Fall 12-14-2018

Delivery of MicroRNA with CXCR4-Targeted Nanoparticles in Metastatic Cancer Treatment

Ying Xie
University of Nebraska Medical Center

Delivery of MicroRNA with CXCR4-Targeted Nanoparticles in Metastatic Cancer Treatment

by

Ying Xie

A DISSERTATION

Presented to the Faculty of

the University of Nebraska Graduate College

in Partial Fulfillment of the Requirements

for the Degree of Doctor of Philosophy

Pharmaceutical Sciences

Graduate Program

Under the Supervision of Professor David Oupický

University of Nebraska Medical Center

Omaha, Nebraska

August, 2018

Supervisory Committee:

Justin L. Mott, M.D., Ph.D. Dong Wang, Ph.D.

Rakesh K. Singh, Ph.D.

Acknowledgements

First and foremost, I would like to express my most profound and sincere thanks to my supervisor Prof. David Oupický for all his mentor and support throughout my four-year study as his PhD student. I have been constantly encouraged and inspired by his unlimited passion to innovation, dedication to science, broad knowledge and critical thinking. It is my great honor and lucky to be his student.

I would also like to sincerely thank my committee members, Profs. Justin L. Mott, Dong Wang and Rakesh K. Singh for their professional suggestions and valuable guidance for my research.

My sincere gratitude also goes to Dr. Jing Li for all the kind help and continuous guidance. I thank Ms. Mary Anne Phillippi, Cody J. Wehrkamp and Dr. Ashley M. Mohr from Dr. Mott's lab for help with miRNA and cholangiocarcinoma-related work. I thank all my former and current labmates for their help and support in and out of the lab. I thank the Department of Pharmaceutical Sciences, University of Nebraska Medical Center for this great opportunity and study experience in this wonderful program. Financial support from China Scholarship Council is gratefully acknowledged.

Last but not least, I would like to thank my family for their endless love and continued support, and all my friends for their company and encouragement along my student life.

Abstract:

Delivery of MicroRNA with CXCR4-Targeted Nanoparticles in Metastatic Cancer Treatment

Ying Xie, Ph.D.

University of Nebraska Medical Center, 2018

Supervisor: David Oupický, Ph.D.

Metastasis is the main contributor to cancer-associated deaths. Inhibition of CXCR4 emerged as one promising approach in metastatic cancer therapy. MiRNAs represent a new class of therapeutics for cancer treatment through RNA interference-mediated gene silencing. Polymeric CXCR4 antagonist (PCX) is a dual-functional polycation to inhibit CXCR4 and deliver nucleic acids. This dissertation hypothesized that blockade of CXCR4 by PCX combined with delivery of miRNA cooperatively enhances metastatic cancer therapy.

In chapter 1, an overview of CXCR4 inhibition, miRNA delivery and CXCR4 targeted nanomedicine in cancer therapy is given.

Chapter 2 reports that PCX can effectively deliver miR-200c mimic and that the combination treatment consisting of PCX and miR-200c results in cooperative antimigration activity by coupling the CXCR4 blockade with epithelial-to-mesenchymal transition inhibition in the cholangiocarcinoma (CCA) cells. The ability of the combined PCX/miR-200c treatment to obstruct two migratory pathways represents a promising antimetastatic strategy in CCA.

Chapter 3 describes that blockade of CXCR4 by PCX combined with the inhibition of hypoxia-inducible miR-210 can cooperatively enhance therapeutic efficacy in

CCA. PCX had a broad inhibitory effect on cell migration, effectively delivered anti-miR-210, and downregulated miR-210 expression in CCA cells. PCX/anti-miR-210 nanoparticles showed cytotoxic activity towards CCA cells and reduced cancer stem-like cells. The nanoparticles reversed hypoxia-induced drug resistance and sensitized CCA cells to gemcitabine and cisplatin combination treatment. Systemic treatment with the nanoparticles in CCA xenograft model resulted in prominent combined antitumor activity.

In chapter 4, PCX effectively delivered both siKRAS and miR-210 inhibitor into pancreatic cancer (PC) cells and induced combined cell killing effect. IP injection of nanoparticles targeted to orthotopic PC tumor. The IP injected combination nanoparticles achieved improved survival in KPC-derived mice through inhibition both primary tumor growth and metastasis. The nanoparticles represent a promising dual-function delivery platform for siRNA/miRNA codelivery and provide safe and effective nanomedicines for metastatic PC therapy.

Results of this thesis and future directions are given in Chapter 5.

Table of Contents

List of Figures

List of Tables

List of Abbreviations

AFM	Atomic force microscope
ALDH	aldehyde dehydrogenase
APC	allophycocyanin
CCA	cholangiocarcinoma
CQ	chloroquine
CSC	cancer stem cell
CXCR4	C-X-C chemokine receptor type 4
DAPI	4′,6-diamidino-2-phenylindole
DEAB	diethylaminobenzaldehyde
DLS	dynamic light scattering
DMAEMA	Dimethylaminoethyl methacrylate
DMEM	Dulbecco's Modified Eagle Medium
EMT	epithelial to mesenchymal transition
EPR	enhanced permeability and retention effect
Erk	extracellular-signal-regulated kinase
EtBr	ethidium bromide
FBS	fetal bovine serum
FDA	Food and Drug Administration

FITC	fluorescein isothiocyanate
FOLFIRINOX	folinic acid, fluorouracil, irinotecan and oxaliplatin
GEM	gemcitabine
HPMA	N-(2-Hydroxypropyl)methacrylamide
H&E	Haemotoxylin and Eosin
IC50	half-maximal inhibition concentrations
IP	intraperitoneal
IV	intravenous
KPC	$Kras^{LSL\text{-}G12D/+}$; $Trp53^{LSL\text{-}R172H/+}$; Pdx-1-Cre
KRAS	Kirsten rat sarcoma viral oncogene homolog
LPA	lysophosphatidic acid
miRNA	microRNA
MFI	mean fluorescence intensity
MMPs	matrix metalloproteinases
NPs	nanoparticles
NCOA3	nuclear receptor co-activator-3
PBS	phosphate buffered solution
PC	pancreatic cancer
PCQ	polymeric chloroquine
PCX	polymeric CXCR4 antagonist

PDI	polydispersity index
PEI	polyethylenimine
PET	positron emission tomography
PLGA	poly(lactic-co-glycolic acid)
qRT-PCR	quantitative real-time polymerase chain reaction
RES	reticuloendothelial system
RISC	RNA inducing silencing complex
RNAi	RNA interference
SDF-1	stromal cell-derived factor 1
siRNA	small interfering RNA
TEM	transmission electron microscope
VEGF	vascular endothelial growth factor
ZEB1	Zinc finger E-box-binding homeobox 1

Chapter 1 – Introduction

Please note that part of the content of this chapter was published in Wiley Interdisciplinary Reviews: Nanomedicine and Nanobiotechnology (Xie, Wang et al, 2018) [1]. As the first author, I wrote the paper. Prof. Oupický, Dr. Jing Li, Dr. Yazhe Wang and Yu Hang gave suggestions to write the manuscript. All the authors agreed with including their work in this dissertation.

Cancer is a major public health problem and a leading cause of mortality worldwide. Metastasis is the main contributor to cancer-associated deaths [2]. The heterogeneity of cancer, combined with multiple gene mutations during tumorigenesis and tumor progression, makes curing cancer a daunting challenge. Recently, combination of chemotherapeutics with RNA interference (RNAi), mainly small interfering RNA (siRNA) and microRNA (miRNA), emerged as an effective strategy in cancer treatment. These combination therapies demonstrate potentially great benefits in targeting multiple cancer-associated pathways, inhibiting metastasis and overcoming adaptive drug resistance [3, 4]. However, this combination treatment is limited by a lack of efficacious delivery systems for simultaneous delivery of small-molecule drugs and siRNA/miRNA. Due to the physicochemical differences between the two types of agents, it is a significant challenge to develop delivery systems for combinations of small molecule drugs and siRNA/miRNA. Among the available delivery systems, polymeric nanoparticles have been the most successful delivery approaches in drug/nucleic acid combinations [4, 5]. Typical polymeric nanoparticles are composed of pharmacologically inert polymer suitable for encapsulation of both types of therapeutic agents. Recently, alternative approaches have focused on the development of pharmacologically active nanoparticles and polymers to achieve delivery of drug/nucleic acid combinations [6-9].

The chemokine receptor CXCR4 is an important emerging target for developing combination delivery strategies for improved cancer therapy [10, 11]. CXCR4 is an especially promising target in antimetastatic therapies because of its crucial role in metastatic spread of multiple types of human cancer [12, 13]. Mounting evidence also supports the potential of improving chemotherapy and immunotherapy through its combination with CXCR4 antagonists [14-17]. As a result, various CXCR4-targeted drug delivery systems, including liposomes, nanoparticles, dendrimers, lipoplexes, and polyplexes have been developed for improved cancer therapy [10]. Recently, our group have reported the synthesis of a series of polycations with the ability to simultaneously inhibit CXCR4 and deliver nucleic acids to cancer cells. We have successfully employed these polymeric CXCR4 inhibitors (PCX) to deliver functional siRNA and miRNA for combination cancer therapy [18-21]. More recently, we have successfully prepared chloroquine-containing polycations as efficient miRNA delivery vectors with improved endosomal escape and antimigratory activity through CXCR4 inhibition in cancer cells [22]. Next, we will introduce these dual functional CXCR4 targeted polycations and discuss the combination strategies based on CXCR4 targeted nanomedicines for cancer therapy.

1.1 CXCR4 as a therapeutic target in cancer

CXCR4 and its chemokine ligand (CXCL12) are two key factors in the tumor growth, metastasis, angiogenesis, and cancer cell-microenvironment interaction, which make them promising targets for cancer therapy.

1.1.1 CXCR4/CXCL12 axis

Chemokine receptors are a large family of proteins that mediate chemotaxis of cells towards a gradient of chemokines. Based on the location of conserved cysteine

residues, chemokine receptors are classified into four groups (C, CC, CXC and CX3C). There are over twenty different chemokine receptors which all belong to the G-protein coupled receptor family. In tumors, the system of chemokines and chemokine receptors modulates the trafficking of cells into and out of the tumor microenvironment and especially mediates crucial steps of the metastasis of tumor cells. Although different types of cancer have varied expression profiles of chemokine receptors, CXCR4 is the most widely expressed chemokine receptor in human cancers. CXCR4 is a G-protein coupled receptor with a seven-transmembrane structure. CXCR4 exerts its biological effect by binding with its specific ligand CXCL12 (also known as stromal derived factor-1, SDF-1). Through activating multiple downstream signaling pathways (mainly including PI3K, MAPK, and Erk1/2), CXCR4/CXCL12 axis regulates a number of different cellular processes, which includes alteration of gene expression, actin polymerization, cell skeleton rearrangement, cell survival, migration and invasion [23, 24].

1.1.2 CXCR4 in cancer and metastasis

CXCR4 expression has been found in more than 20 major human cancer types, including breast, ovarian, prostate, pancreatic, melanoma, and renal cell carcinoma [23]. The upregulation of CXCR4 is highly dependent on multiple transcription factors, growth factors, and hypoxia-inducible factors [25, 26]. A significant correlation between CXCR4 expression and cancer metastasis has been demonstrated by many preclinical and clinical studies. For example, a clinical study concluded that elevated expression of CXCR4 in primary breast tumors is associated with a higher likelihood of developing bone metastases [27]. Another study showed significant correlation between CXCR4 expression and lymph node metastasis [28]. High CXCR4 expression also indicates poor survival and enhanced aggressiveness of cancers and can be used as an independent prognostic marker [29]. CXCR4 can activate focal adhesion complexes and matrix

metalloproteinases, which mediates degradation of extracellular matrix and facilitates the invasion of cancer cells. Then, the CXCL12 concentration gradients drive the movement of CXCR4-expressing cancer cells in the circulation and contribute to the process of extravasation and organ-specific metastasis. For instance, bone marrow, lungs, brain, liver and lymph nodes exhibit elevated expression levels of CXCL12 and represent the most common organs for homing of cancer metastasis in cells that express the CXCR4 receptor [30].

1.1.3 CXCR4 as target for cancer therapy

Various strategies have been developed to inhibit CXCR4/CXCL12 axis for anticancer applications. Among them, specific CXCR4 antagonists showed the best effects. A small molecule CXCR4 antagonist Plerixafor (AMD3100) has already been approved by the FDA for clinical use in stem cell mobilization [31]. Besides small molecules, CXCR4-binding peptides and siRNA silencing of CXCR4 gene have also been reported to be capable of inhibiting CXCR4-mediated processes in anticancer therapy [32-36]. The inhibition of CXCR4 with these therapeutic agents is highly efficacious for cancer therapy through inhibiting metastasis, sensitizing tumors to chemotherapy and radiotherapy, and boosting immunotherapy [37-39]. In the past decade, development of multiple nanomedicines that target CXCR4 have been also reported (**Figure 1.1**). First, CXCR4 can serve as a target for ligand-mediated enhancement of delivery and molecular imaging. CXCR4-binding small molecule organic ligands, CXCR4-binding peptides or anti-CXCR4 antibodies can be attached to the surface of nanoparticles for active targeting to cancer cells for improved therapy and imaging [40, 41]. For example, gold nanoclusters functionalized with AMD3100 were used for targeted positron emission tomography (PET) imaging of CXCR4 in primary tumors and metastases in an orthotopic breast cancer model [42]. Moreover, inhibition of

CXCR4 through CXCR4 siRNA or CXCR4 ligands can be considered as effective approach for cancer therapeutic nanomedicines [36, 43-46]. For example, CXCR4-targeted lipid-coated poly(lactic-co-glycolic acid) (PLGA) nanoparticles modified with AMD3100 systemically delivered sorafenib into liver cancer, resulting in effective sensitization of tumors to sorafenib treatment and lung metastasis inhibition [44].

1.2 Small RNA delivery

RNA interference (RNAi) is a natural biological mechanism in which RNA molecules inhibit gene expression or translation by neutralizing target mRNA molecules. RNAi based agents, mainly including siRNA and miRNA, are able to knock down the oncogenes by targeting related mRNA expression, which make them powerful approaches for cancer therapy [47, 48].

1.2.1 SiRNA

siRNAs are synthetic RNA duplexes (19 to 25 bp in length) with 3' dinucleotide overhangs designed to specifically target a particular mRNA for degradation. SiRNA-mediated RNAi pathway starts with the processing of dsRNA by DICER to siRNA which is then loaded into the RNA inducing silencing complex (RISC) (Figure 1.2). The passenger strand of siRNA is cleaved by AGO2 which is a component of RISC. Then, the guide strand of siRNA guides the activated RISC to the target mRNA. Finally, the complete complementary binding between the guide strand and mRNA leads to the cleavage of mRNA of target gene [4, 48, 49]. Through silencing of key oncogenes, siRNA is capable of modulating or selectively blocking biological processes that are the defining hallmarks of cancer, which make it potentially an effective therapeutic approach for cancer [50].

1.2.2 MiRNA

MiRNAs are small (~22 nucleotide) noncoding endogenous RNAs that post-transcriptionally regulate gene expression. In the nucleus, the transcription of miRNA gene is carried out by RNA polymerase II to produce pri-miRNA, which is then cleaved by Drosha to form pre-miRNA (**Figure 1.2**). Pre-miRNA is transported by Exportin 5 to the cytoplasm. In the cytoplasm, pre-miRNA is processed by Dicer into mature miRNA. Then, miRNA is loaded into RISC. The passenger strand is discarded. The remaining guide strand guides the miRISC to the target mRNA through partially complementary binding. Finally, the target mRNA is inhibited via translational repression, degradation or cleavage [48, 51]. Due to the imperfect pairing, a single microRNA is capable of simultaneously targeting different genes, showing the characteristic of multiple targeting. MiRNAs regulate a wide range of cellular pathways and modulate the expression of nearly 30% of all human proteins. Dysregulation of miRNA often results in pathological states such as cancer. MicroRNAs function as tumor suppressors or oncogenes and play an important role in tumorigenesis, tumor growth, angiogenesis, and metastasis [52]. Hence, inhibition of overexpressed oncogenic microRNAs or restitution of downregulated tumor-suppressor microRNAs provides a highly promising approach to treat cancer [53].

1.2.3 Small RNA delivery

Both siRNA and miRNA are highly effective therapeutic agents for cancer. However, their clinical use is limited by multiple hurdles, such as stability, off-target effect and poor efficiency of delivery. Although proper chemical modification can improve the stability and reduce off-target effect, poor delivery is still a main challenge in translating therapeutic siRNAs/miRNAs into clinic [54, 55]. Since they have similar physicochemical properties (double-stranded RNAs with about 22 nucleotides) and the same intracellular site of action (cytoplasm), similar delivery systems can be utilized for

both siRNA and miRNA. An ideal delivery system is expected to sequentially overcome multiple biological barriers, mainly including nucleases degradation, reticuloendothelial system (RES) clearance, poor tumor tissue penetration and intracellular uptake, lysosomal entrapment, and intracellular RNA release [56, 57].

Viral vectors and non-viral vectors represent the two main types of delivery technologies for siRNA/miRNA. Non-viral vectors show advantages over viral vectors in terms of safety and represent a potential option for clinical application. Widely used non-viral approaches include polymer-based and lipid-based delivery systems. Cationic polymers (polycations) and cationic lipids bind with anionic siRNA/miRNA through electrostatic interactions which leads to the formation of nanosized polyplexes or lipoplexes, which protect them from degradation and facilitate transport across cellular membranes [48]. To meet the requirement of combination RNAi therapy and traditional small molecule therapy, many delivery systems have been reported to co-deliver small molecule agents and RNAi therapeutics in the past decade. Among the available delivery systems, polymeric nanoparticles have been the most successful delivery approaches in drug/RNAi therapeutic combinations. Typical polymeric nanoparticles are composed of pharmacologically inert polymer suitable for encapsulation of both types of therapeutic agents [3]. However, the manufacturing complexity and unsatisfactory drug loading ability of the traditional nanoparticles remain a significant hurdle for their clinical translation. Recently, alternative approaches from our lab have developed pharmacologically active nanoparticles based on polymeric drugs to achieve delivery of drug/nucleic acid combinations [6]. The uniquely designed polymeric drug nanoparticles have several advantages, including simpler formulation and high content of active agents that make them suitable candidates for delivery of drug/RNA combinations. In

particular, a series of CXCR4 targeted polymeric drug nanoparticles represent a new generation of drug/RNAi delivery vectors for combination anticancer therapy.

Both CXCR4 inhibition and siRNA/miRNA delivery are important approaches for cancer therapy. CXCR4 targeted nanomedicines delivering functional siRNA/miRNA represent an effective choice for combinational cancer therapy. These newly developed nanomedicines include polyplexes, lipid nanoparticles, peptide carriers, lipopolymer complexes and fusion proteins (**Table 1**). Among the CXCR4 targeted nanomedicines, we will focus on polymeric CXCR4 antagonists and polymeric chloroquines.

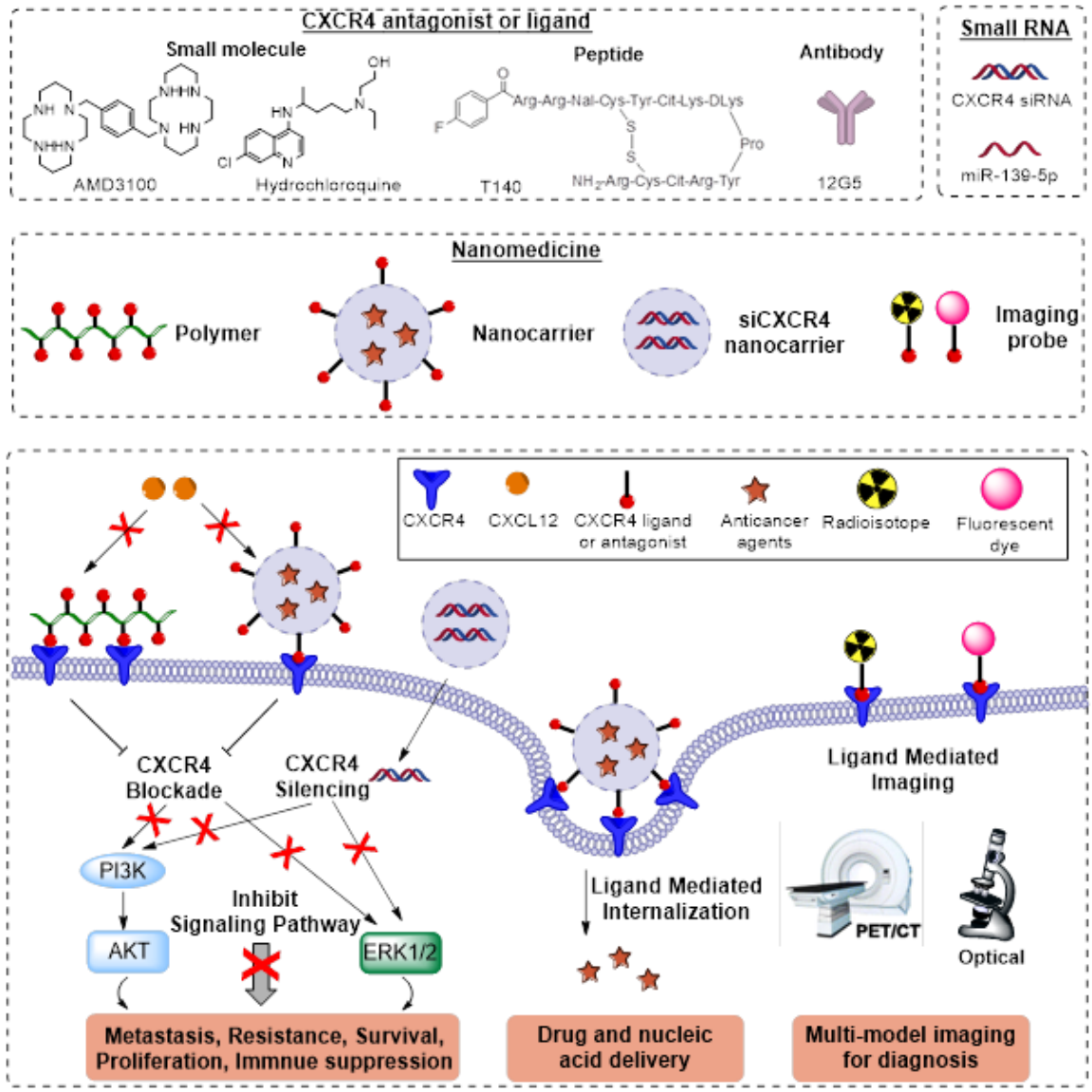

Figure 1.1. Main approaches utilizing CXCR4 in cancer nanomedicine.

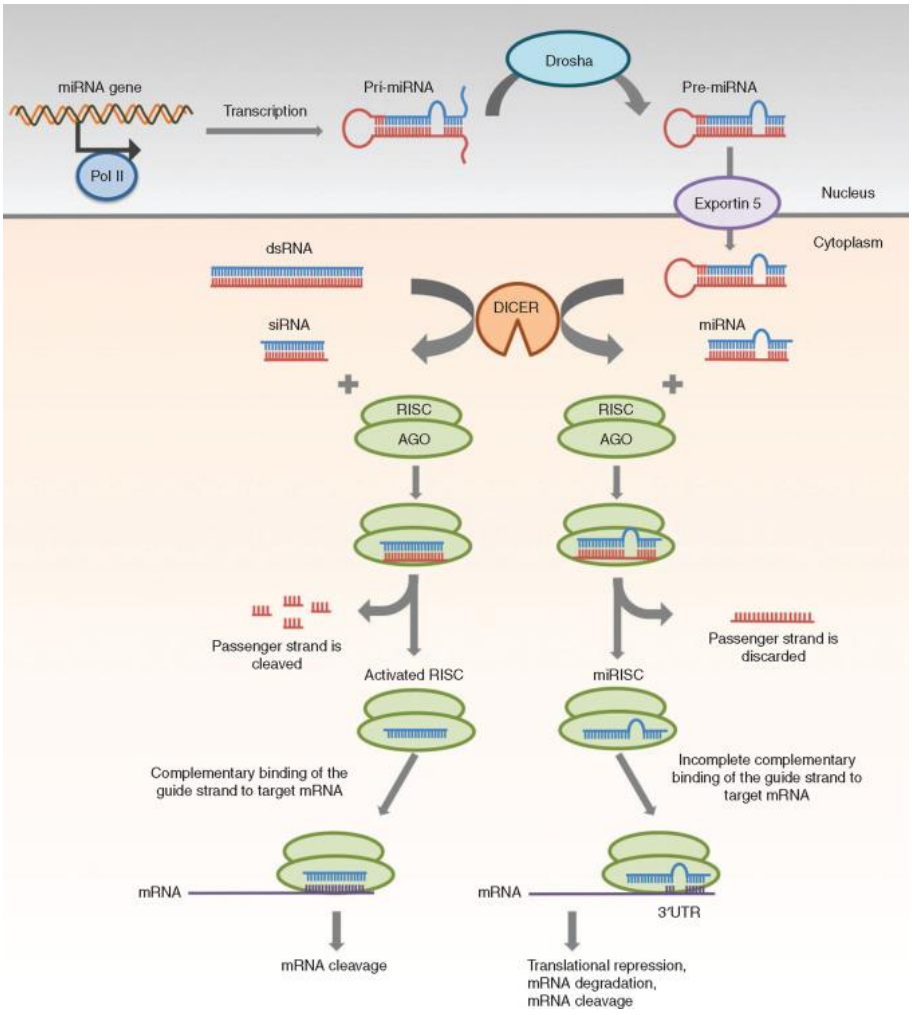

Figure 1.2. Gene silencing mechanisms of siRNA and miRNA. (Reprinted with permission from Ref [48])

Table 1. Example of CXCR4-targeted nanomedicines delivering siRNA/miRNA in cancer therapy.

CXCR4 targeting moiety	Delivery system	Delivered cargo	Application	References
AMD3100	Polyplexes (PCX-1)	PLK1 siRNA	Simultaneously inhibit migration through CXCR4 antagonism and kill cells through siPLK1 (*in vitro*)	[58]
AMD3100	Polyplexes (PCX-1)	NCOA3 siRNA	Increase tumor perfusion by siNCOA3, simultaneously inhibit tumor growth and metastasis (*in vivo*)	[21]
Monocyclam	Polyplexes (PCX-2)	MiR-200c mimic	Combined inhibition of cancer cell invasiveness by CXCR4 antagonism and EMT inhibition (*in vitro*)	[59]
AMD3465	Polyplexes (P-SS-AMD)	MiR-200c mimic	Combined inhibition of cancer cell migration by CXCR4 antagonism and EMT inhibition (*in vitro*)	[60]
Chloroquine	Polyplexes (PCQ)	MiR-210 inhibitor	Facilitate endosome escape, simultaneously inhibit migration and kill cells (*in vitro*)	[22]
AMD3100	Lipid nanoparticles	VEGF siRNA	Overcome tumor evasion of antiangiogenic therapy, inhibit tumor growth and metastasis (*in vivo*)	[61]
Peptide	Modular peptide-based carrier	VEGF siRNA	Targeted siRNA delivery into CXCR4-expressing cancer and endothelial cells for inhibition of migration (*in vitro*)	[62]
CXCR4 siRNA	Lipopolymer complexes	CXCR4 siRNA	Decrease CXCR4 expression for acute myeloid leukemia therapy (*in vitro*)	[63]
CXCR4 siRNA	Fusion protein	CXCR4 siRNA	CXCR4 knockdown by siRNA effectively inhibited breast tumor growth and metastasis (*in vivo*)	[36]

1.3 Cyclam-based polymeric CXCR4 antagonists (PCX)

1.3.1 Polymer design and development

Blockade of CXCR4 with specific antagonists can inhibit metastasis and control the growth of the primary tumors [64]. Cyclam derivatives such as AMD3100 are the most widely investigated CXCR4 antagonists which act through inhibiting CXCL12 binding and subsequent CXCR4 signaling [65-67]. AMD3100 contains six secondary and two tertiary amines (Figure 1.3A). Not all of the eight amines are required for binding to the CXCR4 receptor and its pharmacologic function. The redundant amine groups can be used for chemical modification while still maintaining CXCR4 inhibition activity [68]. The presence of the protonizable amines provides AMD3100 with positive charge, which makes it a suitable building unit for synthesis of polycations for nucleic acid delivery. Based on this rationale, our group have synthesized the first generation of polymeric CXCR4 antagonists (PCX-1) (Figure 1.3A), polymeric AMD3100, by direct Michael-like addition polymerization of AMD3100. The synthesized PCX-1 not only retained the CXCR4 inhibitory activity of parent AMD3100 but also successfully delivered nucleic acids to cancer cells [18, 20].

Although PCX-1 was well suited for the proof-of-principle studies, the ability to control the polymerization reaction was severely compromised by the presence of six reactive secondary amines in the chemical structure of AMD3100, which resulted in the generation of highly branched polymers. The random chemical substitution of AMD3100 in PCX-1 also decreased the relative CXCR4 inhibitory activity when compared with the parent AMD3100. To overcome the disadvantage of PCX-1, we then developed the second generation of the poly(amido amine) CXCR4 antagonists (PCX-2) with improved presentation of the CXCR4-binding moieties and better controlled polymerization. Unlike PCX-1 which was based on AMD3100, the linear PCX-2 was prepared by the

polymerization of newly synthesized CXCR4-inhibiting monocyclam monomers (**Figure 1.3A**). PCX-2 showed improved ability to inhibit CXCR4 when compared with the monomers. PCX-2 inhibited cancer cell invasion *in vitro* and presented CXCR4 antagonism *in vivo* to mobilize leukocytes from bone marrow to peripheral blood. Moreover, the dual function PCX-2 was also capable of delivering DNA into cancer cells [19].

Chemical modification of the PCX polymers was performed to further improve the activity of PCX to systemically deliver functional nucleic acids for cancer therapy. To improve *in vivo* applicability, polyplexes are often modified with poly(ethylene glycol) (PEG) to shield the surface charges and improve colloidal stability by steric stabilization [69, 70]. Accordingly, PEG modification of PCX was investigated by grafting PEG chains to form PEG-PCX. We found that optimized PEG-PCX retained the desirable CXCR4 antagonism and capability of PCX to inhibit cancer cell invasion, while at the same time allowing to improve safety and colloidal stability of the PCX polyplexes [71]. Furthermore, we were able to further balanced the polymer hydrophobicity by grafting PCX with cholesterol and prepared amphiphilic Chol-PCX. When compared with simple PCX polyplexes, the optimized Chol-PCX polyplexes increased colloidal stability and greatly improved siRNA transfection in the presence of serum, all the while retaining strong CXCR4 inhibitory activity [58]. Overall, PEG-PCX and Chol-PCX were successfully developed as potential vectors for systemic *in vivo* delivery of nucleic acids.

1.3.2 PCX-mediated delivery of siRNA and miRNA to cancer cells

After successful development of the CXCR4 inhibiting polymers PCX, we tested their ability to deliver suitable siRNA or miRNA for combined cancer therapy. In the first example, we focused on PCX/siRNA polyplexes for pancreatic cancer (PC) therapy. PC is one of the most aggressive malignancies with intense desmoplasia, widespread

metastasis and inherent chemoresistance. Nuclear receptor co-activator-3 (NCOA3) is a critical modulator of the expression of mucins in PC. Silencing of NCOA3 with siRNA in PC cells downregulates the expression of mainly two mucins, MUC1 and MUC4, which are critical for PC progression [72]. Besides mucins, NCOA3 upregulates the expression of multiple chemokines that are responsible for the recruitment of immune cells to pancreatic tumors, perpetuation of pro-inflammatory conditions, and activation of pancreatic stellate cells. As a result, NCOA3 is a suitable target for siRNA nanomedicine design which aims to modulate PC tumor microenvironment by decreasing desmoplasia, increasing perfusion and enhancing drug delivery to tumor. In addition to the tumor microenvironment modulation by NCOA3 silencing, blockade of CXCR4 is another effective approach to inhibit PC metastasis and progression. We thus combined the two strategies together, using optimized formulation of PCX/siNCOA3 polyplexes to simultaneously target CXCR4 and NCOA3 in PC (**Figure 1.4**). Chol-PCX showed maximum CXCR4 antagonism, NCOA3 silencing and inhibition of PC cell migration *in vitro*. Furthermore, PCX/siNCOA3 polyplexes showed great potential in sensitizing PC cells to chemotherapy. More importantly, the polyplexes showed improved antitumor therapy in an orthotopic mouse model of metastatic PC after systemic delivery. The polyplexes significantly inhibited primary tumor growth, which was because of a decrease in tumor necrosis and increased tumor perfusion. The polyplexes also showed significant antimetastatic effect as demonstrated by effective suppression of metastasis to distant organs. Overall, PCX/siNCOA3 polyplexes represent a highly promising combination approach for modulating tumor microenvironment in metastatic PC [21].

In addition to siRNA delivery, PCX also provide effective delivery activity for therapeutic miRNA as demonstrated in a study focused on delivery of metastasis-regulating miRNA for cooperatively enhanced anti-invasive effect in multiple types of cancer cells. The invasion and metastasis of cancer cells are regulated by multiple

factors, which includes not only CXCR4 but also multiple miRNAs. For example, increasing intracellular levels of miR-200c decreased the extent of the epithelial-to-mesenchymal transition (EMT) and inhibited cell migration and invasion in cancer cells [73]. Combining the CXCR4 antagonism with the action of miR-200c mimic was thus expected to cooperatively enhance the inhibition of the migration of cancer cells. Based on this rationale, we prepared PCX-2 polyplexes carrying miR-200c mimic (Figure 5). PCX-2 polyplexes effectively delivered miR-200c mimic into cancer cells. By coupling the CXCR4 blockade with miR-200c-induced EMT inhibition, the polyplexes achieved cooperative antimigration activity (**Figure 1.5A and B**) [59]. Moreover, an N-(2-hydroxypropyl)methacrylamide (HPMA)-based self-immolative polymeric prodrug of a CXCR4 antagonist, AMD3465 (P-SS-AMD) (**Figure 1.5C**), also effectively delivered miR-200c and led to the combinational inhibition of cancer cell migration [60]. Overall, PCX/miR-200c treatment is an effective antimetastatic strategy that combines inhibition of two important cell motility pathways.

1.3.3 Mechanism of action of PCX polyplexes

Even though we have experimentally confirmed the dual function of PCX/RNA polyplexes to inhibit CXCR4 and deliver small RNA [58], the specific mechanism of action remained unclear because of the seemingly conflicting demands on the system (siRNA delivery vs. CXCR4 inhibition). We have formulated three hypotheses depicted in **Figure 1.6** to explain the mechanism of action. First, as all polyplexes, PCX/RNA are prepared with excess PCX and it is the excess polymer that is responsible for the immediate CXCR4 antagonism. This has been shown by increased CXCR4-dependent anti-migration activity with increasing PCX/siRNA w/w ratio [58]. Second, PCX bound to siRNA is released after intracellular siRNA delivery and polyplex disassembly. This mode of action results in delayed CXCR4 inhibition effect, either via binding intracellular

CXCR4 during recycling or via PCX excretion from the cells and binding the plasma membrane CXCR4 on cancer cells. Third, in case of intracellularly degradable PCX, the small molecule degradation products containing the CXCR4-binding cyclam moieties may further contribute to the CXCR4 inhibition. Improved understanding of the mechanism of action will contribute to further improvement of the antitumor and antimetastatic activity of the PCX polyplexes.

Another concern in developing PCX has been related to optimizing properties of the formulations with two active agents (CXCR4 inhibitor and siRNA/miRNA). Single formulation of two active agents is often technically challenging, and in many cases, it may be easier to use two single-agent formulations. However, several unique properties of PCX greatly simplify the process of optimizing pharmacologic activity of the dual PCX/siRNA polyplexes and justify their development. The most important one is a broad therapeutic window of PCX, which gives us great leeway in optimizing the formulation for effective siRNA/miRNA delivery without significant concerns about the CXCR4 activity. For example, the effective dose (EC_{50}) of the most active PCX is only 0.021 μg/mL, while its toxic dose (LD_{50}) is more than 8,000-times higher (171 μg/mL) [19]. In a typical siRNA (10 nM) silencing experiment with polyplexes formulated at PCX/siRNA w/w ratio of 5, the PCX concentration would be 0.665 μg/mL (i.e., 30-times above EC_{50}). Thus, at the anticipated siRNA concentration range, changes in PCX concentrations will have minimal effect on its CXCR4 activity.

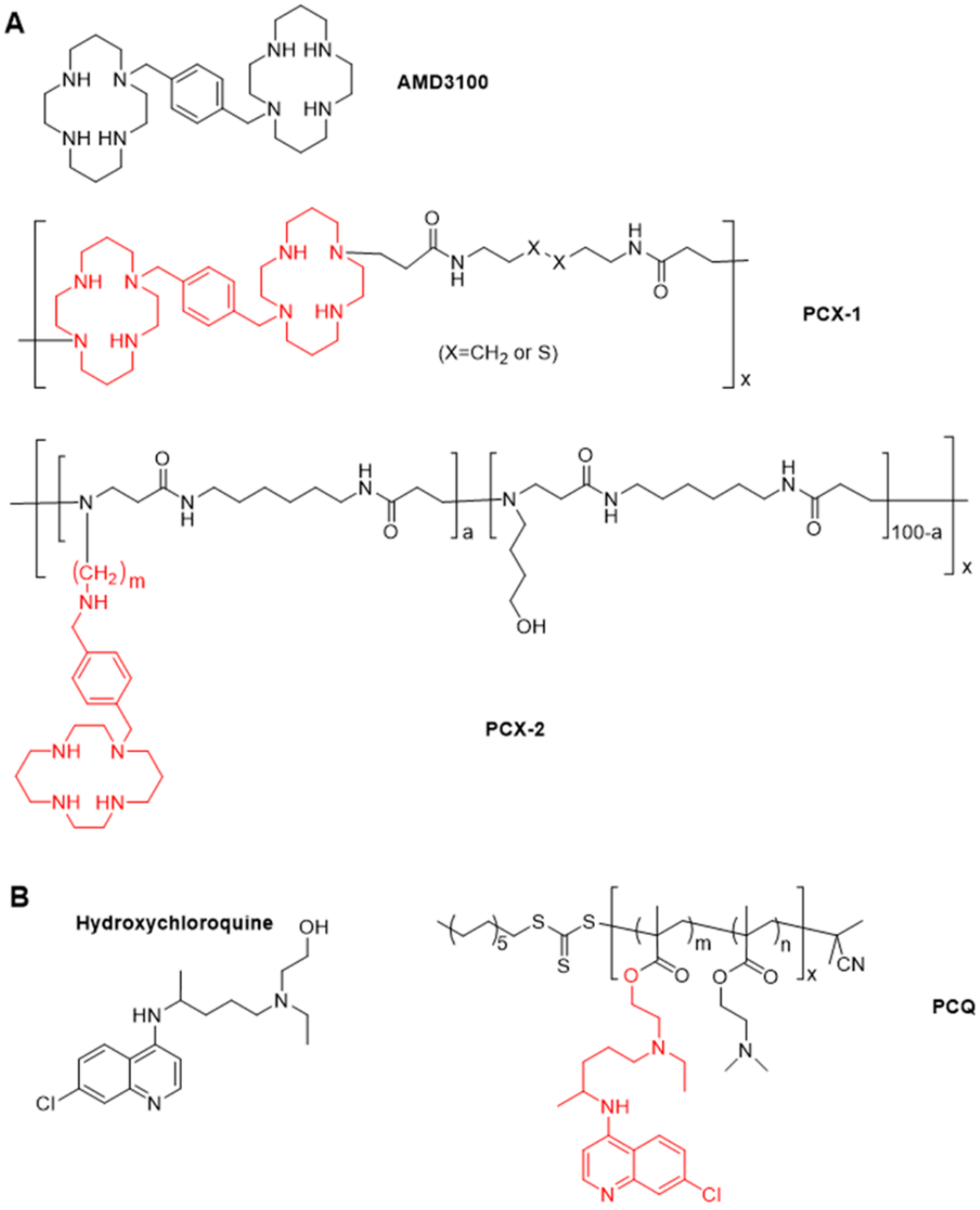

Figure 1.3. Chemical structure of (A) AMD3100 and cyclam-based polymeric CXCR4 antagonists (PCX) and (B) hydroxychloroquine and chloroquine-based CXCR4 antagonists (PCQ) (Red color indicates the CXCR4-binding repeating unit in the polymers).

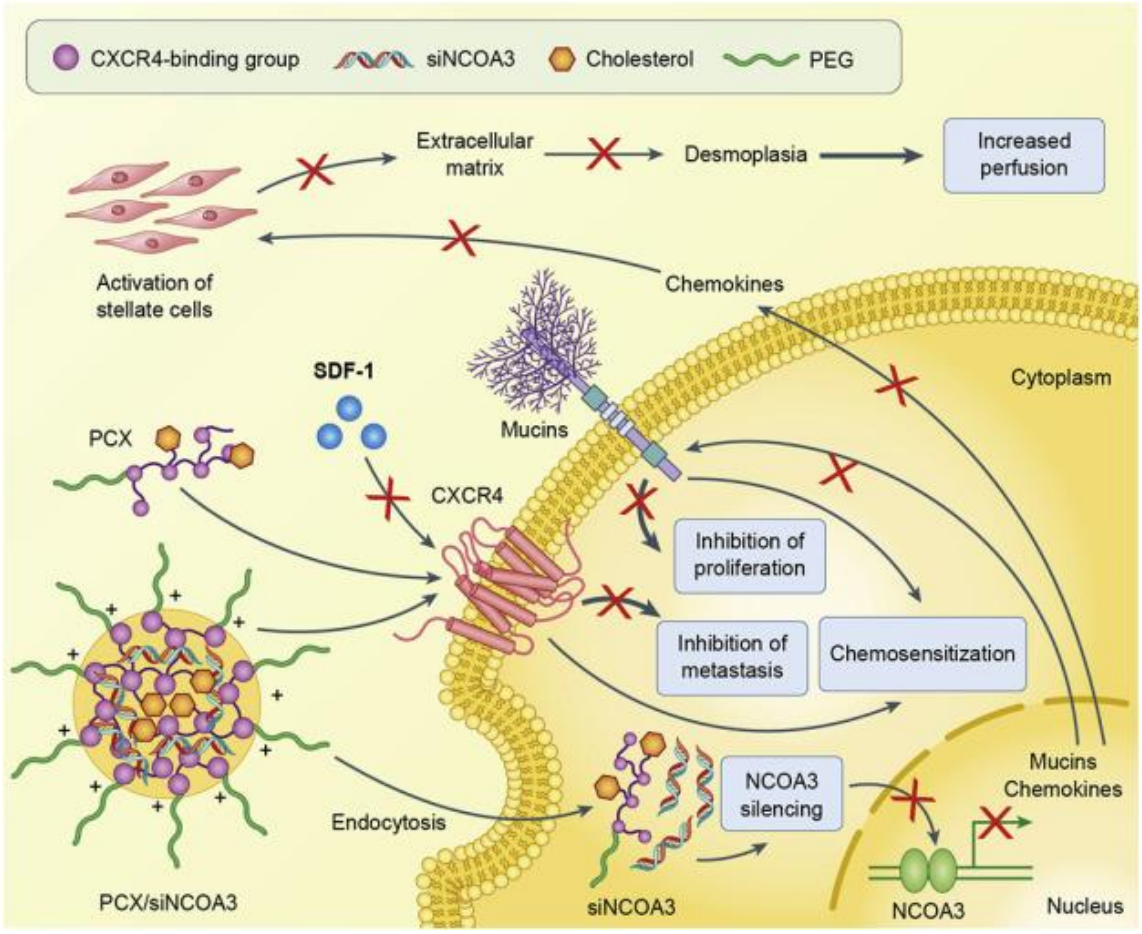

Figure 1.4. Mechanism of action of PCX/siNCOA3 polyplexes in pancreatic cancer therapy. (Reprinted with permission from Ref [21])

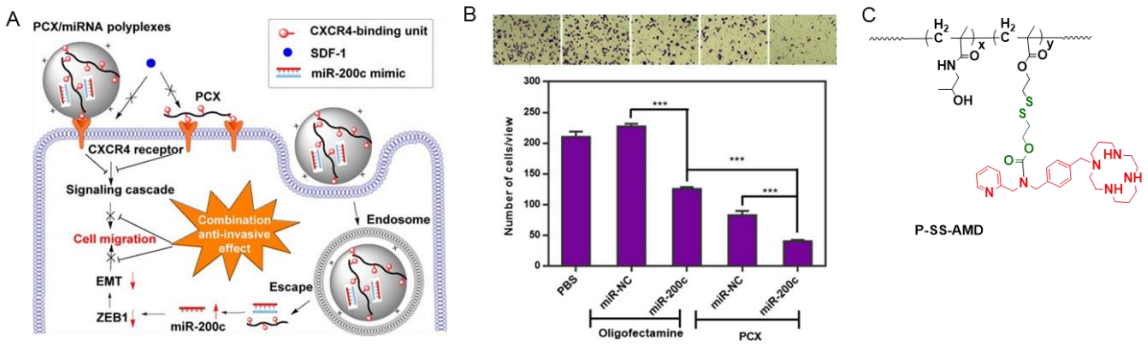

Figure 1.5. (A) Proposed mechanism of action of PCX/miR-200c polyplexes. (B) Combined inhibition of cancer cell migration. (Reprinted with permission from Ref [59]) (C) Chemical structure of an HPMA-based self-immolative polymeric prodrug of a CXCR4 antagonist, AMD3465 (P-SS-AMD). (Reprinted with permission from Ref [60])

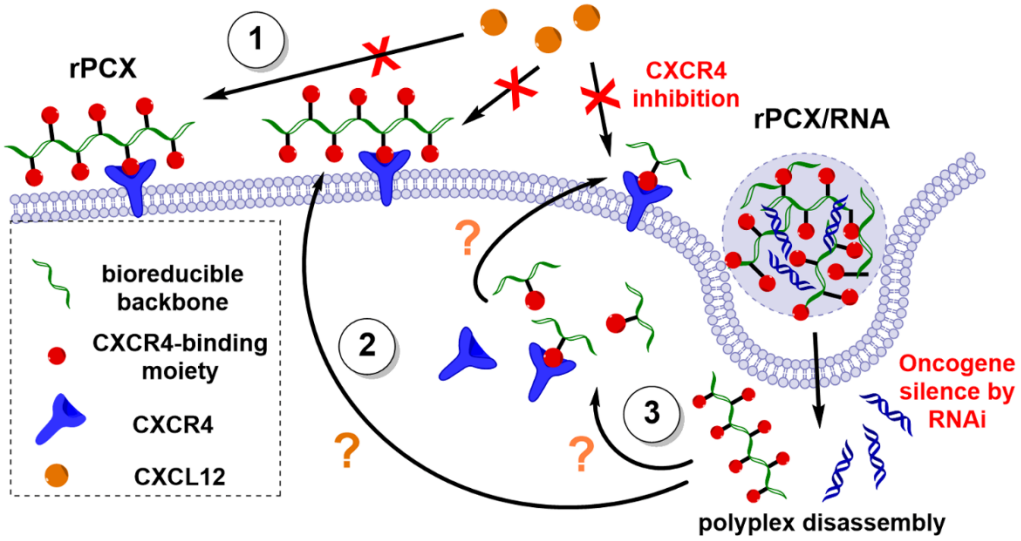

Figure 1.6. Proposed mechanisms of PCX/RNA polyplexes. (1) Excess PCX of the polyplexes formulation is responsible for the immediate CXCR4 antagonism. (2) The disassembly of polyplex releases both small RNA and PCX. Functional small RNA silences oncogene through RNAi mechanism. These released PCX results in delayed CXCR4 inhibition effect via binding intracellular CXCR4 during recycling or via PCX excretion from the cells and binding the plasma membrane CXCR4 on cancer cells. (3) In case of intracellularly bioreducible PCX (rPCX), the small molecule degradation products containing the CXCR4-binding cyclam moieties further contribute to the CXCR4 inhibition.

1.4 Chloroquine-based CXCR4 antagonists (PCQ)

1.4.1 Polymer development

Chloroquine (CQ) is a widely used antimalarial drug. In recent years, the potential benefits of CQ in anticancer therapies have been also reported mainly due to its effects on autophagy and cholesterol metabolism.[74-77] Recently, the ability of CQ to inhibit CXCR4/CXCL12 axis has also been reported and successfully used in the treatment of solid tumors [78]. CQ was able to inhibit CXCL12-mediated invasion and proliferation of PC cells and improve survival of tumor-bearing mice when combined with gemcitabine treatment [79]. Despite its promise, CQ is a poor (mM) inhibitor of CXCR4 when compared with existing specific nM inhibitors like AMD3100. Thus, we aimed to improve the CXCR4-inhibiting activity of CQ by taking advantage of the multivalency effect by conjugating multiple CQ molecules to a polymeric carrier. We have synthesized CQ-containing copolymers (PCQ) by copolymerization of methacryloylated hydroxy-CQ (HCQ) and HPMA. PCQ-1 enhanced inhibition of cancer cell migration and invasion *in vitro*, and improved antimetastatic activity *in vivo* with lower toxicity when compared with the parent HCQ. The effective inhibition of the CXCR4/CXCL12 axis has been confirmed as one mechanism of the PCQ antimetastatic activity [80, 81]. Besides HPMA-based PCQ, our group reported another PCQ drug, chloroquine-modified hydroxyethyl starch (CQ-HES) which was synthesized by conjugation of HES with HCQ by a carbonyldiimidazole coupling. CQ-HES was able to target CXCR4 signaling and improve inhibition of migration and invasion of PC cells when compared with HCQ [82]. Overall, PCQ represents a new generation of safe and effective CXCR4 inhibitors for metastatic cancer therapy.

Besides CXCR4 antagonism, CQ is also a widely used chemical endosomolytic agent to improve *in vitro* transfection of polyplexes. Simple cotransfection of polyplexes

with free CQ enhances the cytoplasmic delivery of nucleic acids [83]. However, CQ cotransfection is difficult to be used *in vivo* because in order to achieve the functional levels, toxic doses of CQ are required. To overcome the limitations of CQ as endosomal agent *in vivo*, covalent conjugation of CQ to the nanoparticles improved siRNA delivery *in vivo* by enhancing endosomal escape [84]. Thus, conjugation of CQ to polycations was also expected to improve endosomal escape of polyplexes. Hence, we aimed to prepare CQ-conjugated polycation for both CXCR4 antagonism and improved endosomal escape. Recently, we reported the synthesis of CQ-containing 2-(dimethylamino)ethyl methacrylate (DMAEMA) copolymers (PCQ-2) by reversible addition–fragmentation chain-transfer polymerization. After careful optimization of both polymer molecular weight and CQ content in the polymer, the best performing PCQ-2 polyplexes presented the expected dual function through not only inhibiting the migration of cancer cells but also facilitating the endosomal escape for cytoplasm delivery of miRNA (**Figure 1.7**) [22].

1.4.2 RNA delivery by PCQ

After successful preparation of PCQ-2, we then aimed to deliver suitable siRNA or miRNA for cancer therapy. Intratumoral hypoxia is a hallmark of cancer due to a structurally and functionally disturbed microcirculation, with deterioration of the diffusion geometry, and of tumor-associated anemia [85]. As a key factor in tumor progression, hypoxia induces cancer metastasis and increases the resistance of cancer cells to chemotherapy, radiotherapy and photodynamic therapy [86-88]. Hypoxia is also able to induce and stabilize CXCR4 expression in cancer [89, 90]. MiR-210 is a major hypoxia-inducible miRNA which is overexpressed in multiple types of cancers [91, 92]. MiR-210 controls a wide range of biological processes, including cell proliferation, apoptosis, differentiation, DNA repair, cell metabolism, metastasis, and antitumor immune

responses [93, 94]. Hence, miR-210 inhibition with anti-miR-210 provides a valid target for the treatment of cancer. Accordingly, we prepared PCQ polyplexes to deliver anti-miR-210. Besides retaining the antimigration activity by CXCR4 antagonism, PCQ polyplexes improved the delivery of anti-miR-210 to cancer cells by facilitating endosomal escape. Moreover, through inhibition of miR-210 function, PCQ/anti-miR-210 polyplexes improved anticancer activity by inducing significant cell killing in cancer cells. These results further validate the use of PCQ as a efficacious polymeric drug platform in combination anti-metastatic and anticancer miRNA therapeutic strategies [22].

1.5 CXCR4-targeted nanoparticles

1.5.1 CXCR4 antagonist nanoparticles

Besides PCX and PCQ, other CXCR4 targeted nanoparticles have also been reported for RNAi cancer therapy. These nanoparticles were typically formed by the physical addition of small molecular CXCR4 inhibitor like AMD3100 to the formulation. AMD3100 can act as both cancer targeting ligand for improved nanoparticles delivery and CXCR4 antagonism for cancer therapy [43, 46, 61]. For example, the Chen's group developed a CXCR4-targeted lipid-based nanoparticles (NP) to specifically deliver vascular endothelial growth factor (VEGF) siRNA as an antiangiogenic substance into liver cancer. AMD3100 was added into the nanoparticles to serve as both a targeting moiety and a sensitizer to antiangiogenic therapy. These AMD3100-modified NPs efficiently delivered VEGF siRNAs into liver cancer and downregulated VEGF expression *in vitro* and *in vivo*. The combination of CXCR4 inhibition by AMD3100 and VEGF siRNA induced synergistic antiangiogenic effects and suppressed primary tumor growth and distant metastasis in orthotopic liver cancer model [61].

1.5.2 CXCR4-silencing nanoparticles

SiRNA silencing of CXCR4 also represents an additional approach to target CXCR4/CXCL12 axis. Multiple studies reported the delivery of CXCR4 siRNA using nanoparticles [36, 63, 95-97]. For example, a lipid-modified polymeric carrier was developed for CXCR4 siRNA delivery to acute myeloid leukemia (AML) cells. CXCR4 siRNA was successfully delivered to mononuclear cells derived from AML patients, which resulted in significant CXCR4 silencing in tested samples. Decreasing CXCR4 expression via lipopolymer/siRNA nanocarriers was proven as a potential option for AML therapy [63]. In another study, a fusion protein containing an anti-HER2 single-chain antibody fragment was reported to deliver CXCR4 siRNA for $HER2^{+}$ breast cancer treatment. CXCR4 knockdown by siRNA effectively inhibited breast tumor growth and metastasis both *in vitro* and *in vivo* [36].

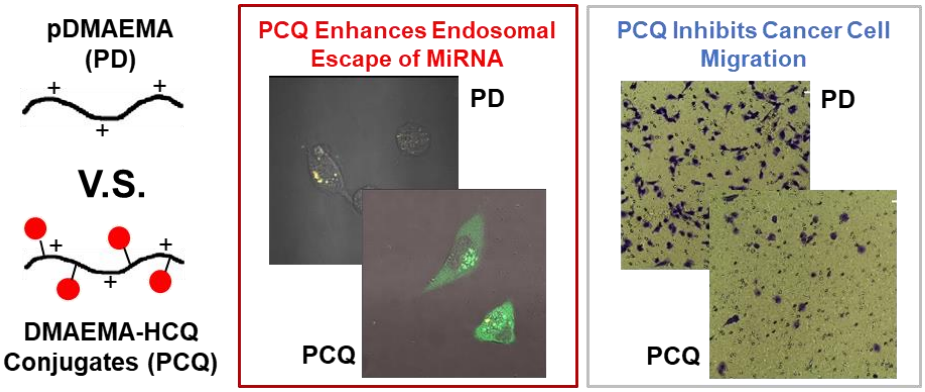

Figure 1.7. Chloroquine containing polycation for improving endosome escape of delivered miRNA and inhibiting cell migration. (Reprinted with permission from Ref [22])

1.6 Summary

The benefits of both CXCR4 inhibition and siRNA/miRNA delivery for improved cancer therapies are clearly established. CXCR4-targeted nanocarriers are greatly potential nanomedicines to deliver functional siRNA/miRNA for combination therapy. The dual function polymeric CXCR4 antagonists simultaneously block the CXCR4/CXCL12 axis and deliver functional siRNA and miRNA to cancer cells, which normally result in the inhibition of primary tumor growth and reduction of metastasis. Using CQ as an alternative CXCR4 inhibitor allows to advantageously combine CXCR4 antagonism with endosomolytic properties of CQ to enhance cytoplasmic delivery of siRNA and miRNA. Besides the PCX and PCQ polymers, CXCR4 inhibitors or CXCR4 siRNA can also be encapsulated into suitable nanocarriers for CXCR4 inhibition. These CXCR4 targeted nanomedicines carrying functional siRNA/miRNA represent a promising choice for combination cancer therapy especially metastasis inhibition.

Chapter 2 - Delivery of miR-200c mimic with poly(amido amine) CXCR4 antagonists for combined inhibition of cholangiocarcinoma cell invasiveness

Please note that part of the content of this chapter was published in Molecular Pharmaceutics (Xie, Wehrkamp et al, 2016) [59]. As the first author, I performed all the work in the paper. Prof. Oupický and co-authors helped to interpret the data and prepare the manuscript. All the authors agreed with including their work in this dissertation.

2.1 Introduction

Cholangiocarcinoma is a malignant neoplasm of the biliary duct system. Intrahepatic cholangiocarcinoma (ICC) arises from the epithelial cells of the intrahepatic bile ducts [98, 99]. ICC is the second most common primary liver malignancy after hepatocellular carcinoma and accounts for 10-25% of all primary hepatic malignancies. The incidence rate of ICC has increased worldwide over the past decade. Despite advances in surgical techniques, chemotherapy and radiotherapy, 5-year survival rate of patients after diagnosis has not increased and remains at ~10% [100]. The ICC is highly fatal mainly due to early invasion and widespread metastasis and the lack of effective therapeutic options [101, 102]. Among others, therapeutic strategies that focus on addressing the invasive character of ICC promise to improve the treatment outcomes.

MicroRNAs are noncoding RNAs with about 22 nucleotides in length. MicroRNA is involved in the regulation of gene expression at a post-transcriptional level through binding to the target sites of messenger RNAs. Growing number of studies confirm the important role of microRNAs in formation and progression of various human cancers, including ICC [103-109]. Recent evidence suggests that migration, invasion and metastasis of ICC are regulated by multiple microRNAs, including miR-21[110], miR-200c [73], and miR-214 [111]. For example, increasing levels of miR-200c decreased the extent of the epithelial-to-mesenchymal transition (EMT) and inhibited cell migration and

invasion in ICC cells [73]. Despite the potential of microRNA for cancer therapy, the clinical translation of therapeutic microRNA is hindered by a lack of efficient delivery systems [112, 113]. The negative charge and low molecular weight of microRNAs make them suitable for formulation in nanoscale delivery systems, thus enabling their use in clinical cancer therapy [114]. Polycations are widely used as miRNA carriers for gene therapy in cancer [3, 115]. For example, cationic polyurethanes-short branch PEI delivered miR-145 to xenograft tumors to reduce tumor growth and metastasis [116].

The chemokine receptor CXCR4 plays a crucial role in metastatic spread of multiple types of cancer, including ICC, making it a potential therapeutic target [117-121]. Stromal cell-derived factor-1 (SDF-1, CXCL12) is the only chemokine ligand for the CXCR4 receptor and is highly expressed in the liver. Binding of SDF-1 to CXCR4 can activate several intracellular signaling transduction pathways that regulate migration and invasion of cancer cells. CXCR4 facilitates the metastatic spread of the primary tumor to sites where SDF-1 is highly expressed. Numerous studies have shown that blocking CXCR4 activation with CXCR4 antagonists inhibits metastasis of multiple tumor types [122-124]. The anti-metastatic effect of CXCR4 inhibition can be enhanced by simultaneous use of nucleic acids that target additional pathways involved in cancer cell migration and invasion. This was demonstrated in a recent study which combined inhibition of the CXCR4 axis with siRNA knockdown of Lipocalin-2 (Lcn2) as a way of synergistically reducing migration in metastatic human breast cancer cells [125].

We have recently developed a series of polymeric CXCR4 antagonists (PCX) capable of delivering various types of nucleic acids, including DNA and siRNA [126-129]. The developed PCX polymers effectively block cancer cell invasion by inhibiting the CXCR4/SDF1 axis, while at the same time, deliver nucleic acids into the cancer cells for improved anticancer effect. The PCX polymers were synthesized from either FDA-

approved CXCR4 antagonist AMD3100 (**Scheme 2.1A**) or novel CXCR4-inhibiting monocyclam inhibitors (**Scheme 2.1B**). In the present study, we hypothesized that combining the CXCR4 axis blockade with the action of miR-200c mimic would enhance the inhibition of the migration of metastatic ICC cells more efficiently than either one of these treatments alone. We expected that in addition to CXCR4 antagonism, the PCX could deliver miR-200c into ICC cells and inhibit EMT by inhibiting zinc finger E-box-binding homeobox 1 (ZEB1) expression, thus enhancing the inhibitory effect on cancer cell migration and invasion (**Scheme 2.1C**). The ability of the combined PCX/miR-200c treatment to obstruct two migratory pathways represents a promising antimetastatic strategy in ICC.

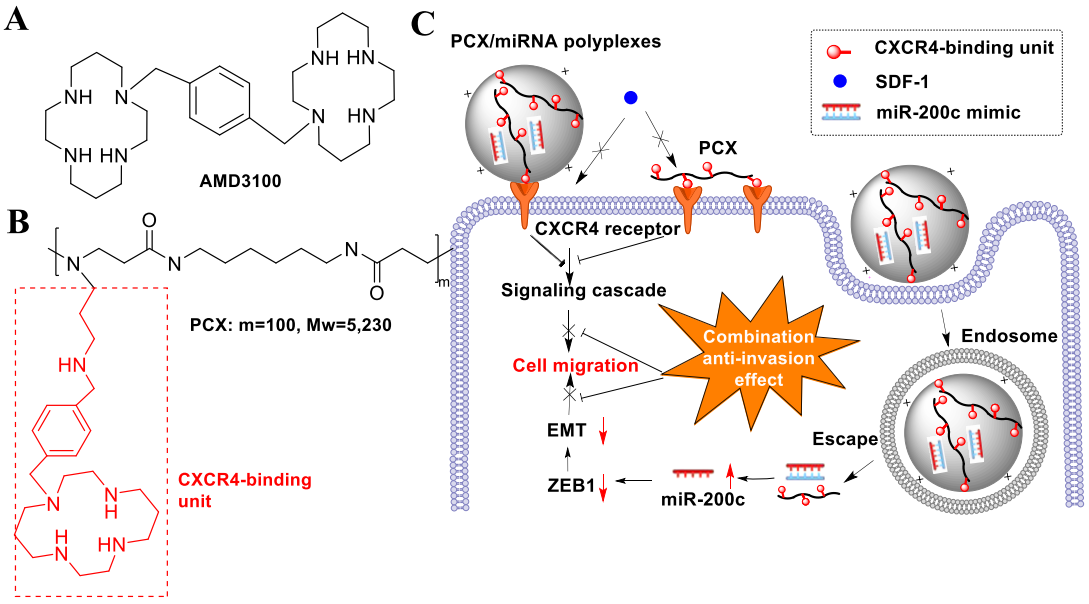

Scheme 2.1. Chemical structure of (A) AMD3100 (Plerixafor) and (B) PCX. (C) Mechanism of action of PCX/miR-200c polyplexes.

2.2 Materials and methods

2.2.1 Materials

Dulbecco's modified Eagle medium (DMEM), Dulbecco's phosphate buffered saline (PBS), and fetal bovine serum (FBS) were from ThermoScientific (Waltham, MA). Cell culture inserts (for 24-well plates, 8.0 μm pores, Translucent PET Membrane, cat# 353097) were purchased from BD Biosciences (Billerica, MA). Human SDF-1α was from Shenandoah Biotechnology, Inc. (Warwick, PA). Oligofectamine was from Invitrogen (Carlsbad, USA) and used as suggested by the supplier. BLOCK-iT™ Fluorescent Oligo (FITC-Oligo) was supplied by ThermoFisher Scientific. MicroRNA-200c mimic (mature microRNA sequence: 5′-UAAUACUGCCGGGUAAUGAUGGA-3′), and negative control miR-NC mimic (mature microRNA sequence: 5′-UCACAACCUCCUAGAAAGAGUAGA -3′) were purchased from Dharmacon (Lafayette, CO). Polymeric CXCR4 antagonist (PCX, M_w = 5230, M_w/M_n = 1.27) was synthesized and characterized as previously described [127]. All other reagents were from Fisher Scientific and used as received unless otherwise noted.

2.2.2 Cell culture

Human malignant intrahepatic cholangiocarcinoma HuCCT1 cell line was kindly provided by Dr. Gregory Gores, Mayo Clinic, Rochester MN. The cell line was derived previously from the malignant ascites fluid from a 56-year-old male patient with intrahepatic cholangiocarcinoma [130]. HuCCT1 cells were grown in high glucose DMEM supplemented with 10% FBS, penicillin (100 U/mL), streptomycin (100 μg/mL), G418 (50 μg/mL), and insulin (0.5 μg/mL) at 37°C with 5% CO_2 in a humidified chamber [130, 131].

2.2.3 Surface expression of CXCR4

HuCCT1 cells were detached with enzyme-free Cell Dissociation Buffer (Thermo Scientific) and suspended in a staining buffer. Cells were stained live with allophycocyanin (APC)-conjugated anti-CXCR4 antibody (Abcam, USA) for 1 h at 4 °C. Isotype-matched negative control was used in the panel of mAb to assess background fluorescence intensity. Samples were analyzed on a BD FACSCalibur flow cytometer (BD Bioscience, Bedford, MA). The results were processed using FlowJo software (Tree Star Inc., Ashland, OR).

2.2.4 Preparation and physicochemical characterization of PCX/microRNA polyplexes

The ability of PCX to condense microRNA was determined by electrophoresis in a 2% agarose gel containing 0.5 μg/mL ethidium bromide (EtBr). PCX/microRNA polyplexes were formed by adding predetermined volume of PCX to a microRNA solution (20 μM in 10 mM HEPES pH 7.4) to achieve the desired w/w ratio and vigorously vortexed for 10 s. Polyplexes were then incubated at room temperature for 30 min before further use. Polyplexes prepared at different PCX-to-microRNA weight ratios were loaded (20 μL of the sample containing 1.0 μg of microRNA) and run for 30 min at 100 V in 0.5×Tris/Borate/EDTA buffer. The gels were visualized under UV illumination on a KODAK Gel Logic 100 imaging system. MicroRNA release from polyplexes was analyzed by heparin displacement assay. The polyplexes were prepared at a w/w ratio of 12 and incubated with increasing concentrations of heparin for 30 min at room temperature. The samples (20 μL of the sample containing 0.5 μg of microRNA) were then analyzed by agarose gel electrophoresis. Hydrodynamic diameter and zeta potential of the polyplexes were determined by dynamic light scattering (DLS) using a ZEN3600 Zetasizer Nano-ZS (Malvern Instruments Ltd., Massachusetts, United States).

2.2.5 Cellular uptake and intracellular trafficking of polyplexes

Flow cytometry analysis was used to study the cellular uptake of polyplexes. HuCCT1 cells (5×10^4) were seeded in 24-well plates and cultured to reach about 50% confluence. The cells were incubated at 37 °C with PCX/FITC-Oligo polyplexes at a FITC-Oligo concentration of 200 nM for 4 h. The cells were then trypsinized, washed with cold PBS, filtered through 35 μm nylon mesh, and subjected to analysis using a BD FACSCalibur flow cytometer (BD Bioscience, Bedford, MA). The results were processed using FlowJo software. Intracellular localization was observed seperately by confocal laser scanning microscope. Cells were cultured on 20 mm glass-bottom cell culture dish (Nest) at 1×10^5 cells/dish. After 24 h, the medium was exchanged with fresh medium and PCX/FITC-Oligo polyplexes were added (200 nM FITC-Oligo). After incubation for 4 h, the cells were washed twice with PBS and stained with LysoTracker® Red DND-99 (Life Technology, USA) for 30 min, fixed with 4% paraformaldehyde for 10 min, and stained with Hoechst 33258 for 10 min. The cells were rinsed 3 times with PBS and visualized by LSM 710 Laser Scanning Microscope (Zeiss, Jena, Germany).

2.2.6 Quantitative real-time PCR (qRT-PCR)

The expression levels of miR-200c were evaluated by TaqMan qRT-PCR. mirVana™ miRNA Isolation Kit (Ambion™, USA) was used for total RNA extraction from cultured cells. 10 ng of total RNA was converted into cDNA using specific primers for miR-200c (or the internal control Z30 (Applied Biosystems, Foster City, CA)) and the TaqMan microRNA reverse transcription kit (Applied Biosystems). qRT-PCR was performed using TaqMan Universal Master Mix II, No AmpErase UNG (2×) and specific primers for miR-200c or Z30 (Applied Biosystems, Foster City, CA) on a Rotor-Gene Q instrument (QIAGEN) according to the manufacturer's instructions. MicroRNA expression levels were expressed relative to the internal control according to the comparative threshold cycle (Ct) method.

2.2.7 Western blot

Cultured cells were lysed with RIPA Lysis buffer by incubation on ice for 10 min. After centrifugation at 12,000 g for 10 min, the supernatants were collected and the concentrations of proteins were quantified by the BCA protein assay kit (Promega, USA). The protein samples were denatured by boiling for 5 min, loaded onto 10% SDS-PAGE gel for electrophoresis (at 120 V for 2 h), and then transferred (at 300 mA for 1 h) to a nitrocellulose membrane. After blocking with 5% non-fat dried milk at room temperature for 1 h, the membrane was incubated overnight at 4 °C with ZEB1 rabbit monoclonal antibody (Cell Signaling Technology, USA), then washed and incubated with the secondary anti-rabbit IgG HRP-linked Antibody (Cell Signaling Technology, USA) for 1 h. Finally, membranes were again washed and visualized using Pierce™ ECL Western Blotting Substrate (Thermo Scientific, USA). Quantification of western blot bands was performed using ImageJ software (National Institutes of Health, Bethesda, MD), and the data were expressed as relative ZEB1 level compared with untreated cells.

2.2.8 Wound healing assay

HuCCT1 cells (2×10^5) were seeded into 6-well plates and cultured in complete DMEM to reach about 50% confluence. Cells were then treated with PCX/miR-200c polyplexes (w/w=12) containing 200 nM miR-200c for 4 h. The polyplex solution was then removed and replaced with fresh medium. Oligofectamine/microRNA lipoplexes were transfected into cells according to the manufacturer's protocol. When the cells reached confluence at 48 h post-transfection, an artificial wound was created in the monolayer with a sterile plastic 1 mL micropipette tip. Next, the cell monolayers were rinsed gently with PBS and further incubated. Pictures of the wounds were taken using a phase-contrast microscope at different time points.

2.2.9 Transwell migration assay

HuCCT1 cells (2×10^5) were seeded into 6-well plates and cultured in complete DMEM to reach 50% confluence. The cultured cells were subsequently treated with

PBS, Oligofectamine/miR-NC, Oligofectamine/miR-200c, PCX/miR-NC, PCX/miR-200c at microRNA concentration of 200 nM. After 48 h incubation, the cells were trypsinized and suspended in medium without serum. Subsequently, 5×10^4 cells were seeded in the top chambers in 300 µL of serum-free medium and 500 µL of complete medium containing 10% FBS was added to the lower transwell chambers. After 24 h, the non-migrated cells in the top chamber were removed with a cotton swab. The migrated cells were then fixed and stained by dipping the inserts into staining Diff-Quick solution. The images were taken by EVOS xl microscope. Three 20× visual fields were randomly selected for each insert and each group was conducted in triplicate.

2.2.10 Cytotoxicity

Toxicity of the polyplexes was evaluated by Cell Titer Blue assay in HuCCT1 cells. The cells were plated in 96-well microplates at a density of 5,000 cells/well. After 24 h, the cultured cells were treated with PBS, Oligofectamine/miR-NC, Oligofectamine/miR-200c, PCX/miR-NC, PCX/miR-200c at microRNA concentration of 200 nM. After further 48 h incubation, the medium was removed and replaced with a mixture of 100 µL serum-free media and 20 µL of CellTiter-Blue reagent (CellTiter-Blue® Cell Viability Assay, Promega). After 2 h incubation, the Fluorescence (560/590nm) was measured on Synergy 2 Microplate Reader (BioTek, VT). The relative cell viability (%) was calculated as $[\text{Fluorescence}]_{\text{sample}}/[\text{Fluorescence}]_{\text{untreated}} \times 100\%$.

2.2.11 Statistical analysis

Data are presented as the mean ± SD. The statistical significance was determined using ANOVA followed by Bonferroni *post hoc* correction with $p < 0.05$ as the minimal level of significance.

2.3 Results and discussion

2.3.1 CXCR4 expression and CXCR4-mediated migration in HuCCT1 cells

Surface expression of CXCR4 in HuCCT1 cells was confirmed by flow cytometry (**Figure 2.1A**). Over 36% of the HuCCT1 cells were CXCR4-positive with enhanced fluorescence intensity per cell. We then assessed the involvement of CXCR4 in the migration of the cells. A migration assay was performed to test whether SDF-1 induced migration of HuCCT1 cells and whether this migration could be inhibited by CXCR4 antagonists. As shown in **Figure 2.1B**, substantially increased migration across the transwell insert membrane was observed in HuCCT1 cells stimulated with the chemoattractant SDF-1. In agreement with previous reports in other cholangiocarcinoma cells, the cell migration could be significantly inhibited by CXCR4 antagonist AMD3100 [119].

2.3.2 Preparation and physicochemical characterization of PCX/microRNA polyplexes

The ability of PCX to form polyplexes with microRNA was first evaluated by agarose gel electrophoresis. As shown in **Figure 2.2A**, PCX was able to fully condense microRNA above a PCX/microRNA (w/w) ratio of 2. PCX condensation of the microRNA was observed already at low w/w ratios (0.5-1) as indicated by the smear of the ethidium bromide stained microRNA and as strong fluorescence in the starting well of the gel. At higher PCX/microRNA w/w ratios (above 2), condensed microRNA was completely protected from ethidium bromide binding and no fluorescence signal was observed. The stability of the PCX/microRNA polyplexes against dissociation was then determined by heparin displacement assay (**Figure 2.2B**). For PCX/microRNA polyplexes prepared at w/w 12, heparin was able to dissociate the polyplexes and release microRNA above 200

μg/mL heparin. Hydrodynamic size and zeta-potential of PCX/microRNA polyplexes prepared at various w/w ratios were measured by DLS. Polyplexes with all the tested w/w ratios exhibited size in a narrow range from 160 to 180 nm with polydispersity indexes <0.2 (**Figure 2.2C**). The size distribution of polyplexes showed a log-transformed normal distribution (**Figure 2.2D**). As expected, increased w/w ratio used in the preparation of the polyplexes resulted in an increase of the zeta potential (**Figure 2.2E**).

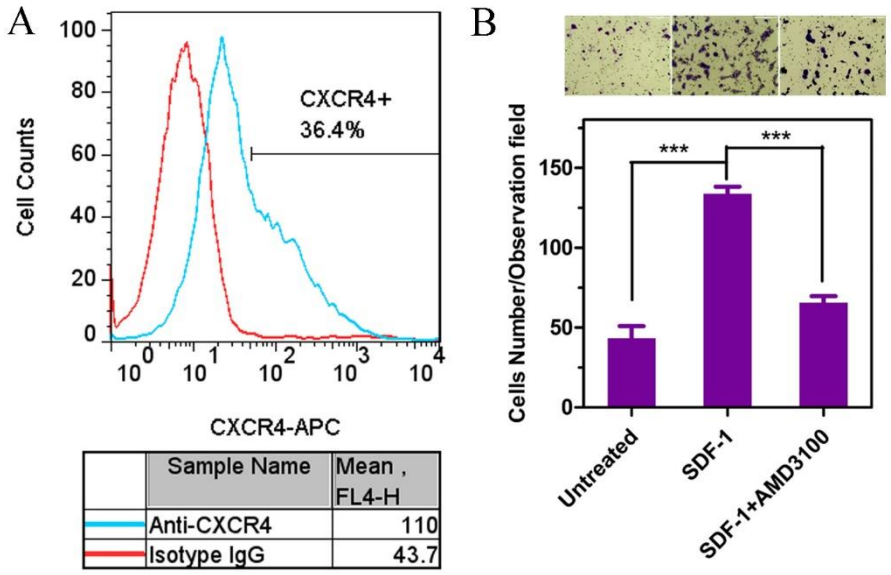

Figure 2.1. Characterization of the CXCR4 status of HuCCT1 cells. (A) Flow cytometric histograms show CXCR4 expression on HuCCT1 cell surface. The percent of CXCR4-positive cells and mean fluorescence intensity were analyzed using FlowJo software. (B) Inhibition of CXCR4-mediated cell migration. HuCCT1 cells were treated with AMD3100 (300 nM) and allowed to migrate through transwell membranes upon stimulation with SDF-1 for 24 h. Three 20× imaging areas were randomly selected for each insert and each group was conducted in triplicate. Data are shown as mean ± SD (n = 3). ***$p < 0.001$.

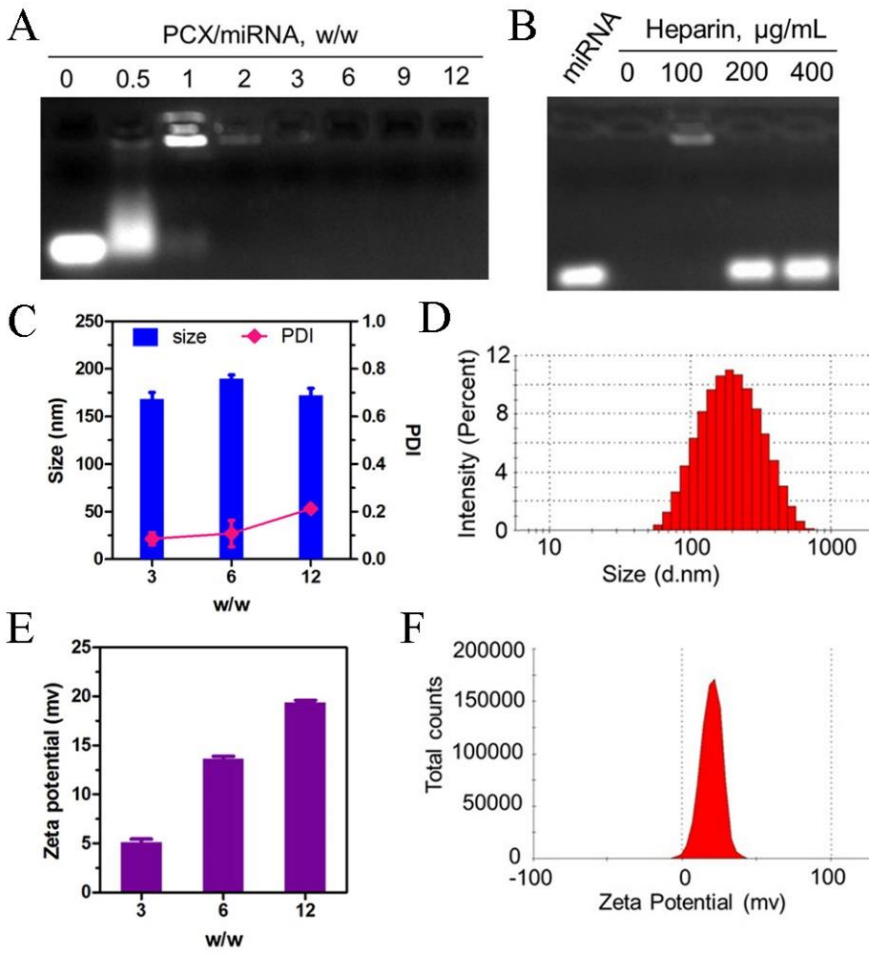

Figure 2.2. Physicochemical characterization of PCX/microRNA polyplexes. (A) MicroRNA condensation by PCX in 10 mM HEPES buffer (pH 7.4) using agarose gel electrophoresis. (B) Heparin induced microRNA release from the polyplexes. Polyplexes were prepared at w/w 12 and incubated with increasing concentrations of heparin. (C) Hydrodynamic size of PCX/microRNA polyplexes. (D) Size distribution of PCX/microRNA (w/w=12). (E) Zeta-potential of PCX/microRNA polyplexes. (F) Zeta-potential of PCX/microRNA (w/w=12) as determined by dynamic light scattering. Data shown as mean ± SD (n = 3).

2.3.3 Cellular uptake and intracellular trafficking

To study the cellular uptake and intracellular trafficking of the polyplexes, we used a fluorescently labeled FITC-Oligo (200 nM) instead of microRNA in the preparation of the polyplexes. HuCCT1 cells were treated with PCX/FITC-Oligo for 4 h before flow cytometry analysis. As shown in **Figure 2.3A**, PCX polyplexes exhibited significant cellular uptake in HuCCT1 cells as indicated by the enhanced fluorescence intensity when compared with untreated cells or cells treated with free FITC-Oligo. Increasing the w/w ratios in preparation of the polyplexes resulted in enhanced cell uptake, both in terms of the mean fluorescence intensity per cell (**Figure 2.3B**) and the percentage of cells that have taken up the polyplexes (**Figure 2.3C**). PCX polyplexes prepared at highest tested w/w = 12 showed the highest cell uptake and were thus selected for subsequent studies.

We further evaluated the intracellular trafficking of the PCX polyplexes using confocal microscopy. PCX/FITC-Oligo polyplexes (green) prepared at w/w 12 were incubated with the cells for 4 h. Lysosomes were stained with Lysotracker Red (red) and cell nuclei were stained with Hoechst 33258 (blue). As shown in **Figure 2.3D**, the fluorescence of the FITC-Oligo was distributed mainly in the cytoplasm and no FITC-Oligo signal was found in the cell nucleus. Limited extent of the co-localization of the FITC-Oligo signal with the LysoTracker signal in lysosomes (red) indicated efficient endosomal escape of the PCX polyplexes.

2.3.4 MicroRNA transfection

miR-200c and its negative control miR-NC were used to evaluate the microRNA transfection efficiency of the PCX polyplexes. The levels of miR-200c in HuCCT1 cells were measured using TaqMan qRT-PCR (**Figure 2.4**). PCX polyplexes exhibited high microRNA transfection efficiency, as indicated by a nearly 9,500-fold increase in

intracellular miR-200c levels when polyplexes prepared at w/w=12 were used. Similar to the results of the cell uptake experiment (**Figure 2.3**), increasing the w/w ratio in preparing the polyplexes resulted in significantly enhanced transfection efficiency.

Having confirmed the ability of PCX to effectively deliver miR-200c to the HuCCT1 cells, we then evaluated the effect of the delivered miR-200c on the target intracellular pathway. We used Western blot to analyze the cellular levels of one of the downstream targets of miR-200c, namely the zinc finger E-box-binding homeobox 1 (ZEB1). ZEB1 is an inducer of the epithelial-to-mesenchymal transition (EMT) in cancer cells and its overexpression is associated with cancer cell migration and invasion [73, 132, 133]. As shown in **Figure 2.5**, delivery of miR-200c using PCX polyplexes resulted in a significant decrease (46.3%) in cellular ZEB1 protein levels in the HuCCT1 cells when compared with the control PCX/miR-NC polyplexes. This finding confirms that the miR-200c was delivered by the PCX polyplexes into the cytoplasm and efficiently released in its active state to successfully downregulate the target ZEB1 protein.

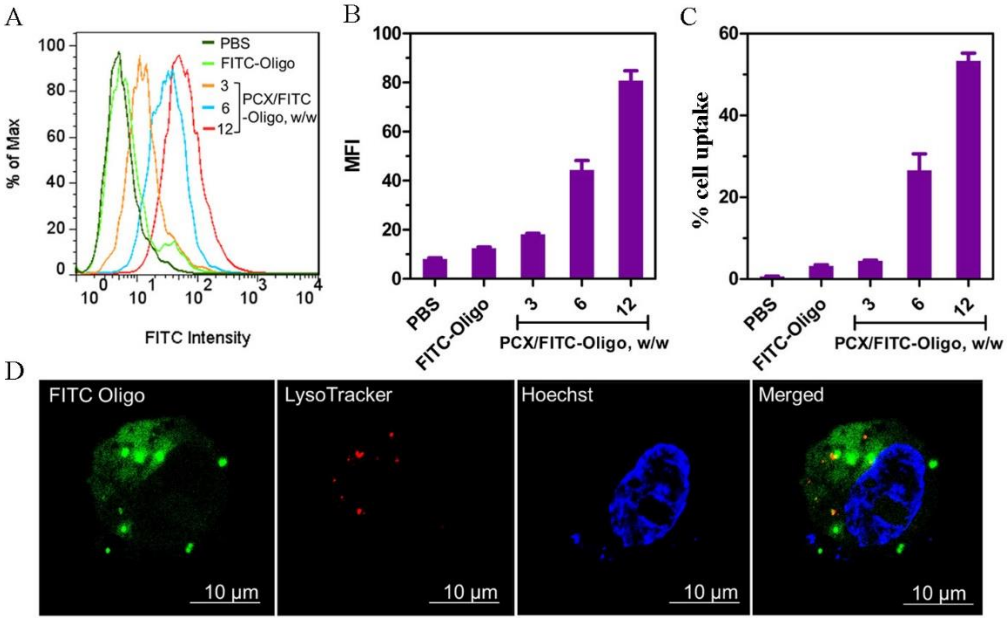

Figure 2.3. Cellular uptake and intracellular trafficking of PCX polyplexes. (A) Overlayed histogram of flow cytometry analysis of cells treated with PCX/FITC-Oligo polyplexes at various w/w ratio (200 nM FITC-Oligo). Quantification of cellular uptake is shown by (B) mean fluorescence intensity (MFI) and (C) % cell uptake. Data are shown as mean ± SD (n = 3). (D) Intracellular trafficking of PCX/FITC-Oligo in HuCCT1 cells by CLSM after 4 h incubation.

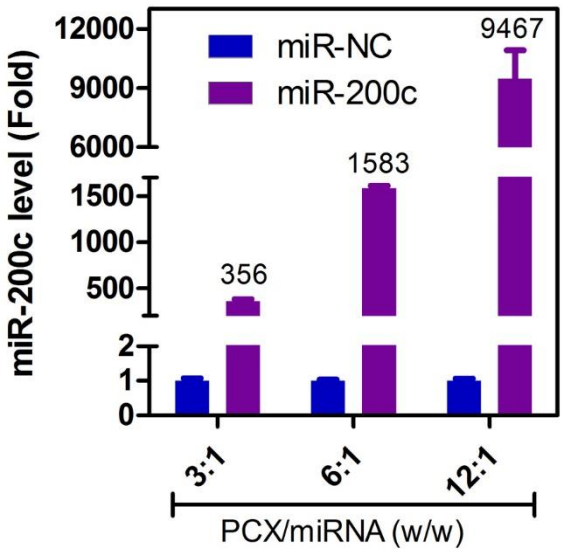

Figure 2.4. Transfection activity of PCX/microRNA polyplexes. miR-200c level was detected by TaqMan qRT-PCR in HuCCT1 cells. Data are shown as mean ± SD (n = 3).

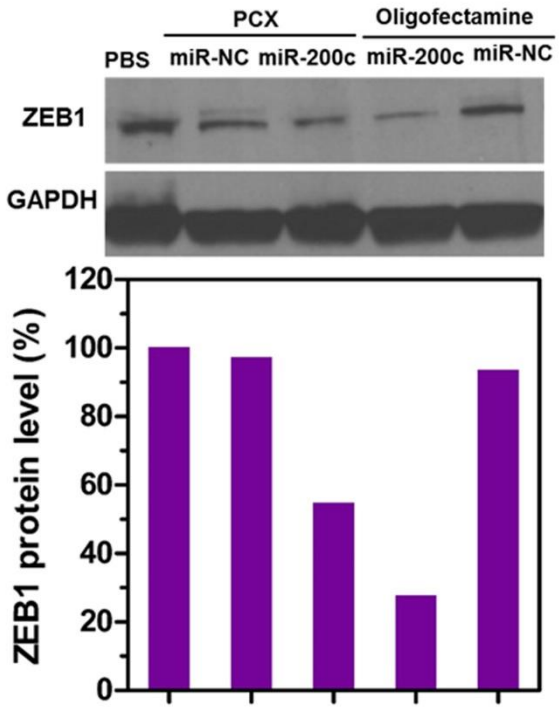

Figure 2.5. Effect of miR-200c delivery on the expression of ZEB1 protein. Quantification of Western blot bands was performed using ImageJ software and the data are expressed as relative ZEB1 levels relative to untreated cells.

2.3.5 Cell migration

After confirming the ability of the PCX polyplexes to deliver functional microRNA to the human cholangiocarcinoma cells, we evaluated the cooperative effect of the inhibition of ZEB1 by miR-200c and CXCR4 inhibition by PCX on the migration of the cells. Before proceeding, we first confirmed that the selected polyplex formulations have no significant adverse effect on cell viability that could negatively affect their migratory properties. As shown in **Figure 2.6**, the cells treated with all the PCX polyplexes as well as the control Oligofectamine lipoplexes exhibited nearly 100% viability after 48 h incubation, indicating no adverse effects on cell proliferation. The migration of the cancer cells was then assessed using a wound healing assay and a transwell cell migration assay.

Wound healing assay was conducted to study the combined inhibitory activity of PCX/miR-200c polyplexes on migration of HuCCT1 cells. The cells were treated with PCX/miR-200c polyplexes and an artificial wound was created 48 h post-transfection. The healing status of the wound, which represents the extent of cell migration, was measured after 24 and 48 h. As shown in **Figure 2.7**, the untreated (PBS) wound reached nearly complete closure after 48 h. The cells treated with control PCX/miR-NC exhibited significant inhibition of wound healing (56% closure) after 48 h, which is consistent with the CXCR4 antagonistic activity of PCX and its effect on cell migration. The combination treatment with PCX/miR-200c polyplexes further enhanced the extent of inhibition (40% closure) due to the cooperative activity of the CXCR4 antagonism of PCX and the effect of miR-200c on ZEB1. ZEB1 has previously been implicated in the migration-inhibitory effect of miR-200c, suggesting ZEB1 may be a functional mediator of this effect in HuCCT1 cells. As expected, no inhibition of wound healing was observed when the control miR-NC was delivered using Oligofectamine. When used to deliver

miR-200c, Oligofectamine lipoplexes exhibited partial inhibition of wound closure (61% closure).

To further confirm the cooperative activity of PCX and miR-200c on the inhibition of cancer cell migration, transwell assay was also performed. HuCCT1 cells were transfected with PCX/miR-200c polyplexes as before and 10% FBS was applied to the lower chamber as the chemoattractant to induce the transwell cell migration. As shown in **Figure 2.8**, the migration of HuCCT1 cells was significantly inhibited following treatment with control Oligofectamine/miR-200c. Treatment with another control, PCX/miR-NC, resulted in marked migration inhibition due to the CXCR4 antagonism of PCX. Combined treatment with PCX/miR-200c achieved the highest inhibition level of cell migration (~81%) among all the tested formulations, confirming the cooperative effect of PCX and miR-200c.

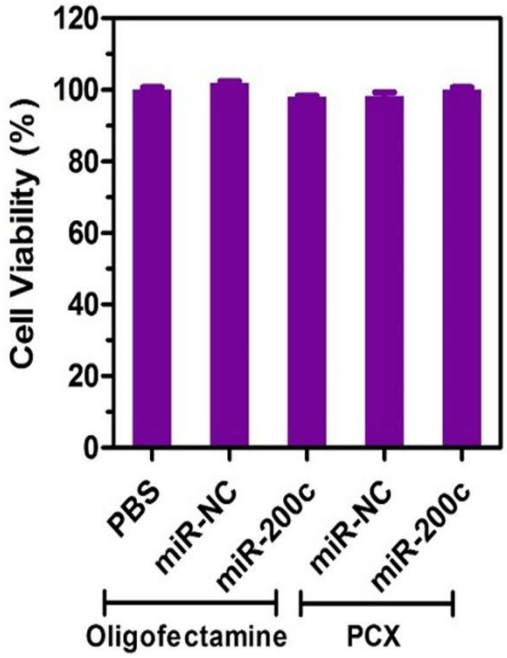

Figure 2.6. Cell viability was measured using Cell Titer Blue assay in HuCCT1 cells. HuCCT1 cells were treated with PCX polyplexes or control Oligofectamine complexes for 48 h. Data are shown as mean ± SD (n = 3).

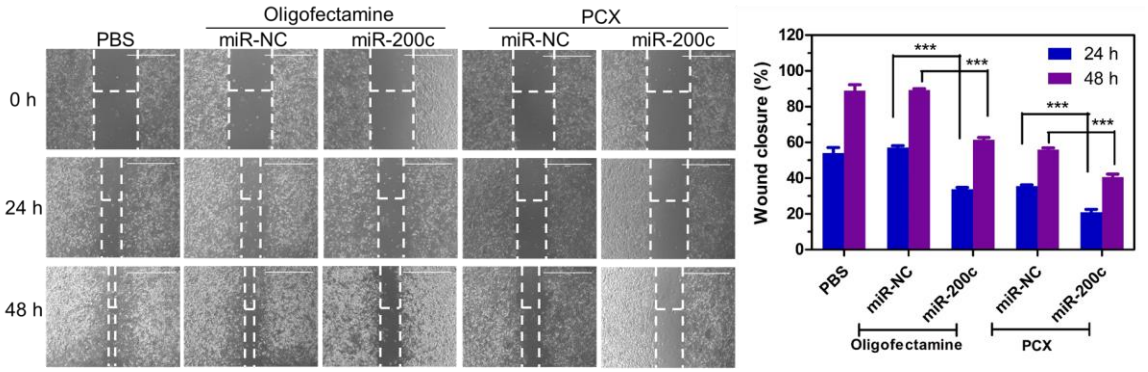

Figure 2.7. Inhibition of wound healing. Cells were treated with formulations for 48 h. Then an artificial wound was created in the monolayer with a 1 mL pipette tip. 4× imaging areas of the wounds were taken using a microscope at different time points. Wound closure was expressed as % initial wound size (mean ± SD; n = 3) (Scale bar = 1000 μm). Data are shown as mean ± SD (n = 3). ***$p < 0.001$.

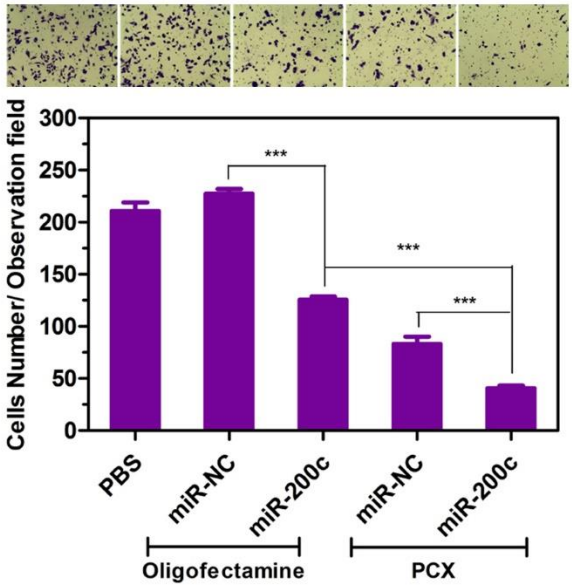

Figure 2.8. Inhibition of cancer cell migration. HuCCT1 cells were transfected with Oligofectamine lipoplexes or PCX polyplexes for 48 h and then allowed to migrate through Transwell upon stimulation with 10% FBS for 24 h. Three 20× imaging areas were randomly selected for each insert and each group was conducted in triplicate. Data are shown as mean ± SD (n = 3). ***$p < 0.001$.

2.4 Conclusion

In this study, CXCR4-inhibiting polycation (PCX) was used to deliver miR-200c mimic with the goal of improving the inhibition of cholangiocarcinoma cell migration. The results show that PCX can inhibit the cancer cell migration due to its CXCR4 antagonism. The ability of PCX to form polyplexes with nucleic acids was used for simultaneous delivery of miR-200c mimic into cells. The delivery of miR-200c resulted in reduced expression of the EMT inducer ZEB1. The combination treatment consisting of PCX and miR-200c resulted in cooperative anti-migration activity, most likely by coupling the CXCR4 axis blockade with EMT inhibition in the cholangiocarcinoma cells. Our results provide a promising strategy for a combination therapy involving multiple migration pathways in metastatic cholangiocarcinoma.

Chapter 3 – Cholangiocarcinoma therapy with nanoparticles that combine downregulation of microRNA-210 with inhibition of cancer cell invasiveness

Please note that part of the content of this chapter was published in Theranostics (Xie, Wang et al, 2018) [134]. As the first author, I performed all the experiments in the paper except the synthesis of PCX by Yu Hang and Lee Jaramillo. Prof. Oupický and co-authors helped to interpret the data and prepare the manuscript. All the authors agreed with including their work in this dissertation.

3.1 Introduction

Cholangiocarcinoma (CCA) is an aggressive cancer of the biliary duct system. CCA is a deadly disease with dismal prognosis as evident from its low 10% five-year survival rates. Surgery is the only curative option for CCA. However, over 70% of CCA patients are diagnosed at late stage and not eligible for surgical resection [135, 136]. The high mortality of CCA is attributed to the early invasion and widespread metastasis. No effective treatment options exist for metastatic CCA [137]. Advanced CCA is currently treated with a combination of gemcitabine (GEM) and cisplatin (CDDP). Unfortunately, the therapeutic outcome of systemic GEM/CDDP treatment is poor due to drug resistance [138, 139]. These therapeutic challenges highlight the urgent need to develop new therapeutics to inhibit metastasis and reverse drug resistance in CCA therapy.

CXCR4 overexpression has been found in more than 20 major human cancer types, including CCA [23, 140]. The upregulation of CXCR4 is highly dependent on multiple transcription factors, growth factors, and hypoxia-inducible factors. The hypoxic tumor microenvironment can induce CXCR4 based on activation of the hypoxia-inducible factor-1α (HIF1α) and transcript stabilization [89]. The binding of CXCL12 to CXCR4

activates intracellular signaling to promote migration and invasion of cancer cells. CXCR4 then facilitates the metastasis of the primary tumor cells to these sites where CXCL12 is highly expressed [11, 141]. Inhibition of the signaling pathway with CXCR4 antagonists decreases the motility and invasion of CCA cells [119, 142]. Inhibition of CXCR4 also can reverse drug resistance and improve chemotherapy, as documented by chemosensitizing effect of a CXCR4 antagonist AMD3100 to GEM in human CCA cells [17, 143]. Several studies reported that CXCR4 inhibition reduced the stemness of cancer cells to overcome drug resistance [144, 145]. Current evidence strongly supports the potential of CXCR4 inhibition to reverse drug resistance and inhibit metastasis in CCA.

MiRNAs can act as tumor suppressors or oncogenes and play an important role in tumorigenesis, tumor growth, angiogenesis, and metastasis [146]. A growing number of studies confirm the important role of miR-25, miR-34a, and let-7c in CCA formation and progression [106, 107, 147, 148]. Recent evidence already suggests that miRNA therapy can inhibit CCA growth, metastasis, and improve survival in animal models [149-151]. Hypoxia in CCA induces the upregulation of miR-210, which helps the cancer cells to adapt to the hypoxic microenvironment through multiple biological pathways [152, 153]. Oncogenic activity of miR-210 is responsible for cell proliferation, apoptosis, metastasis, DNA repair, cell metabolism, and antitumor drug resistance [93, 154, 155]. Hence, inhibition of miR-210 provides a promising target for the treatment of CCA.

Despite the great potential of miRNAs in metastatic cancer, their clinical translation has been limited by a lack of efficient and safe systemic delivery systems [112, 156]. We have reported on a series of polymeric CXCR4 antagonists (PCX) capable of delivering miRNA, siRNA, and DNA [19, 59, 60, 157]. PCX simultaneously inhibit cancer cell invasion by CXCR4 axis blockade and deliver nucleic acids into

various cancer cells for improved anticancer effect. PCX were synthesized from AMD3100 and modified with cholesterol to improve the stability of their nanoparticles for better systemic delivery [21, 58]. Due to the key roles of CXCR4 and miR-210 in CCA, we hypothesized that combining inhibition of CXCR4 by PCX and inhibition of hypoxia-inducible miR-210 would cooperatively enhance the therapy of CCA through reducing invasiveness, inducing cell killing and overcoming drug resistance (**Scheme 3.1**). To test this hypothesis, we used PCX modified with cholesterol to prepare PCX/anti-miR-210 nanoparticles and to evaluate their delivery activity and anticancer efficacy in CCA both *in vitro* and *in vivo*.

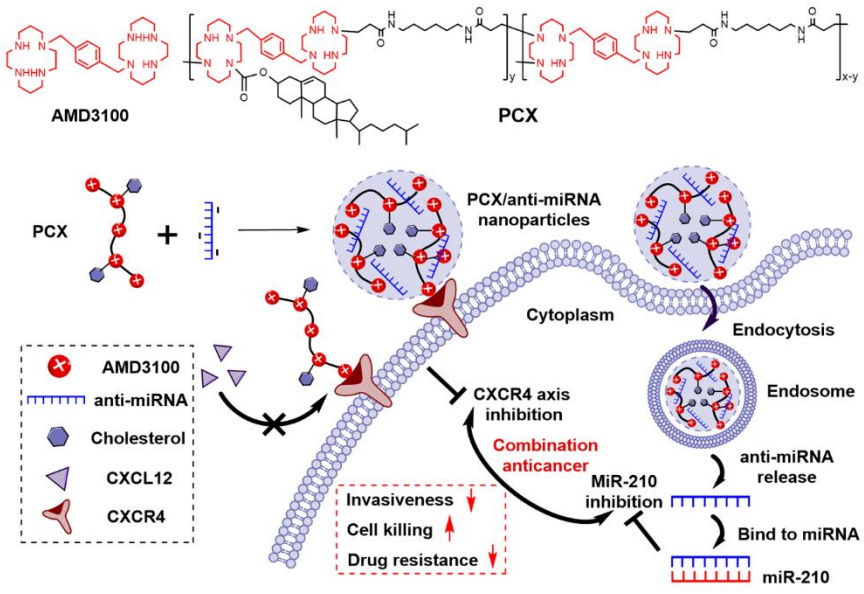

Scheme 3.1. Proposed mechanism of action of PCX/anti-miR-210 nanoparticles.

3.2 Materials and methods

3.2.1 Materials

Cholesterol-modified polymeric CXCR4 inhibitors PCX (Mw = 16.7 kDa, Mw/Mn = 1.9, cholesterol wt% =16.8%) was synthesized and characterized as previously described [58]. Succinimidyl ester of Alexa Fluor® 647 carboxylic acid was from Life Technologies (Eugene, OR). AlexaFluor 647 labeled PCX polymers (AF647-PCX) were produced according to manufacturer's instructions and purified by dialysis to remove unreacted dye. AMD3100 was from Biochempartner (Shanghai, China). Dulbecco's modified Eagle medium (DMEM), Dulbecco's phosphate buffered saline (PBS), and fetal bovine serum (FBS) were from Thermo Scientific (Waltham, MA). Hsa-miR-210-3p-Hairpin Inhibitor (anti-miR-210, mature miRNA sequence: 5′-CUGUGCGUGUGACAGCGGCUGA-3′), negative control miR-NC inhibitor (anti-miR-NC, mature miRNA sequence: 5′-UCACAACCUCCUAGAAAGAGUAGA-3′), and carboxyfluorescein (FAM) labeled FAM-anti-miRNA were purchased from Dharmacon (Lafayette, CO). Cell culture inserts (for 24-well plates, 8.0 μm pores, Translucent PET Membrane, cat# 353097) were purchased from BD Biosciences (Billerica, MA). Real-time (RT)-PCR primers were purchased from Invitrogen (Carlsbad, CA). Allophycocyanin (APC) mouse anti-human CXCR4 antibody and APC mouse lgG2a, κ isotype controls were from BD Biosciences (San Jose, CA). All other reagents were from Fisher Scientific and used as received unless otherwise noted.

3.2.2 Cell culture

Human malignant cholangiocarcinoma Mz-ChA-1 cell line was kindly provided by Dr. Gregory Gores, Mayo Clinic, Rochester, MN. Mz-ChA-1 cells were grown in high-glucose DMEM supplemented with 10% FBS, penicillin (100 U/mL), streptomycin (100

μg/mL), G418 (50 μg/mL), and insulin (0.5 μg/mL) at 37 °C with 5% CO2 in a humidified chamber. To induce hypoxia, cells were incubated in an atmosphere of 2% O2, 5% CO2, and 93% N2 at 37 °C.

3.2.3 Cellular surface expression of CXCR4

Mz-ChA-1 cells were detached with enzyme-free Cell Dissociation Buffer (Thermo Scientific) and suspended in a staining buffer. Cells were stained live with allophycocyanin (APC)-conjugated anti-CXCR4 antibody for 1 h at 4 °C. Isotype matched negative control was used in the panel of mAb to assess background fluorescence intensity. Samples were analyzed on a BD FACS Calibur flow cytometer (BD Bioscience, Bedford, MA). The results were processed using FlowJo software (Tree Star Inc., Ashland, OR).

3.2.4 Analysis of pERK signaling by Western blot

Mz-Cha-1 cells were treated with AMD3100 (300 nM), PCX (3 μg/mL) for 4 h followed by 20 min incubation with SDF-1 (100 ng/mL). Then, cells were lysed by RIPA Lysis buffer. After centrifugation at 12,000 g for 10 min, the supernatants were collected and the concentrations of proteins were quantified by the BCA protein assay kit (Promega, USA). The protein samples were denatured by boiling for 5 min, loaded onto 10% SDS-PAGE gel for electrophoresis (at 120 V for 2 h), and then transferred (at 300 mA for 1 h) to a nitrocellulose membrane. After blocking with 5% non-fat dried milk at room temperature for 1 h, the membrane was incubated overnight at 4 °C with pERK rabbit monoclonal antibody (Cell Signaling Technology, USA), then washed and incubated with the secondary anti-rabbit IgG HRP-linked Antibody (Cell Signaling Technology, USA) for 1 h. Finally, membranes were again washed and visualized using Pierce™ ECL Western Blotting Substrate (Thermo Scientific, USA). Quantification of

western blot bands was performed using ImageJ software (National Institutes of Health, Bethesda, MD). GAPDH and Erk were used as housekeeping controls. Quantification of Western blot bands was performed using ImageJ software.

3.2.5 FBS-induced transwell migration assay

Mz-ChA-1 cells (2×10^5) were seeded into 6-well plates and cultured in complete DMEM medium. The cultured cells were subsequently treated with AMD3100 (300 nM) or PCX (3 μg/mL). After 48 h of incubation, the cells were trypsinized and suspended in medium without serum. Subsequently, 3×10^4 cells were seeded in the top chambers in 300 μL of serum-free medium and 500 μL of complete medium containing 10% FBS was added to the lower transwell chambers. After 12 h, the nonmigrated cells in the top chamber were removed with a cotton swab. The migrated cells were fixed in 100% methanol and stained with 0.2% Crystal Violet solution for 10 min at room temperature. The images were taken by EVOS xl microscope. Three 20× visual fields were randomly selected for each insert, and each group was conducted in triplicate.

3.2.6 Phospholipid lysophosphatidic acid (LPA)-induced transwell migration assay

Mz-ChA-1 cells (2×10^5) were seeded into 6-well plates and cultured in complete DMEM medium. The cultured cells were subsequently treated with AMD3100 (300 nM) or PCX (3 μg/mL). After 48 h of incubation, the cells were trypsinized and suspended in medium without serum. Subsequently, 6×10^4 cells were seeded in the top chambers in 300 μL of serum-free medium and 500 μL of serum-free medium containing LPA (20 μM) was added to the lower transwell chambers. After 12 h, the nonmigrated cells in the top chamber were removed with a cotton swab. The migrated cells were fixed in 100% methanol and stained with 0.2% Crystal Violet solution for 10 min at room temperature.

The images were taken by EVOS xl microscope. Three 20× visual fields were randomly selected for each insert, and each group was conducted in triplicate.

3.2.7 Preparation and characterization of nanoparticles

PCX/anti-miRNA nanoparticles were prepared by adding predetermined volume of PCX to an anti-miRNA solution (20 μM in 10 mM HEPES pH 7.4) to achieve the desired w/w ratio and vigorously vortexed for 10 s. Nanoparticles were then incubated at room temperature for 20 min before further use. The ability of PCX to condense anti-miRNA was determined by electrophoresis in a 2% agarose gel containing 0.5 μg/mL ethidium bromide (EtBr). Nanoparticles formed at various polycation-to-anti-miRNA weight ratios were loaded (20 μL of the sample containing 0.5 μg of microRNA) and run for 15 min at 100 V in 0.5 × Tris/Borate/EDTA buffer. The gels were visualized under UV illumination with a KODAK Gel Logic 100 imaging system. Hydrodynamic diameter and zeta potential of the nanoparticles were determined by dynamic light scattering (DLS) using a ZEN3600 Zetasizer Nano-ZS (Malvern Instruments Ltd., Massachusetts, USA). Morphology was observed under transmission electron microscopy (TEM, Tecnai G2 Spirit, FEI Company, USA) using NanoVan® negative staining (Nanoprobes, USA). Anti-miRNA release from nanoparticles was analyzed by heparin displacement assay. The nanoparticles (w/w = 2) were incubated with increasing concentrations of heparin for 30 min at room temperature. The samples (20 μL of the sample containing 0.5 μg of anti-miRNA) were then analyzed by agarose gel electrophoresis. For the serum stability test, free anti-miRNA solution and nanoparticles (w/w = 2) solution were incubated with FBS (v:v = 1:1) at 37 °C, respectively. Each sample was collected at a specified time interval (0.5, 1, 2, 4, 8, and 24 h) and analyzed by gel electrophoresis. Prior to gel electrophoresis, nanoparticles solution was pre-treated with heparin to displace anti-miRNA from the nanoparticles.

3.2.8 Cellular uptake and intracellular trafficking of nanoparticles

Flow cytometry analysis was performed to study the cellular uptake of the nanoparticles. Mz-ChA-1 cells (5×10^4) were seeded in 24-well plates. After 24 h growth, the cells were incubated for 4 h with nanoparticles prepared with AF647-PCX and FAM-anti-miRNA (w/w =2, 100 nM FAM-anti-miRNA). The cells were then trypsinized, washed with cold PBS, and subjected to analysis using a BD FACS Calibur flow cytometer (BD Bioscience, Bedford, MA). The results were processed using FlowJo software. Intracellular localization of AF647-PCX/FAM-anti-miRNA was also observed by confocal laser scanning microscopy. Cells were cultured on a 20 mm glass-bottom cell culture dish (Nest) using 1×10^5 cells per dish. After 24 h, the medium was replaced with fresh medium and AF647-PCX/FAM-anti-miRNA nanoparticles were added (100 nM FAM-anti-miRNA). After incubation for 4 h, the cells were washed twice with PBS, stained with Hoechst 33258 for 10 min. The cells were visualized using a LSM 800 Laser Scanning Microscope (Zeiss, Jena, Germany). Moreover, to follow the endosomal release of nanoparticles, AF647-PCX/anti-miRNA nanoparticles were incubated with cells for 4 h. Then, the cells were washed twice with PBS and stained with LysoTracker Red DND-99 (Life Technology, USA) for 30 min. Finally, the cells were rinsed three times with PBS and visualized with confocal microscope.

3.2.9 Quantitative real-time polymerase chain reaction (qRT-PCR)

Cells were seeded in 12-well plates at 1×10^5 cells per well 24 h prior to treatment. Then, the cells were incubated with the nanoparticles containing anti-miRNA (100 nM) in 1 mL of medium for 48 h. The expression levels of miR-210 were evaluated by TaqMan qRT-PCR. The mirVana miRNA Isolation Kit (Ambion, USA) was used for total RNA extraction from cultured cells. 10 ng of total RNA was converted into cDNA using specific primers for miR-210 (or the internal control Z30, Applied Biosystems,

Foster City, CA) and the TaqMan microRNA reverse transcription kit (Applied Biosystems). qRT-PCR was performed using TaqMan Universal Master Mix II, No AmpErase UNG (2×) and specific primers for miR-210 or Z30 (Applied Biosystems, Foster City, CA) on a Rotor-Gene Q instrument (QIAGEN) according to the manufacturer's instructions. MiRNA expression levels were expressed relative to the internal control according to the comparative threshold cycle (Ct) method.

3.2.10 Apoptosis

Firstly, apoptosis was analyzed using the Annexin V-FITC/PI Apoptosis Detection Kit (BioLegend, USA). Briefly, cells were seeded in 12-well plates at a density of 1×10^5 cells per well 24 h prior to treatment. The cells were incubated with the nanoparticles containing anti-miRNA (100 nM) in 1 mL of medium for 48 h. The Annexin V-FITC apoptosis detection was performed using flow cytometry in accordance with the manufacturer's protocol, and the data were processed using FlowJo. Apoptosis percentage was also quantified by nuclear morphology and visualized by treatment with the fluorescent DNA-binding dye, DAPI (4′, 6-diamidine-2′-phenylindole dihydrochloride). Briefly, cells were stained with 2 μg/mL of DAPI for 30 minutes at 37 °C. Apoptotic nuclei (condensed, fragmented) were counted and presented as a percent of total nuclei. At least 100 cells were counted per well and experiments were performed in triplicate. Caspase 3/7 activity was measured by enzymatic fluorophore release (Apo-One) according to the manufacturer's protocol (Promega).

3.2.11 Cytotoxicity of polymers and nanoparticles

Cytotoxicity of PCX and nanoparticles was tested in Mz-ChA-1 cells by Cell Titer Blue assay. Cells were plated in 96-well microplates at a density of 5000 cells/well. After 24 h, cells were incubated with the PCX for another 48 h prior to measuring cell viability.

Toxicity of the nanoparticles carrying anti-miRNA was also evaluated. Briefly, cells were plated in 96-well microplates at a density of 5000 cells/well. After 24 h, cells were incubated with the nanoparticles containing miRNA (100 nM) for another 48 h prior to measuring cell viability. The medium was then removed and replaced with a mixture of 100 µL serum-free media and 20 µL of CellTiter-Blue reagent (CellTiter-Blue Cell Viability Assay, Promega). After a 2 h incubation, fluorescence (560/590 nm) was measured on a SpectraMax iD3 Multi-Mode Microplate Reader (Molecular Devices, CA). The relative cell viability (%) was calculated as [I]treated/[I]untreated × 100%.

3.2.12 Colony formation

Cells were transfected with nanoparticles containing miRNA (100 nM) for 4 h. Then, transfected cells were reseeded in 6-well plates (200 cells per plate). Cells were allowed to grow for 14 days. Cells were fixed in 100% methanol and stained with 0.2% Crystal Violet solution for 10 min. Finally, plates were washed with distilled water and photographed. Number of colonies in each well were quantified.

3.2.13 Aldefluor activity

Cells were transfected with nanoparticles containing miRNA (100 nM) for 4 h and then replaced with fresh medium for incubation for 48h. Then, Aldefluor kit (Stem Cell Technologies, Durham, NC, USA) was used to analyze ALDH enzymatic activity according to the manufacturer's instructions. Cells were suspended in Aldefluor assay buffer containing ALDH substrate (BODIPY-aminoacetaldehyde) and incubated for 30 min at 37 °C. As the negative control, cells were treated with 50 mM diethylaminobenzaldehyde (DEAB) inhibitor before adding ALDH substrate. The cells were subjected to analysis using a BD FACSCalibur flow cytometer (BD Bioscience, Bedford, MA).

3.2.14 Tumor spheroid formation

Cells were transfected with nanoparticles containing miRNA (100 nM) for 4 h and then cells were dissociated and plated in ultralow attachment 6-well plates (Corning, New York) at a density of 5000 viable cells per well. Cells were cultured in serum-free DMEM/F12 medium containing 5 μg/mL insulin (Sigma-Aldrich, St. Louis, MO, USA), 0.4% bovine serum albumin (Sigma-Aldrich, St. Louis, MO, USA), 10 ng/mL basic fibroblast growth factor (Invitrogen, Waltham, MA, USA), and 20 ng/mL human recombinant epidermal growth factor (Invitrogen, Waltham, MA, USA) and observed after 14 days.

3.2.15 Chemotherapy sensitization

Cell viability assay was performed to study the activity of nanoparticles to sensitize cells to chemotherapy. Cells were seeded in 96-well microplates at a density of 5000 cells/well. After 24 h, cells were incubated with indicated concentrations of gemcitabine/cisplatin (GEM/CDDP, w/w=10), PCX/anti-miR-NC (100 nM) plus GEM/CDDP and PCX/anti-miR-210 (100 nM) plus GEM/CDDP, respectively. After incubation for another 48 h, CellTiter-Blue assay were performed to measure cell viability. The IC50 were calculated in GraphPad Prism using a built-in dose–response analysis as the total drugs (Gemcitabine plus cisplatin) concentration that achieves 50% growth inhibition relative to untreated cells (n = 3). Moreover, synergy calculations were performed to study the combinational effects between PCX/anti-miR-210 and GEM/CDDP. Briefly, cells were seeded in 96-well microplates at a density of 5000 cells/well. After 24 h, cells were incubated with indicated concentrations of gemcitabine/cisplatin (GEM/CDDP, w/w=10), PCX/anti-miR-210 and PCX/anti-miR-210 plus GEM/CDDP, respectively. After incubation for another 48 h, CellTiter-Blue assay were performed to measure cell viability. The data from cell viability assays were

analyzed using Combenefit software (Cancer Research UK Cambridge Institute). The "Mapped Surface" views (Bliss model) were selected as graphical outputs for the synergy distribution.

3.2.16 CCA xenograft tumor model

All animal experiments followed a protocol approved by the University of Nebraska Medical Center Institutional Animal Care and Use Committee. Animals were placed in a facility accredited by the Association for Assessment and Accreditation of Laboratory Animal Care upon arrival. Male athymic nu/nu mice (6 weeks) were purchased from Charles River Laboratories. The xenograft tumor model was generated by subcutaneous injection of 5×10^6 Mz-ChA-1 cells in 1:1 mixture of PBS/Matrigel (100 µL) into the flank region of the mouse. Tumor hypoxia was evaluated using pimonidazole hydrochloride (60 mg/kg) given by intraperitoneal injection. The mice were sacrificed 30 min after the pimonidazole injection, the tumors were excised, and frozen tumor sections were stained with FITC-Mab1 antibody using the Hypoxyprobe-1 Plus Kit (Hypoxyprobe Inc., Burlington) and imaged with the confocal microscope.

3.2.17 Biodistribution

Xenograft tumor mice (~300 mm^3) were injected with AF647-PCX/FAM-miRNA nanoparticles (w/w=2, 2.4 mg/kg AF647-PCX, 1.2 mg/kg FAM-miRNA) through tail vein. The mice were sacrificed 24 h post administration, and the tumors and major organs were harvested and subjected to ex vivo fluorescence imaging using Xenogen IVIS 200 (Ex = 640 nm, Em = 680 nm). The fluorescence from each organ was analyzed by the instrument software. Then, the isolated tumors were embedded in an OCT compound, cut into 10 µm sections, stained with DAPI, and imaged with the confocal microscope.

3.2.18 *In vivo* therapeutics effect

When the tumor sizes reached about 150-200 mm^3 at days 10 post-tumor inoculation, mice were randomly assigned to 5 groups (n = 5) and injected with PBS, GEM/CDDP, PCX/anti-miR-NC, PCX/anti-miR-210 and PCX/anti-miR-210 + GEM/CDDP, respectively. PCX/anti-miRNA (w/w=2, 2.4 mg/kg PCX, 1.2 mg/kg anti-miRNA) were injected at days 11, 13, 15 and 17 through tail vein. GEM/CDDP (15 mg/kg GEM, 1.5 mg/kg CDDP) were given at days 12 and 16 by intraperitoneal injection. Tumor volume was monitored by measuring the perpendicular size of the tumors using digital calipers. The estimated volume was calculated according to the following formula: tumor volume (mm^3) = 0.5 × length × $width^2$. Body weight of the mice was also recorded. On days 22, mice were sacrificed, and all tumor tissues and major organs were harvested, fixed in 4% paraformaldehyde, sectioned, and stained with H&E. The apoptosis of tumor cells was determined using the Caspase 3 immunohistochemical staining according to the manufacturer's instructions. Blinded histological analysis of the tissues was conducted by a trained pathologist at the UNMC core facility.

3.2.19 Statistical analysis

Data are presented as the means ± SD. The statistical significance was determined using ANOVA followed by Bonferroni post hoc correction with $p < 0.05$ as the minimal level of significance.

3.3 Results and Discussion

3.3.1 The expression of CXCR4 in human CCA cells

We analyzed the expression of CXCR4 in human CCA cells Mz-ChA-1 in normoxic (20% oxygen) and hypoxic (2% oxygen) conditions. The expression of CXCR4 mRNA was quantified with qRT-PCR. Hypoxia increased the CXCR4 expression 5.8-fold when compared with normoxic cells (**Figure 3.1A**). Surface expression of the CXCR4 receptor was then analyzed by flow cytometry (**Figure 3.1B**). The percentage of CXCR4-positive cells increased from 31% under normoxia to 91% in hypoxia. These results confirmed that hypoxia induces the CXCR4 expression in CCA cells. High CXCR4 expression typically leads to increased cell motility, migration and invasion, which leads to enhanced metastasis [158].

3.3.2 Cytotoxicity of polymer PCX

To avoid the effect of PCX cytotoxicity on the migration activity, we carefully selected a safe concentration of PCX. PCX at the concentration of 3 μg/mL showed no cytotoxicity in either normoxia or hypoxia (**Figure 3.2**).

3.3.3 Inhibition of pErk

AMD3100 is a highly specific nM inhibitor of CXCR4. Here, 300 nM of AMD3100 was selected as an effective and safe positive control of CXCR4 inhibitor. To confirm the CXCR4 inhibition activity of PCX in CCA cells, the downstream extracellular-signal-regulated kinase (Erk) signaling pathway of CXCR4 was checked by Western blot analysis. Erk is a main downstream signaling pathway of CXCR4/CXCL12 axis and regulates cell survival, migration and invasion. As shown in **Figure 3.3**, AMD3100 specifically inhibited SDF-1-induced phosphorylation of Erk in Mz-Cha-1 cells. PCX

retained the activity to inhibit pErk in a similar efficiency as AMD3100, which confirmed the CXCR4 inhibiting capability of PCX.

3.3.4 Inhibition of FBS-induced cancer cell migration

The anti-migration activity of PCX was evaluated and compared with a small molecule CXCR4 inhibitor AMD3100. As shown in **Figure 3.4**, hypoxia increased the FBS-induced migration of the CCA cells ~3 fold when compared with normoxic conditions. AMD3100 effectively inhibited the migration under both normoxia (57% inhibition) and hypoxia (63% inhibition). Interestingly, PCX showed better anti-migration activity and almost completely inhibited migration of the CCA cells in both conditions (95 % inhibition in normoxia, 97% inhibition in hypoxia). To further understand why PCX presented such a superior activity, we hypothesized that PCX affected additional signaling pathways involved in cell motility.

3.3.5 Inhibition of LPA-induced cancer cell migration

The bioactive phospholipid lysophosphatidic acid (LPA) and its G-protein-coupled receptors play an important role in cancer migration, invasion and metastasis through regulating GTPases Ras, Rho, and Rac pathways. These LPA-regulated GTPases are normally overexpressed in human CCA and involved in the invasion and metastasis process. Inhibition of LPA signaling represents an effective approach to inhibit CCA cells migration [159-162]. Here, we performed a migration assay using LPA as the chemoattractive agent. As shown in **Figure 3.5**, LPA treatment induced the migration of CCA cells. Hypoxia also increased the LPA-induced migration when compared with normoxic conditions. As expected, AMD3100 failed to inhibit the migration under both normoxia and hypoxia. However, PCX effectively inhibited LPA-induced migration with 59 % inhibition observed in normoxia and 65% inhibition found in hypoxia. AMD3100

reduced CCA cells invasiveness through CXCR4 pathway. However, PCX inhibited invasiveness not only through CXCR4 pathway but also LPA signaling. These findings support the utility of PCX as a potential antimetastatic therapy due to more efficient prevention of CCA migration through multiple pathways than conventional CXCR4 inhibitor.

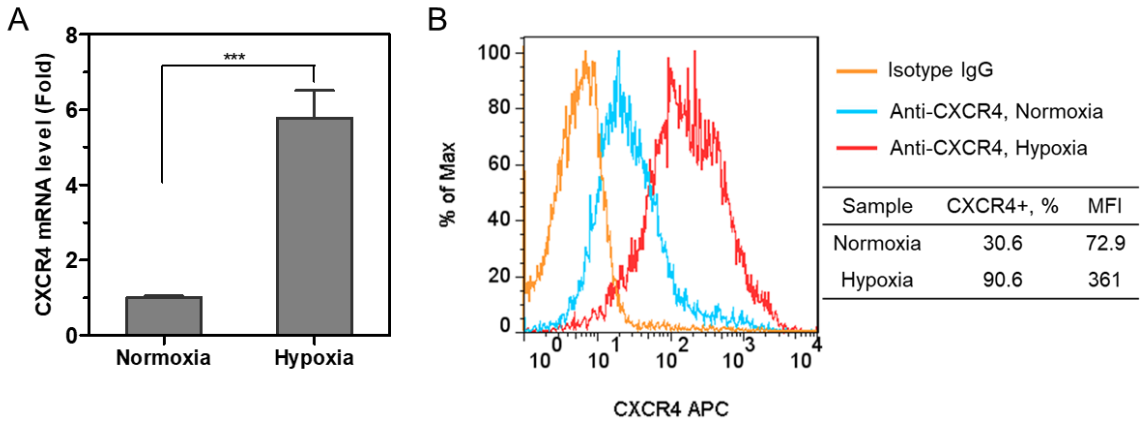

Figure 3.1. CXCR4 level analysis. (A) CXCR4 mRNA expression in Mz-ChA-1 cells quantified by qRT-PCR. (B) CXCR4 expression on Mz-ChA-1 cell surface measured by flow cytometry. The percent of CXCR4-positive cells and mean fluorescence intensity (MFI) were analyzed using FlowJo software.

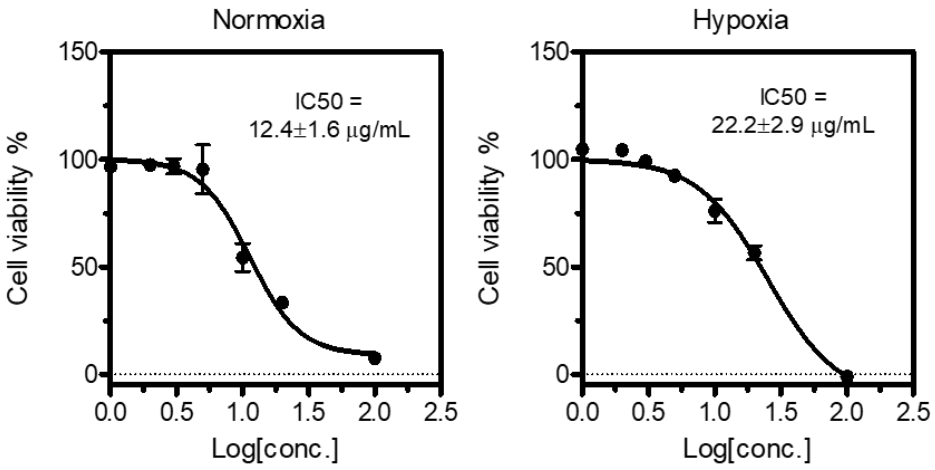

Figure 3.2. Cytotoxicity of PCX in Mz-ChA-1 cells after incubation for 48 h by CellTiter-Blue viability assay.

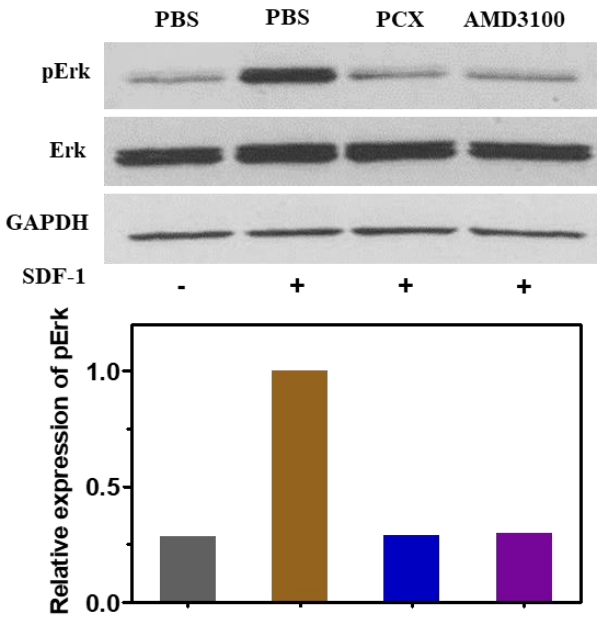

Figure 3.3. Inhibition of pErk by PCX. Mz-Cha-1 cells were treated with AMD3100 (300 nM), PCX (3 μg/mL) for 4 h followed by 20 min incubation with SDF-1 (100 ng/mL). Then, cells were lysed for Western blot analysis. GAPDH and Erk were used as housekeeping controls. Quantification of Western blot bands was performed using ImageJ software.

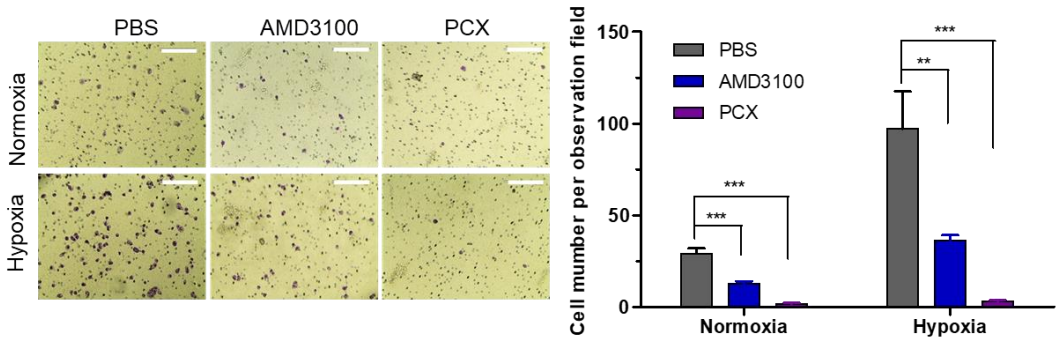

Figure 3.4. Inhibition of FBS-induced cancer cell migration in normoxia and hypoxia. Mz-ChA-1 cells were treated with AMD3100 (300 nM) or PCX (3 μg/mL) for 48 h and then allowed to migrate through a transwell membrane insert (3 × 104 cells per insert) upon stimulation with 10 % FBS for 12 h. Three 20× imaging areas were randomly selected for each insert and each group was conducted in triplicate. Data are shown as mean ± SD (n = 3). **P < 0.01, ***P < 0.001.

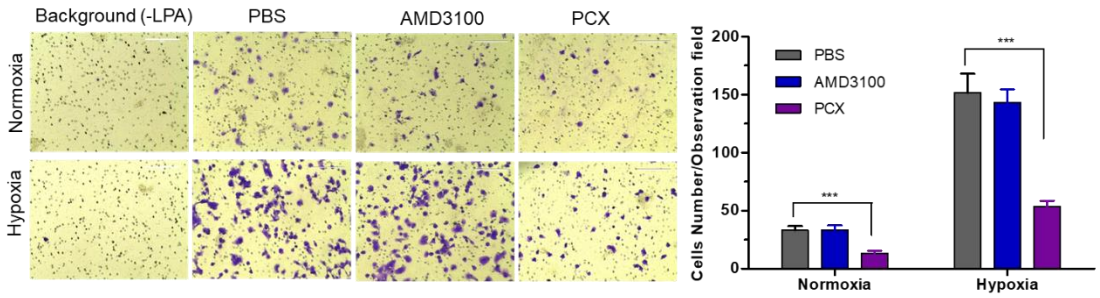

Figure 3.5. Inhibition of lysophosphatidic acid (LPA)-induced cancer cell migration in normoxia and hypoxia. Mz-ChA-1 cells were treated with AMD3100 (300 nM) or PCX (3 μg/mL) for 48 h and then allowed to migrate through a transwell membrane insert (6 × 104 cells per insert) upon stimulation with LPA (20 μM) for 12 h. Three 20× imaging areas were randomly selected for each insert and each group was conducted in triplicate. Data are shown as mean ± SD (n = 3). ***P < 0.001.

3.3.6 Preparation and characterization of nanoparticles

Besides inhibiting CXCR4, PCX are polycations that form polyplexes with nucleic acids. The ability of PCX to form nanoparticles with miRNA was first evaluated using agarose gel electrophoresis. Nanoparticles were prepared by adding PCX to anti-miRNA solution at increasing polycation/anti-miRNA ratios (**Figure 3.6A**). PCX fully condensed the miRNA at and above PCX/miRNA (w/w) ratios of 2. Partial condensation was observed at lower w/w ratios (0.5-1) as indicated by the smear of the RNA in the gel. Hydrodynamic size and ζ-potential of PCX/anti-miRNA nanoparticles (w/w = 2) were measured by dynamic light scattering. As shown in **Figure 3.6B**, nanoparticles exhibited size of 67.5 ± 0.3 nm with low polydispersity index (0.10 ± 0.05). The nanoparticles presented positive surface charge with ζ potential of 21.5 ± 1.3 mv (**Figure 3.6C**). The shape and morphology of the nanoparticles were analyzed by transmission electron microscopy (TEM) (**Figure 3.6D**) and they were found as uniform particles with mostly spherical morphology. Release of the miRNA from the particles was analyzed by heparin displacement assay. The nanoparticles completely released miRNA above 160 μg/mL heparin (**Figure 3.6E**). Poor stability against degradation by serum nucleases hinders the *in vivo* application of miRNA. We studied the serum stability of PCX/anti-miRNA nanoparticles in 50% FBS at 37 °C using gel electrophoresis (**Figure 3.6F**). Naked anti-miRNA was rapidly degraded within 2 h of serum incubation. The PCX/anti-miR-210 nanoparticles protected the anti-miRNA for at least 8 h. Intact anti-miRNA was observed even after serum incubation for 24 h. This result confirmed the improved serum stability provided by the PCX particles.

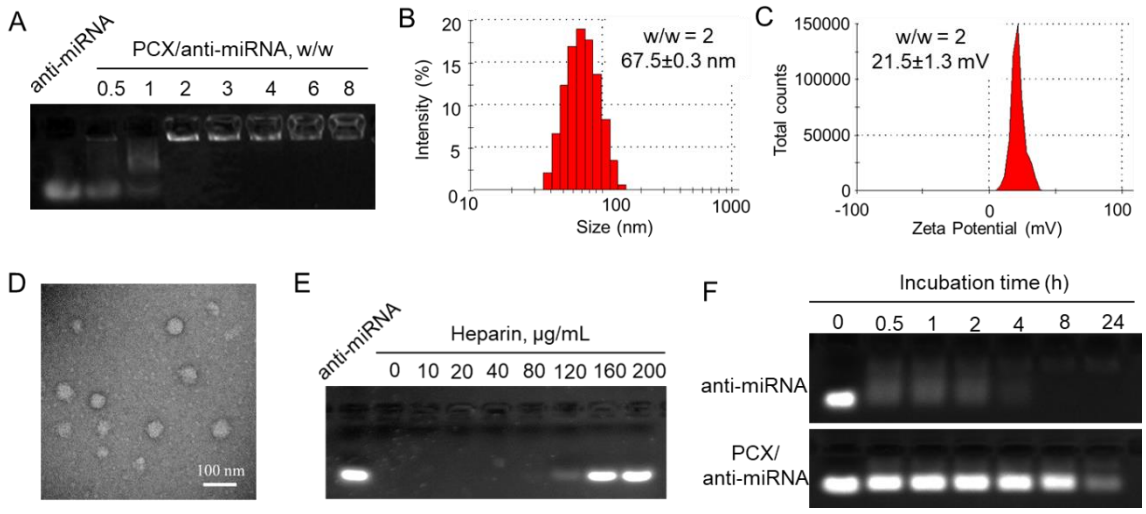

Figure 3.6. Physicochemical characterization of PCX/anti-miRNA nanoparticles. (A) anti-miRNA condensation by PCX using agarose gel electrophoresis. (B) Hydrodynamic size distribution of PCX/anti-miRNA nanoparticles (w/w=2). (C) ζ-potential of PCX/anti-miRNA nanoparticles (w/w=2). (D) TEM image of PCX/anti-miRNA nanoparticles (w/w=2). (E) Heparin induced anti-miRNA release from the PCX/anti-miRNA nanoparticles (w/w=2) with increasing concentrations of heparin. (F) Serum stability assays of naked anti-miRNA and PCX/anti-miRNA nanoparticles. Agarose gel electrophoresis of samples after treatment with serum.

3.3.7 *In vitro* delivery of anti-miRNA

After preparation and characterization of the nanoparticles, we examined their delivery to CCA cells. We prepared PCX nanoparticles using fluorescently labeled PCX (AF647-PCX) and anti-miRNA (FAM-anti-miRNA). Mz-ChA-1 cells were incubated in normoxic conditions with the AF647-PCX/FAM-anti-miRNA (w/w = 2) for 4 h and observed under confocal microscope. As shown in **Figure 3.7A**, both AF647-PCX (red) and FAM-anti-miRNA (green) were observed in the Mz-ChA-1 cells after 4 h of incubation, indicating effective uptake and internalization of the nanoparticles. Partial colocalization of the PCX and miRNA fluorescence (yellow) suggested that at least part of the particles remained assembled in the cells. Disassembly of the significant fraction of the nanoparticles was evident from the separation of the PCX and miRNA fluorescence signals. The disassembly of the nanoparticles is important for delivery of bioavailable miRNA inhibitors.

Cell uptake was also quantified by flow cytometry (**Figure 3.7B**). We found that ~96% CCA cells have internalized both PCX and anti-miRNA. We also quantified the cellular uptake of nanoparticles in hypoxia and found no difference in the uptake percentage or mean fluorescence intensity when compared with the above results in normoxia (Figure **3.8A**). The lack of difference despite large increase in CXCR4 expression in hypoxic cells suggests that CXCR4 was not directly involved in the cell uptake of the particles. This conclusion was further supported by a competition assay in which pretreatment of cells with AMD3100 failed to inhibit the internalization of the nanoparticles (**Figure 3.8B**).

Endosomal escape is an important step in delivery of cytoplasmically active nucleic acids like miRNA. Intracellular distribution and trafficking of the PCX nanoparticles were studied using confocal microscopy. Mz-ChA-1 cells were incubated

with PCX/FAM-anti-miRNA nanoparticles for 4 h and lysosomes were stained with LysoTracker Red (**Figure 3.7C**). The fluorescence of the FAM-miRNA (green) was localized predominantly in the cytoplasm with only a limited extent of co-localization with the LysoTracker signal (red). This result confirmed endosomal escape of the nanoparticles.

After reaching cytoplasm, free anti-miRNA can inhibit targeted mature miRNA and result in therapeutic effect. Transfection activity was evaluated using nanoparticles prepared with anti-miR-210 and its negative control (anti-miR-NC). CCA cells were treated with PCX/ miRNA under normoxia or hypoxia and miR-210 expression was measured using qRT-PCR (**Figure 3.7D**). As expected, hypoxia induced a 6-fold upregulation of miR-210 expression. Incubation with PCX/anti-miR-210 significantly downregulated the miR-210 levels under both normoxia (~57% decrease) and hypoxia (~85% decrease). PCX/anti-miR-NC had no effect on miR-210 expression. These results confirmed effective delivery of functional anti-miR-210 into CCA cells and inhibition of the targeted miRNA by the PCX nanoparticle.

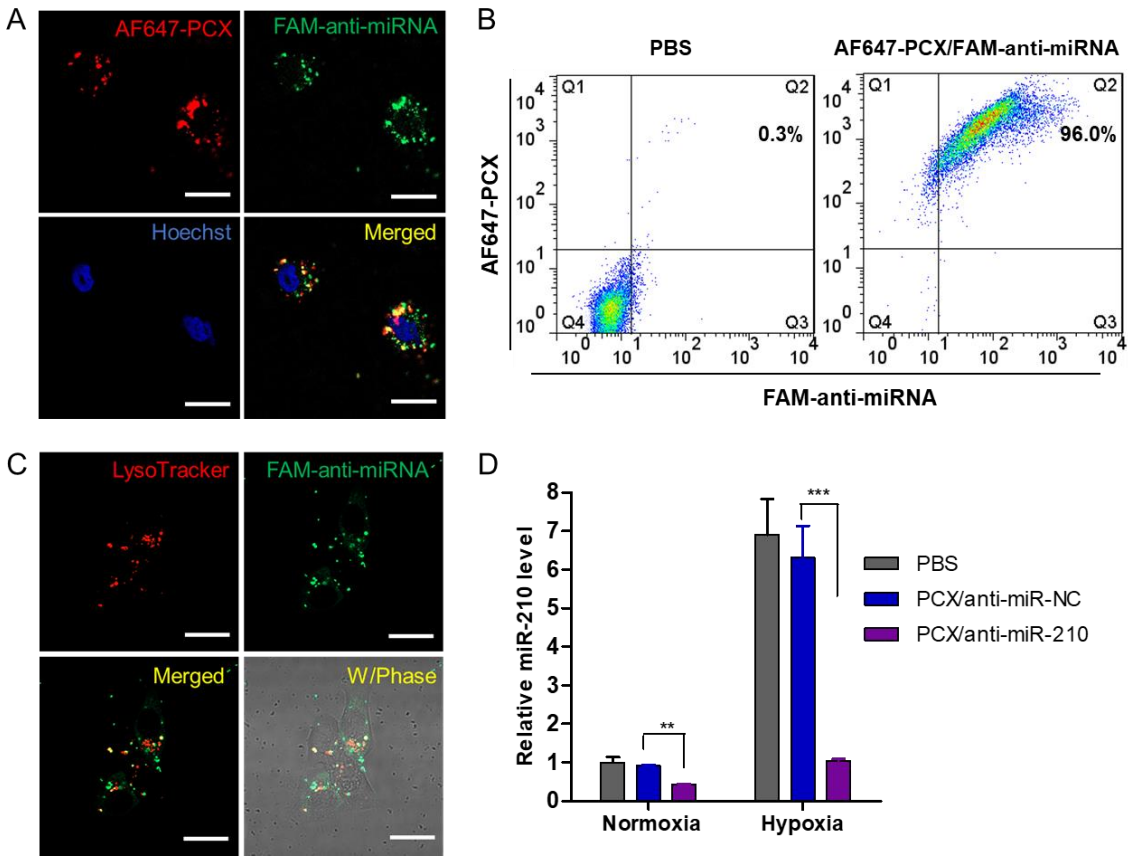

Figure 3.7. Effective delivery of anti-miRNA to CCA cells. (A) Confocal microscopic images of Mz-ChA-1 cells incubated with AF647-PCX/FAM-anti-miRNA for 4 h. (B) Flow cytometry analysis of cells treated with AF647-PCX/FAM-anti-miRNA for 4 h. (C) Intracellular trafficking of AF647-PCX/anti-miRNA in cells after 4 h of incubation. (D) MiR-210 expression in normoxic and hypoxic conditions measured by TaqMan qRT-PCR in Mz-ChA-1 cells after treatment with PCX/anti-miRNA for 48 h. Data are shown as mean ± SD (n = 3). $^{**}P < 0.01$, $^{***}P < 0.001$.

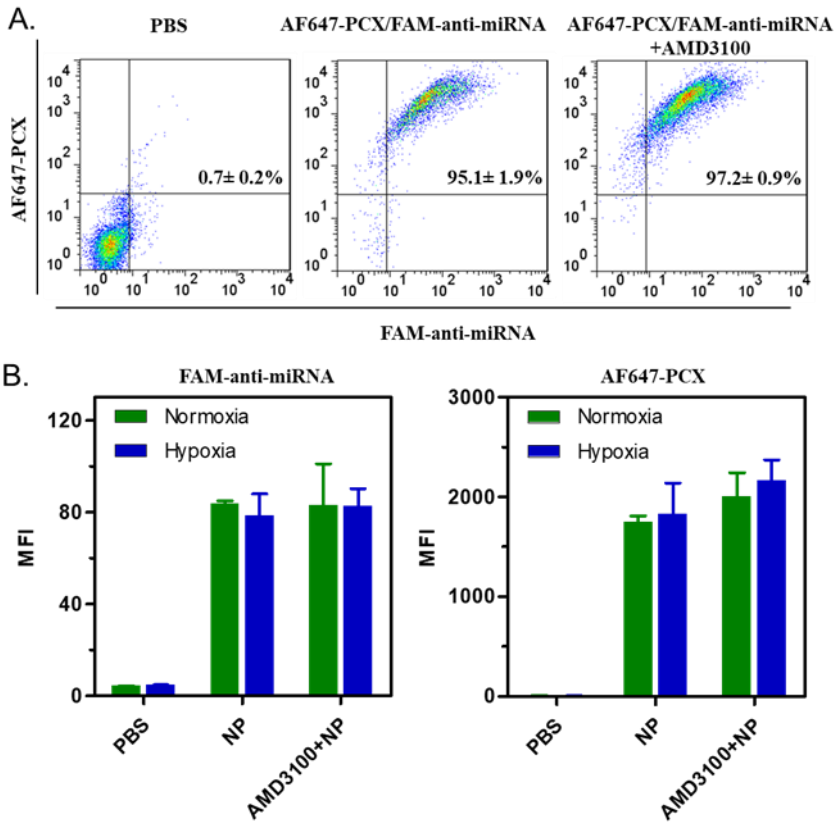

Figure 3.8. Flow cytometry analysis of cellular uptake. (A) Flow cytometry analysis of cells treated with nanoparticles (NP) AF647-PCX/FAM-anti-miRNA for 4 h under hypoxia. Pretreatment of Mz-ChA-1 cells with AMD3100 (100 μM) for 0.5 h for cellular uptake competition assay. (B) Quantification of cellular uptake is shown by mean fluorescence intensity (MFI) under normoxia and hypoxia.

3.3.8 Anticancer activity *in vitro*

The CCA cell killing activity of PCX/anti-miR-210 was first studied by determining apoptosis in the treated cells using Annexin V assay (**Figure 3.9A**). PCX/anti-miR-210 treatment increased the number of apoptotic cells (~32 %) and necrotic cells (~13 %) compared with the control groups. This pro-apoptotic effect of the nanoparticles was further corroborated by staining with DAPI and evaluation based on nuclear morphology. Upon treatment with PCX/anti-miR-210, Mz-ChA-1 cells demonstrated at least a 26% increase in apoptosis compared to cells treated with PCX/anti-miR-NC (**Figure 3.9B**). The PCX/anti-miR-210 nanoparticles also increased caspase 3/7 activity (~3.2 fold) in the CCA cells (**Figure 3.9C**), validating that the nanoparticles induced caspase activation, apoptotic nuclear morphology, and externalization of phosphatidylserine. Next, we studied the contribution of PCX/anti-miR-210 nanoparticles to the overall cell killing activity in Mz-ChA-1 cells using cell viability assay (**Figure 3.9D**). PCX/anti-miR-210 exhibited significantly higher cell killing activity (~28 %) than the untreated and miR-NC controls. Colony formation assay was also performed to study the effect of the nanoparticles on tumorigenic potential of the CCA cells (**Figure 3.9E**). Treatment with PCX/anti-miR-210 reduced colony formation by 92 % compared to PBS. As expected, CXCR4 inhibition by PCX alone had no direct cell killing effect in the CCA cells. Overall, the combined results from the anticancer activity assays confirmed promising activity of

the PCX/anti-miR-210 nanoparticles in CCA cells due to their effect on apoptosis and colony formation.

Cancer stem cells play important roles in growth, recurrence, and metastasis. CXCR4/CXCL12 axis is involved in modulating the cancer stem cell niche. Inhibition of CXCR4/CXCL12 can decrease cancer stem cells through reducing phosphorylation of ERK and STAT3 [163, 164]. Knockdown of miR-210 previously reduced stemness of cancer cells by rescuing the expression of Myc antagonist protein [165]. The combined inhibition of CXCR4 and miR-210 was thus expected to cooperatively reduce stemness of the CCA cells. Aldehyde dehydrogenase (ALDH) is a reliable marker for cancer stem cells which exhibit high ALDH enzymatic activity. The Mz-ChA-1 cells were treated with the particles, incubated with Aldefluor fluorescent reagent, and ALDH activity analyzed by flow cytometry (**Figure 3.9F**). In the untreated cells, the ALDH positive subpopulation of CCA cells was 4.6 %. Treatment with PCX/anti-miR-NC reduced the ALDH+ population to 1.4 %. Further decrease to 0.8% was observed in cells treated with the combined PCX/anti-miR-210 nanoparticles. Tumor spheroid formation assay was then used to validate the effect of the nanoparticles on cancer stem cells. Compared with the untreated (PBS) control group with large and abundant tumor spheroids, PCX/anti-miR-NC reduced the formation of large spheres. PCX/anti-miR-210 treatment further reduced the activity of cancer cells to form tumor spheroids as indicated by the formation of small and fragmentary spheroids (**Figure 3.9G**). Based on the combined evidence from the

ALDH and tumor spheroid assays, we confirmed that both CXCR4 antagonism by PCX and miR-210 inhibition by anti-miR-210 contributed to the reduction of stemness in CCA cancer cell.

3.3.9 Chemosensitizing effect of the nanoparticles

Chemotherapy using GEM and CDDP has limited therapeutic effect in CCA patients due to drug resistance. Cancer stem cells have been shown to be involved in drug resistance through multiple cellular and molecular mechanisms. Decrease of the cancer stem cell population thus emerged as a promising approach to overcome therapy resistance and improve efficacy of cancer therapy [166]. After confirming the ability of the nanoparticles to decrease stemness of the CCA cells, we aimed to study whether PCX/anti-miRNA nanoparticles could reverse drug resistance and sensitize CCA cancer cells to chemotherapy. Mz-ChA-1 cells were treated with GEM/CDDP or GEM/CDDP+PCX/anti-miRNA under both normoxia and hypoxia. Then, cell viability was measured and half-maximal inhibition concentrations (IC50) of the GEM/CDDP combination were calculated. Treatment with PCX/anti-miR-NC (anti-miRNA 100 nM) in normoxia had no direct cell killing effect but the CXCR4 inhibition by the particles sensitized the cells to the effects of GEM/CDDP as indicated by the decrease of IC50 from 1.48 μg/mL to 0.49 μg/mL (**Figure 3.10A**). Combining the CXCR4 inhibition with miR-210 inhibition further enhanced the chemosensitizing effect of the particles (IC50 ~0.14 μg/mL). Incubation of the CCA cells in hypoxic conditions greatly increased

resistance to GEM/CDDP treatment as shown by the more than 3-fold increase of IC50 to >5 μg/mL. Both PCX/anti-miR-NC and PCX/anti-miR-210 nanoparticles sensitized the cancer cells to GEM/CDDP therapy in hypoxic conditions.

The chemosensitizing effect of the PCX/anti-miR-210 nanoparticles was further investigated using synergy analysis. Cell viability was measured in CCA cells treated with different doses and ratios of PCX/anti-miR-210 and GEM/CDDP. Combenefit software was then used to calculate synergy scores for each combination. A positive score (0-100) indicates synergy, a score of 0 is additive, and a negative score indicates antagonism. Higher score indicates stronger synergistic effect. The mapped surface of synergy/antagonism with the Bliss model is shown in **Figure 3.10B**. In normoxia, PCX/anti-miR-210 and GEM/CDDP showed synergistic cell killing effect with a score of ~30. Much stronger synergy of PCX/anti-miR-210 and GEM/CDDP was achieved under hypoxia with a score of ~60. These results confirmed that PCX/anti-miR-210 sensitized the CCA cells to chemotherapy in a synergistic manner and reversed hypoxia-induced drug resistance.

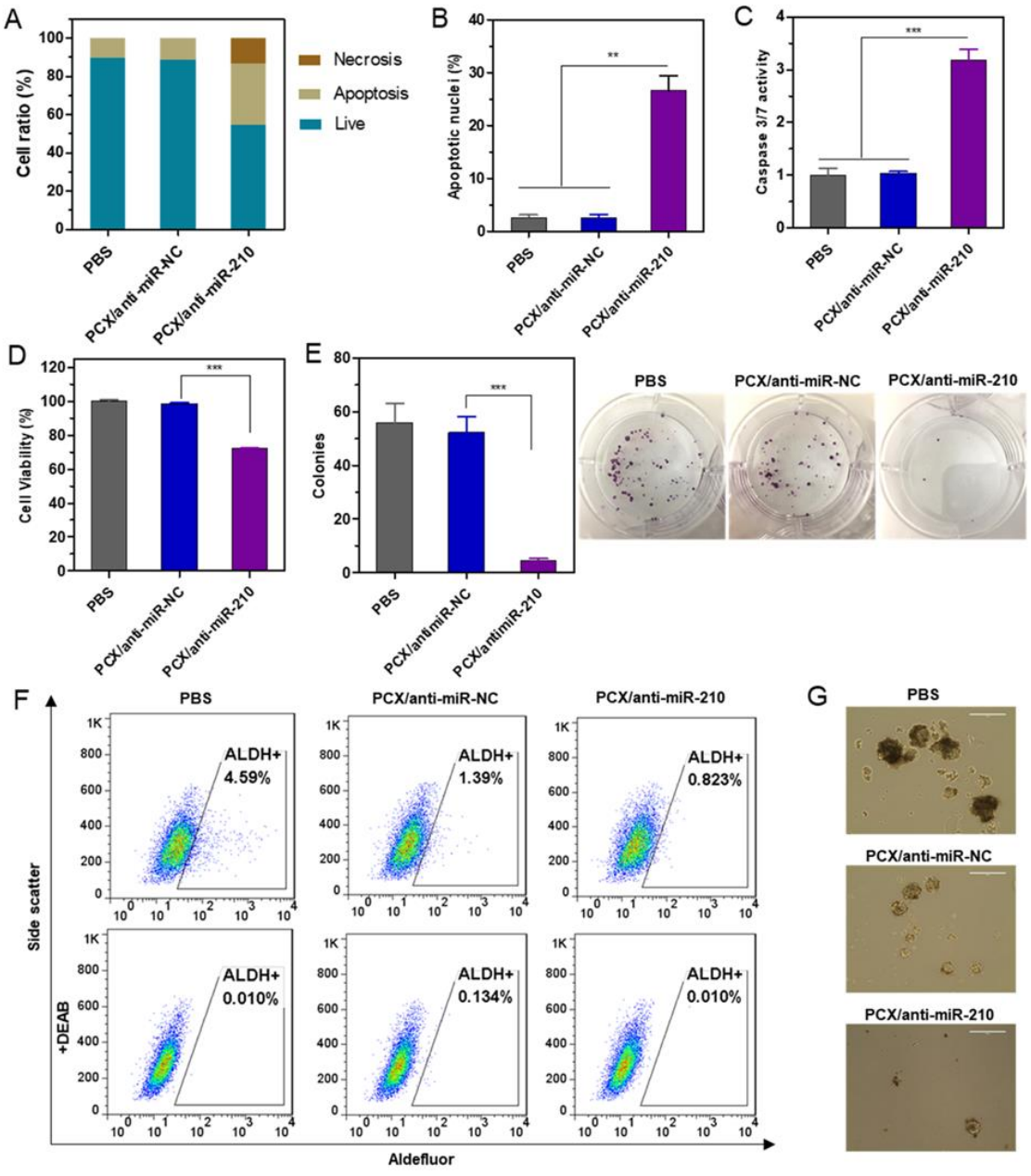

Figure 3.9. Therapeutic effect of nanoparticles *in vitro*. (A) Mz-ChA-1 cells were treated with PCX/anti-miRNA nanoparticles (100 nM anti-miRNA) for 48 h. Flow cytometry analysis of apoptosis was performed using the Annexin V-FITC/PI staining. (B) Apoptotic nuclei were counted after DAPI staining and expressed as a percent of total nuclei. (C) Quantitation of caspase 3/7 activity in cells. (D) Cell viability measured by CellTiterBlue assay after treatment for 48 h. Results are normalized to the viability of PBS treated

cells. (E) Quantification and representative images of colonies from the colony formation assay for 14 days. (F) ALDH activity in the CCA cells by flow cytometry after treatment with nanoparticles. Upper panels: Representative plot showing the percentage of ALDH-positive population. Lower panels: negative control after addition of ALDH inhibitor DEAB. (G) Tumor spheroid formation in CCA cells treated with the nanoparticles and then cultured for 14 days. Data are shown as mean ± SD (n = 3). $^{**}P < 0.01$, $^{***}P < 0.001$.

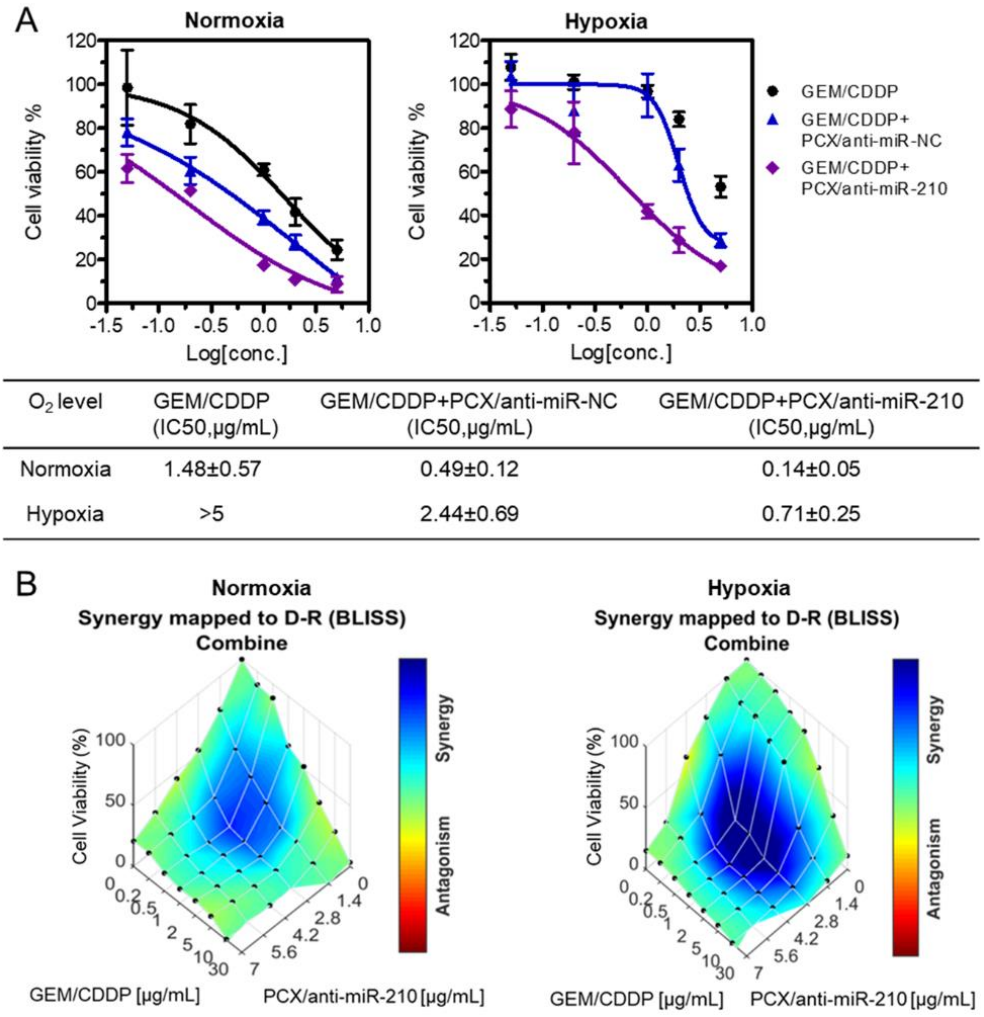

O_2 level	GEM/CDDP (IC50,μg/mL)	GEM/CDDP+PCX/anti-miR-NC (IC50,μg/mL)	GEM/CDDP+PCX/anti-miR-210 (IC50,μg/mL)
Normoxia	1.48±0.57	0.49±0.12	0.14±0.05
Hypoxia	>5	2.44±0.69	0.71±0.25

Figure 3.10. Nanoparticles sensitize CCA cells to chemotherapy. (A) Cell viability assay of Mz-ChA-1 cells after treatment with gemcitabine/cisplatin (GEM/CDDP, w/w=10), GEM/CDDP + PCX/anti-miR-NC, and GEM/CDDP + PCX/anti-miR-210 (anti-miRNA100 nM) for 48 h under both normoxia and hypoxia. IC50 values in combined GEM/CDDP concentrations calculated from the dose–response curves. Data are shown as mean ± SD (n = 3). (B) Synergy calculations of the combination effects between PCX/anti-miR-210 and GEM/CDDP treatments. Cells were treated with indicated concentrations of GEM/CDDP (w/w=10) and PCX/anti-miR-210 plus GEM/CDDP for 48 h. The data were analyzed using Combenefit software (Cancer Research UK Cambridge Institute).

3.3.10 Biodistribution

Following the promising *in vitro* findings, we explored the delivery efficacy of the nanoparticles to tumors *in vivo*. Fluorescently labeled nanoparticles (AF647-PCX/FAM-anti-miRNA) were administered intravenously into mice bearing xenograft Mz-ChA-1 tumors. Following animal sacrifice 24 h post injection, we measured ex vivo fluorescence (AF647) in the excised tissues to analyze the biodistribution (**Figure 3.11A and B**). We observed significant tumor accumulation of the nanoparticles. As expected, the nanoparticles were also found in the liver, spleen and lung. To evaluate the ability of the nanoparticles to deliver both PCX and anti-miRNA into the tumors, frozen tumor sections were observed under confocal microscope (**Figure 3.11C**). Both AF647-PCX (red) and FAM-anti-miRNA (green) fluorescence were clearly present in the tumor. The high colocalization (yellow) of AF647-PCX and FAM-anti-miRNA also indicated good stability of the nanoparticles during systemic delivery.

3.3.11 *In vivo* therapeutic effect

Therapeutic efficacy of the nanoparticles was tested in xenograft CCA model in nude mice. We have confirmed presence of hypoxic tumor microenvironment needed for the mechanism of action of our PCX/anti-miR-210 nanoparticles using pimonidazole staining in frozen tumor sections (**Figure 3.12**). Systemic intravenous treatment with the PCX/anti-miR-210 nanoparticles effectively inhibited tumor growth (51%) when compared with untreated (PBS) mice (**Figure 3.13A**). Treatment with control PCX/anti-miR-NC nanoparticles or with the GEM/CDDP chemotherapy showed negligible effect on the tumor growth. The results showed that only CXCR4 blockade by PCX/anti-miR-NC nanoparticles did not inhibit CCA tumor growth significantly. Downregulation of miR-210 and inhibition of CXCR4 by PCX/anti-miR-210 nanoparticles cooperatively achieved antitumor activity. GEM/CDDP presented chemotherapeutic resistance and failed to

inhibit tumor growth. We have used suboptimal dose of GEM/CDDP (GEM 15 mg/kg, CDDP 1.5 mg/kg) to better demonstrate the benefits of the nanoparticles. When we treated the animals with the combination of PCX/anti-miR-210 and GEM/CDDP, we observed greatly enhanced tumor growth inhibition (~79%), indicating PCX/anti-miR-210 nanoparticles sensitized the tumors to chemotherapy. At the end of the study, tumors were photographed (**Figure 3.13B** and **C**) and the weights of the tumors recorded (**Figure 3.13D**). The mean tumor weight in the PCX/anti-miR-210 group (~0.34 g) was significantly lower than the weight in the PCX/anti-miR-NC group (~0.68 g) and the untreated group (~0.81 g). Combination PCX/anti-miR-210 with GEM/CDDP resulted in the lowest tumor weight (~0.15 g). These findings confirmed strong antitumor and chemosensitizing effect of the PCX/anti-miR-210 nanoparticles in CCA. Immunohistochemical staining of cleaved caspase-3 (CC3) in the tumors was used to validate the proapoptotic activity of the nanoparticles (**Figure 3.13F**). When compared with the PBS group (2% CC3 positive cells), the PCX/anti-miR-210 treatment increased the fraction of apoptotic CC3 positive cells to ~10%. Combination of PCX/anti-miR-210 and GEM/CDDP showed even higher proapoptotic activity, with 19% of CC3 positive cells. Analysis of the H&E tumor sections also suggested considerably enhanced necrosis in the PCX/anti-miR-210 and GEM/CDDP combination group when compared with the control groups. As shown by the unchanged body weight during the treatment, PCX/anti-miR-210 had no apparent signs of gross toxicity (**Figure 3.13E**). The H&E staining of major organs demonstrated no obvious tissue damage when compared to the PBS group (**Figure 3.14**). Due to the low dose of the chemotherapy drugs in this study, we have observed no reduction in body weight or presence of tissue injury caused by the GEM/CDDP either.

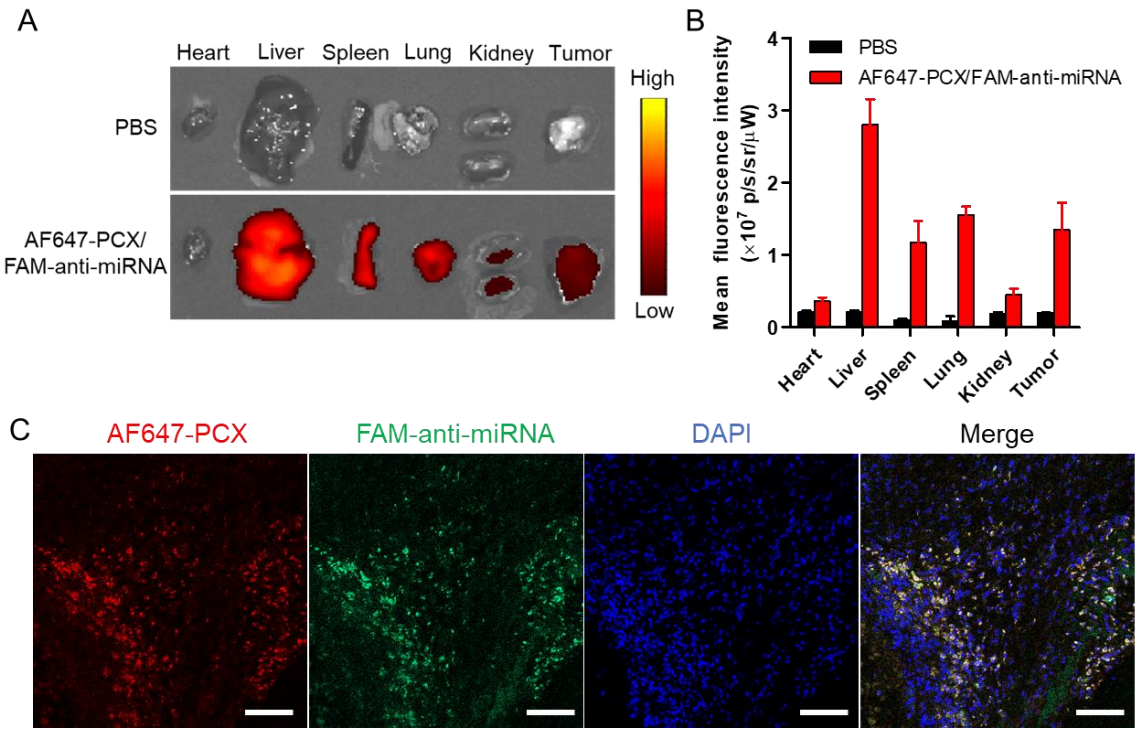

Figure 3.11. Biodistribution of the nanoparticles in xenograft MZ-ChA-1 tumor after intravenous injection. (A) Ex vivo images of the tumors and other tissues 24 h postinjection of AF647-PCX/FAM-anti-miRNA nanoparticles (Ex = 640 nm, Em = 680 nm). (B) Semiquantitative analysis of the nanoparticle biodistribution 24 h postinjection. Results are expressed as mean fluorescence intensity ± SD (n = 3). (C) Confocal images of frozen tumor sections. PCX is shown in red (AF647), anti-miRNA in green (FAM) and the nucleus in blue (DAPI).

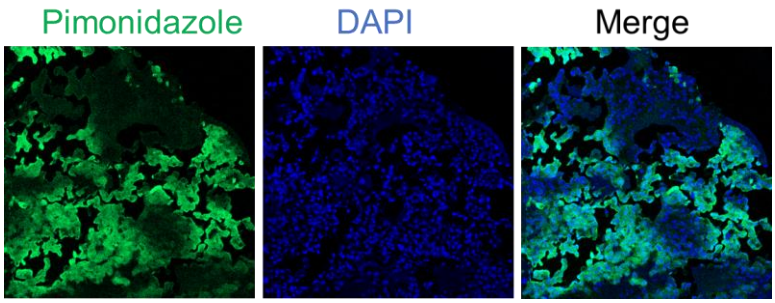

Figure 3.12. Hypoxia visualization in xenograft Mz-ChA-1 tumors. Representative confocal images of frozen tumor sections stained with the pimonidazole antibody (green).

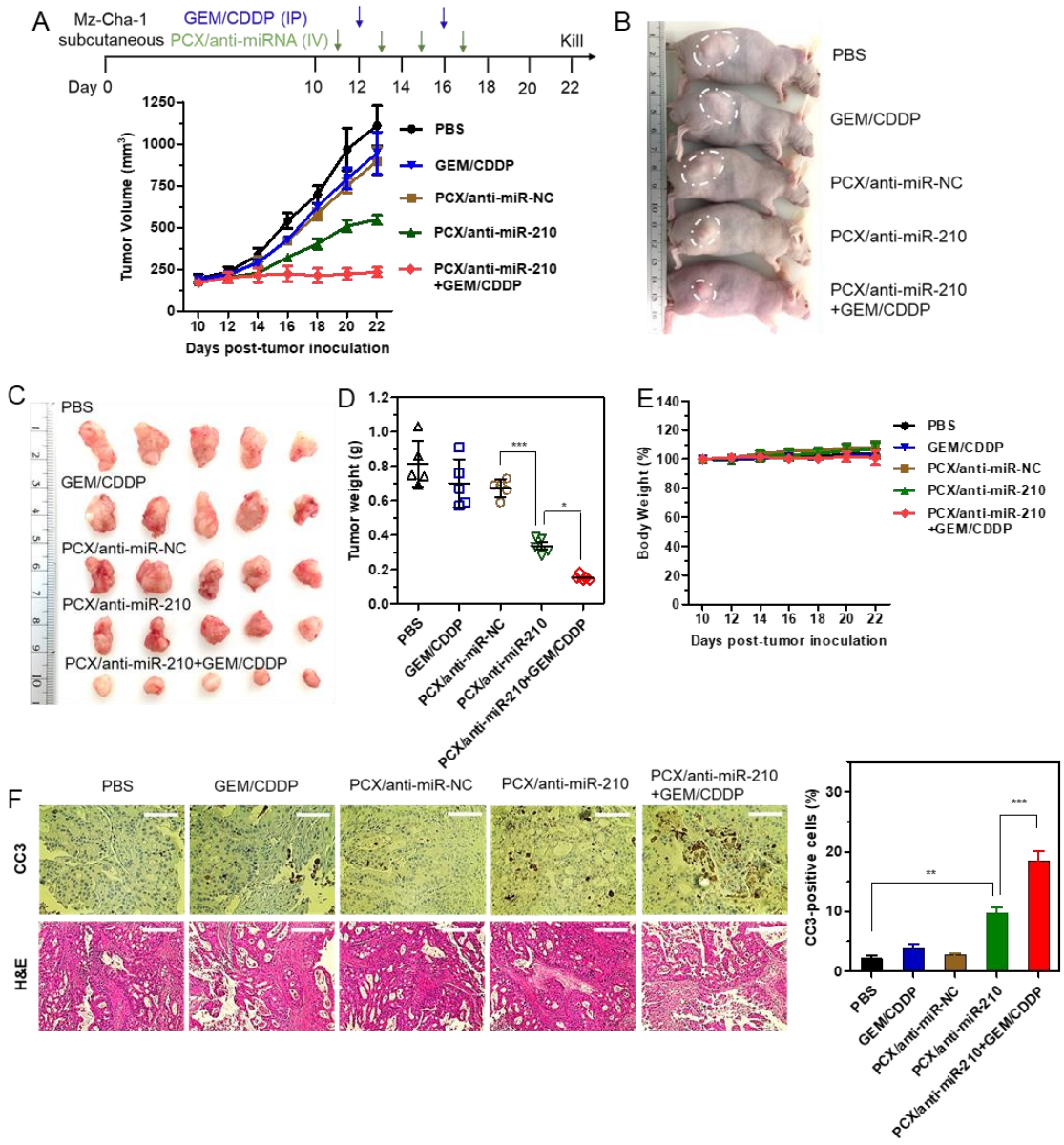

Figure 3.13. Antitumor efficacy in CCA xenograft model. (A) Mz-ChA-1 tumor growth after intravenous injection of PCX/anti-miRNA (2.4 mg/kg PCX, 1.2 mg/kg anti-miRNA) and intraperitoneal injection of GEM/CDDP (15 mg/kg GEM, 1.5 mg/kg CDDP). Data are shown as mean ± SD (n = 5). (B) Representative images of the mice on day 22. (C) Tumor tissues resected from mice on day 22. (D) Weights of tumors collected from the sacrificed mice. Data are shown as mean ± SD (n = 5). (E) Body weight during the treatment. Data are shown as mean ± SD (n = 5). (F) Cleaved caspase-3

immunohistochemistry analysis (magnification 40×) and H&E staining (magnification 20×) of tumor tissues after various treatments. The percentage (%) of cleaved caspase-3 positive cells in tumors. Data are shown as mean ± SD (n = 3). $*P < 0.05$, $**P < 0.01$, $***P < 0.001$

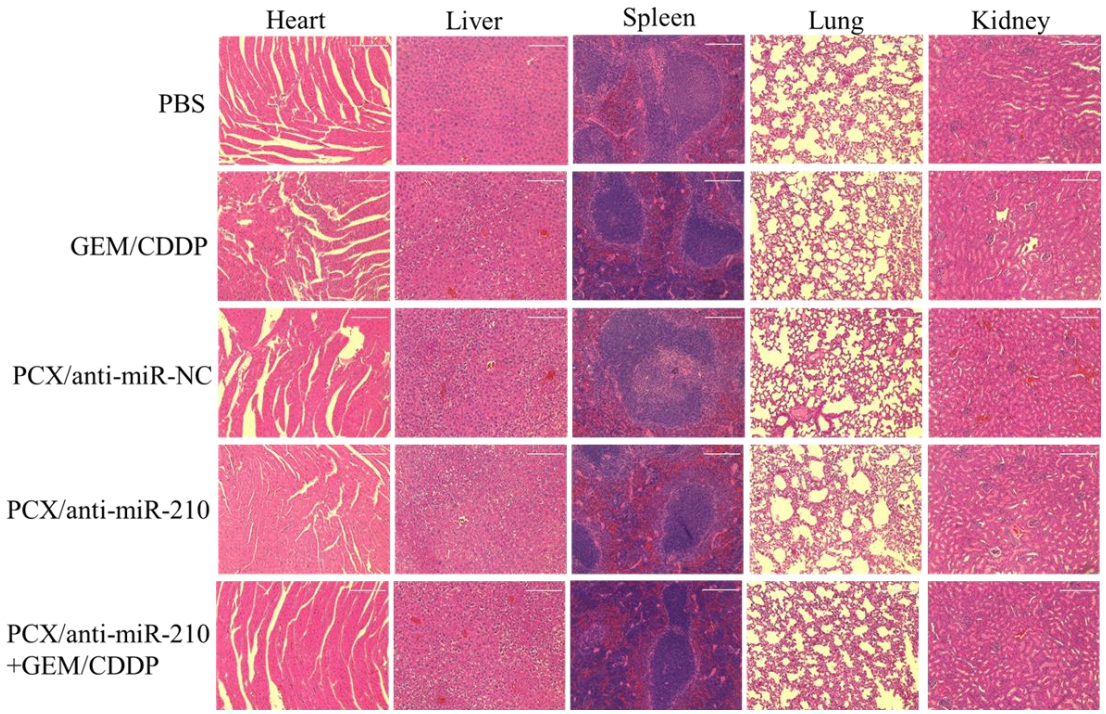

Figure 3.14. Histological observation of tissue sections from major organs of mice after treatment. The organ sections were stained with hematoxylin and eosin (H&E). The images were taken under a light microscope (×40).

3.4 Conclusion

In this study, we have developed an innovative combination nanoparticle treatment approach through simultaneous inhibition of CXCR4 and miR-210. The results showed that CXCR4-inhibiting polycation PCX could efficiently block the hypoxia-induced migration of CCA cells apparently through CXCR4 and LPA pathways. PCX/anti-miRNA nanoparticles delivered functional anti-miRNA to the CCA cells and downregulated miR-210 expression, which resulted in significant cell killing through induction of apoptosis. PCX/anti-miR-210 nanoparticles sensitized CCA cells to GEM/CDDP chemotherapy by reducing stemness and synergistically reversed hypoxia-induced drug resistance. The combination nanoparticles achieved effective systemic delivery to CCA xenograft tumors and enhanced antitumor therapy *in vivo* through direct tumor growth inhibition and chemotherapy sensitization. The nanoparticles represent promising dual-function delivery platform for miRNA delivery and provide safe and effective nanomedicines for systemic CCA therapy. Future studies will focus on the evaluation of the nanoparticles in orthotopic and metastatic CCA animal models to facilitate their clinical translation.

Chapter 4 – Delivery of siRNA and miRNA with CXCR4 targeted nanoparticles for metastatic pancreatic cancer therapy

4.1. Introduction

Pancreatic cancer (PC) is among the most lethal human cancers with a 5-year survival of less than 5% and predicted to be the second leading cause of cancer-related death by 2030 in United States [167, 168]. The high mortality of PC is mainly due to late diagnosis, widespread metastasis, poor delivery of therapeutics and resistance to available therapies [169, 170]. FOLFIRINOX has resulted in the best therapeutic efficacy in PC patient to date, but the median survival still remains only 11.1 months [171]. These therapeutic challenges highlight the urgent need to develop new therapeutics for PC therapy.

The C-X-C receptor type 4 (CXCR4) and its ligand (CXCL12) play a key role in in tumor growth, metastasis, angiogenesis and tumor microenvironment, which make them potential targets for PC therapy [11, 12]. The binding of CXCL12 to CXCR4 activates multiple pathways including SHH, Wnt and MMP to promote migration and invasion of cancer cells. CXCR4 then facilitates metastasis of the primary tumor cells to CXCL12 expressing sites including liver, lymph nodes, lung, and bone marrow [141, 172]. Inhibition of CXCR4/CXCL12 axis with CXCR4 antagonists decreased the invasion and metastasis of PC cells [38, 173, 174]. Current evidence strongly supports the potential of CXCR4 inhibition to inhibit metastasis in PC.

Small interfering RNA (siRNA) and microRNA (miRNA) are promising therapeutics for PC through RNA interference-mediated oncogene silencing. SiRNAs are synthetic RNA duplexes (19–25 bp in length) designed to specifically target a particular mRNA for degradation. MicroRNAs (miRNAs) are small noncoding RNAs (~22

nucleotide) that post-transcriptionally regulate gene expression via imperfect pairing. A miRNA typically targets multiple genes simultaneously and regulated multiple signaling pathways involved in various cancers including PC [175-179]. The combination delivering of siRNA and miRNA represents an attractive strategy to improve anticancer efficacy via simultaneously silencing a specific oncogene strongly and regulating a broad range of cancer related genes [180, 181].

Oncogene mutations of the GTPase KRAS are highly prevalent in PC and emerged as key drivers of PC initiation, progression and metastasis [182-184]. Inhibition of oncogenic KRAS with genetic manipulation inhibits PC progression in mice [185]. However, KRAS remains a largely undruggable therapeutic target; Pharmaceutical companies and academic laboratories failed to develop small molecule inhibitors of KRAS after decades of trying. SiRNA targeting $KRAS^{G12D}$, which is the most common KRAS mutation, improved overall survival of mice models and represented an effective KRAS targeted therapeutic for PC therapy [186]. Moreover, miR-210 is another attractive target for cancer therapy. Hypoxia in PC induces the overexpression of miR-210, which facilitates the adaptation of cancer cells to the hypoxic microenvironment via multiple signaling pathways [91, 187-189]. MiR-210 participates in the regulation of cancer proliferation, apoptosis, metastasis, DNA repair, cell metabolism, and drug resistance [94, 154, 190, 191]. Inhibition of miR-210 provides an effective option for the treatment of PC.

Despite the potential of siRNA and miRNA in PC therapy, their clinical translation is mainly limited by lack of delivery system. SiRNA/miRNA have similar physicochemical properties (double-stranded RNAs with ~22 nucleotides) and the same intracellular site of action (cytoplasm). Similar delivery systems enable to deliver both siRNA and miRNA. Polycations stand among the most investigated delivery platforms, which form

polyplexes with siRNA/miRNA and promote their delivery by protecting them from degradation and overcoming multiple biological barriers [156, 192]. Traditional polycations are pharmacologically inert with no inherent anticancer activity. Pharmacologically active polycations present as a new class of combination cancer therapies with advantages including simple formulation and high content of active agents [6]. Polymeric CXCR4 antagonists (PCX), which are mainly composed of FDA-approved CXCR4 inhibitor AMD3100, are able to block CXCR4/CXCL12 axis and deliver siRNA or miRNA for combined cancer therapy [21, 59, 157]. Considering the key roles of CXCR4, KRAS and miR-210 in PC, we hypothesized that combining inhibition of CXCR4, silence of KRAS and inhibition of hypoxia-inducible miR-210 would cooperatively enhance the therapy of PC. To test this hypothesis, we used PCX to form nanoparticles with both siKRAS and miR-210 inhibitor and evaluated their delivery activity and anticancer efficacy in PC both *in vitro* and *in vivo*.

4.2. Materials and methods

4.2.1 Materials

Cholesterol-modified polymeric CXCR4 inhibitors PCX was synthesized and characterized as previously described. Succinimidyl ester of Alexa Fluor® 647 carboxylic acid was from Life Technologies (Eugene, OR). AlexaFluor 647 labeled PCX polymers (AF647-PCX) were produced according to manufacturer's instructions and purified by dialysis to remove unreacted dye. AMD3100 was from Biochempartner (Shanghai, China). Dulbecco's modified Eagle medium (DMEM), Dulbecco's phosphate buffered saline (PBS), trypsin, penicillin, streptomycin and fetal bovine serum (FBS) were from Thermo Scientific (Waltham, MA). Hsa-miR-210-3p-Hairpin Inhibitor (anti-miR-210, mature miRNA sequence: 5′-CUGUGCGUGUGACAGCGGCUGA-3′), negative control miR-NC inhibitor (anti-miR-NC, mature miRNA sequence: 5′-UCACAACCUCCUAGAAAGAGUAGA-3′), siRNA targeting KRAS (siKRAS, sense sequence, 5′-GUUGGAGCUGAUGGCGUAGdTdT-3′), negative control siRNA (siNC, sense sequence, 5′- UCACAACCUCCUAGAAAGAGUAGA-3′) and carboxyfluorescein (FAM) labeled FAM-siRNA were purchased from Dharmacon (Lafayette, CO). Cell culture inserts (for 24-well plates, 8.0 μm pores, Translucent PET Membrane, cat# 353097) were purchased from BD Biosciences (Billerica, MA). Real-time (RT)-PCR primers were purchased from Invitrogen (Carlsbad, CA). Allophycocyanin (APC) mouse anti-human CXCR4 antibody and APC mouse lgG2a, κ isotype controls were from BD Biosciences (San Jose, CA). All other reagents were from Fisher Scientific and used as received unless otherwise noted.

4.2.2 Cell culture

Primary tumor cell line KPC8060 derived from KPC pancreatic ductal adenocarcinoma mouse model ($Kras^{LSL\text{-}G12D/+}$; $Trp53^{LSL\text{-}R172H/+}$; Pdx-1-Cre) were provided by Dr. James Grunkemeyer at UNMC. KPC cells were grown in high-glucose DMEM supplemented with 10% FBS, penicillin (100 U/mL) and streptomycin (100 µg/mL) at 37 °C with 5% CO2 in a humidified chamber.

4.2.3 Preparation and characterization of nanoparticles

PCX/(siRNA+miRNA) nanoparticles were prepared by adding predetermined volume of PCX to a siRNA and miRNA solution (siRNA:miRNA = 1 (mol:mol), 20 µM in 10 mM HEPES pH 7.4) to achieve the desired w/w ratio and vigorously vortexed for 10 s. Nanoparticles were then incubated at room temperature for 20 min before further use. The ability of PCX to condense siRNA and miRNA was determined by electrophoresis in a 2% agarose gel containing 0.5 µg/mL ethidium bromide (EtBr). Nanoparticles formed at various polycation-to-(siRNA+miRNA) weight ratios were loaded (20 µL of the sample containing 0.5 µg of miRNA and siRNA) and run for 15 min at 100 V in 0.5 × Tris/Borate/EDTA buffer. The gels were visualized under UV illumination with a KODAK Gel Logic 100 imaging system. Hydrodynamic diameter and zeta potential of the nanoparticles were determined by dynamic light scattering (DLS) using a ZEN3600 Zetasizer Nano-ZS (Malvern Instruments Ltd., Massachusetts, USA). Morphology was observed under transmission electron microscopy (TEM, Tecnai G2 Spirit, FEI Company, USA) using NanoVan® negative staining (Nanoprobes, USA). The morphology was also observed using MultiMode Atomic force microscopy (AFM) NanoScope IV system (Bruker Instruments, Santa Barbara, CA) operating in tapping mode.

4.2.4 Quantitative real-time polymerase chain reaction (qRT-PCR)

Cells were seeded in 12-well plates at 5×10^4 cells per well 24 h prior to treatment. Then, the cells were incubated with the nanoparticles containing anti-miRNA (50 nM) and siRNA (50 nM) in 1 mL of medium for 48 h. The mirVana miRNA Isolation Kit (Ambion, USA) was used for total RNA extraction from cultured cells. The expression levels of miR-210 were evaluated by TaqMan qRT-PCR. 10 ng of total RNA was converted into cDNA using specific primers for miR-210 (or the internal control Z30 (Applied Biosystems, Foster City, CA)) and the TaqMan microRNA reverse transcription kit (Applied Biosystems). qRT-PCR was performed using TaqMan Universal Master Mix II, No AmpErase UNG (2×) and specific primers for miR-210 or Z30 (Applied Biosystems, Foster City, CA) on a Rotor-Gene Q instrument (QIAGEN) according to the manufacturer's instructions. MiRNA expression levels were expressed relative to the internal control according to the comparative threshold cycle (Ct) method. Expression of the KRAS was quantified using SYBR Green RT-PCR. 0.5 μg total RNA was reverse-transcribed to cDNA using QuantiTect reverse transcription kit (Qiagen): the relative amount of mRNA was determined by RT-PCR on a Rotor-Gene Q instrument (QIAGEN). The GAPDH primer assay and QuantiFast SYBR Green PCR kit (Qiagen) were used following themanufacturer's protocol. The following primers were used: KRAS (forward 5′-CGCAGACTTACTTCCCCGGC; reverse,

5′-CGCTCAATTCCTCAACCACG). Relative mRNA expression levels were calculated from the Ct values of the target genes and the housekeeping gene GAPDH.

4.2.5 DAPI staining assay

Apoptosis percentage was also quantified by nuclear morphology and visualized by treatment with the fluorescent DNA-binding dye, DAPI (4′, 6-diamidine-2′-phenylindole dihydrochloride). Briefly, cells were stained with 2 μg/mL of DAPI for 30

minutes at 37 °C. Apoptotic nuclei (condensed, fragmented) were counted and presented as a percent of total nuclei. At least 100 cells were counted per well and experiments were performed in triplicate.

4.2.6 Colony formation

Cells were transfected with nanoparticles containing siRNA and miRNA for 4 h. Then, transfected cells were reseeded in 12-well plates (200 cells per plate). Cells were allowed to grow for 7 days. Cells were fixed in 100% methanol and stained with 0.2% Crystal Violet solution for 10 min. Finally, plates were washed with distilled water and photographed. Number of colonies in each well were quantified.

4.2.7 KPC-derived orthotopic PC model

All animal experiments followed a protocol approved by the University of Nebraska Medical Center Institutional Animal Care and Use Committee. Orthotopic KPC-derived model was established by orthotopic injection of KPC cells into the tail of the pancreas. Briefly, KPC cells were trypsinized, washed and resuspended in 1:1 mixture of PBS/Matrigel. Female C57Bl/6 mice (6 weeks old) from Charles River Laboratories were anesthetized by IP injection of ketamine/xylazine solution. The surgical site was sterilized and a 1-cm incision was made in the peritoneum at the mid-abdomen region below the sternum by scissors. 2.5×10^4 of KPC cells (40 µL) were injected into the head of pancreas. The abdomen was closed with a 2-layer suture with 5-0 chromic catgut and soft staple. The skin staples were removed 10 days after surgery.

4.2.8 Blood circulation time

KPC mice were IV or IP injected with AF647-PCX/FAM-siRNA nanoparticles. At 0, 0.25, 1, 4, and 24 h post injection, about 100 µL blood from the venous plexus of mice

was collected in heparin-treated tubes and imaged with Xenogen IVIS 200 (Ex = 640 nm, Em = 680 nm). The fluorescence from each tube was analyzed by the instrument software.

4.2.9 Biodistribution

KPC mice were IV or IP injected with AF647-PCX/FAM-siRNA nanoparticles. At 4 and 24 h post injection, the mice were sacrificed and imaged using Xenogen IVIS 200 (Ex = 640 nm, Em = 680 nm). The tumors and major organs were also harvested and subjected to ex vivo fluorescence imaging (Ex = 640 nm, Em = 680 nm). The fluorescence from each organ was analyzed by the instrument software. Then, the isolated tumors were embedded in an OCT compound, cut into 10 μm sections, stained with CD31 antibody (Cy3) and DAPI, and imaged with a confocal microscope.

4.2.10 Anticancer activity

At day 14 post-tumor inoculation, mice were randomly assigned to 5 groups (n = 5) and IP injected with PBS, PCX/(siNC+miR-NC), PCX/(siNC+miR-210), PCX/(siKRAS+miR-NC), and PCX/(siKRAS+miR-210), respectively. PCX/(siRNA+miRNA) nanoparticles (w/w=2, 5 mg/kg PCX, 1.25 mg/kg siRNA, 1.25 mg/kg miRNA) were injected at days 14, 16, 18, 20, 22, 24 and 26. Body weight of the mice was recorded. On days 28, blood was drawn from the venous plexus of the eyes of mice for whole blood analysis and serum biochemistry test. Mice were sacrificed, and all tumor tissues and major organs were harvested, fixed in 4% paraformaldehyde, sectioned, and stained with H&E. Blood were collected Blinded histological analysis of the tissues was conducted by a trained pathologist at the UNMC core facility.

4.2.11 Statistical analysis

Data are presented as the means ± SD. The statistical significance was determined using ANOVA followed by Bonferroni post hoc correction with $p < 0.05$ as the minimal level of significance.

4.3. Results and discussion

4.3.1 Preparation and characterization of nanoparticles

The ability of PCX to condense siRNA and miRNA was evaluated using agarose gel electrophoresis. PCX was added to siRNA and miRNA solution at increasing polymer/(siRNA+miRNA) weight ratios (**Figure 4.1A**). SiRNA and miRNA was fully condensed at and above PCX/(siRNA+miRNA) (w/w) ratios of 2. Partial condensation was observed at lower w/w ratios (0.5-1). Hydrodynamic size and ζ-potential of PCX/(siRNA+miRNA) nanoparticles (w/w = 2) were measured by dynamic light scattering (**Figure 4.1B** and **C**). Nanoparticles presented sizes of 57.3 ± 0.4 nm with low polydispersity index (0.12 ± 0.02). The nanoparticles exhibited a positive surface charge with ζ potential of 19.5 ± 1.6 mV. The shape and morphology of nanoparticles was further analyzed by transmission electron microscopy (TEM) and atomic force microscopy (AFM). The nanoparticles were uniform particles with a mostly spherical morphology (**Figure 4.1D** and **E**).

4.3.2 *In vitro* delivery of siRNA and miRNA

Transfection activity was evaluated using nanoparticles loaded with siKRAS and anti-miR-210. KPC cells were treated with PCX/(siRNA+anti-miRNA) nanoparticles. Then, KRAS mRNA and miR-210 expression was measured using qRT-PCR. PCX/(siKNC+anti-miNC) failed to decrease KRAS mRNA and miR-210 levels. Incubation with PCX/(siKRAS+anti-miNC) downregulated KRAS mRNA level (**Figure 4.2A**). Treatment with PCX/(siNC+anti-miR-210) decreased miR-210 level in KPC cells (**Figure 4.2B**). PCX/(siKRAS+anti-miR-210) nanoparticles significantly downregulated both KRAS mRNA (~54% decrease) and miR-210 levels (~53% decrease). These results

confirmed effective delivery of functional siKRAS and anti-miR-210 into KPC cells and inhibition of the targeted gene and miRNA by the PCX nanoparticle.

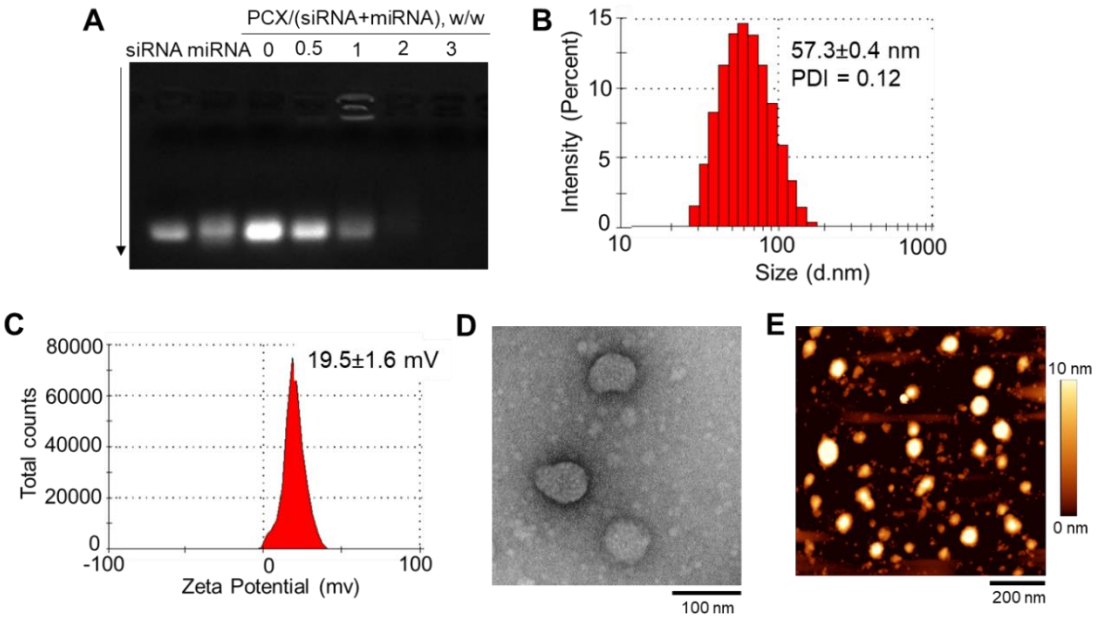

Figure 4.1. Physicochemical characterization of PCX/(siRNA+anti-miRNA) nanoparticles. (A) Condensation of siRNA and anti-miRNA by PCX using agarose gel electrophoresis. (B) Hydrodynamic size distribution of PCX/(siRNA+anti-miRNA) nanoparticles (w/w=2). (C) ζ-potential of PCX/(siRNA+anti-miRNA) nanoparticles (w/w=2). (D) TEM image of PCX/(siRNA+anti-miRNA) nanoparticles (w/w=2). (E) AFM image of PCX/(siRNA+anti-miRNA) nanoparticles (w/w=2).

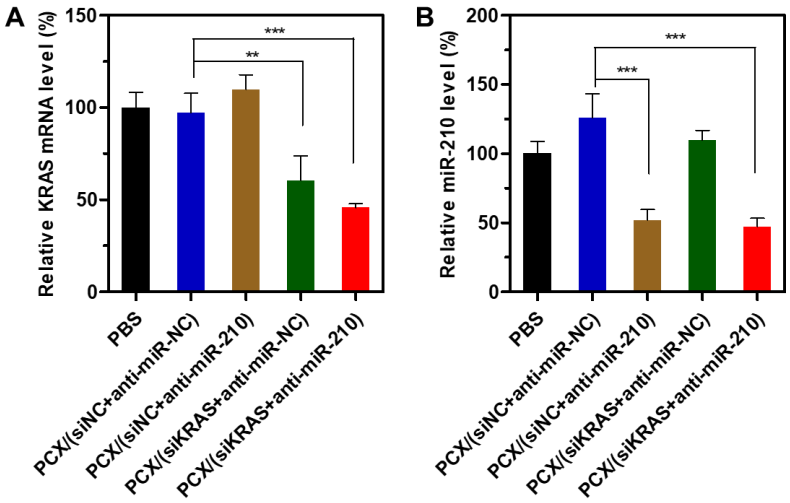

Figure 4.2. *In vitro* delivery of siRNA and miRNA. (A) KRAS mRNA and (B) miR-210 expression in KPC cells after treatment with PCX/(siRNA+anti-miRNA) for 48 h. Data are shown as mean ± SD (n = 3). $^{**}P < 0.01$, $^{***}P < 0.001$.

4.3.3 Anticancer activity *in vitro*

The pro-apoptotic activity of PCX/(siRNA+anti-miRNA) was first studied by staining with DAPI and evaluation based on nuclear morphology. Upon treatment with PCX/(siKRAS+anti-miR-210), KPC cells demonstrated at least a 40% increase in apoptosis compared to cells treated with PCX/(siNC+anti-miR-NC) (**Figure 4.3A**). PCX/(siNC+anti-miR-210) and PCX/(siKRAS+anti-miR-NC) treatment induced only 10% and 15% apoptosis, respectively. These results confirmed the combinational pro-apoptotic activity through co-delivery of siKRAS and anti-miR-210 by PCX nanoparticles. Colony formation assay was also performed to study the effect of the nanoparticles on the tumorigenic potential of KPC cells. In comparison with PCX/(siNC+anti-miR-NC) group, treatment with PCX/(siKRAS+anti-miR-210) presented co-operative activity to reduce colony formation by delivery of both siKRAS and anti-miR-210 (**Figure 4.3B**).

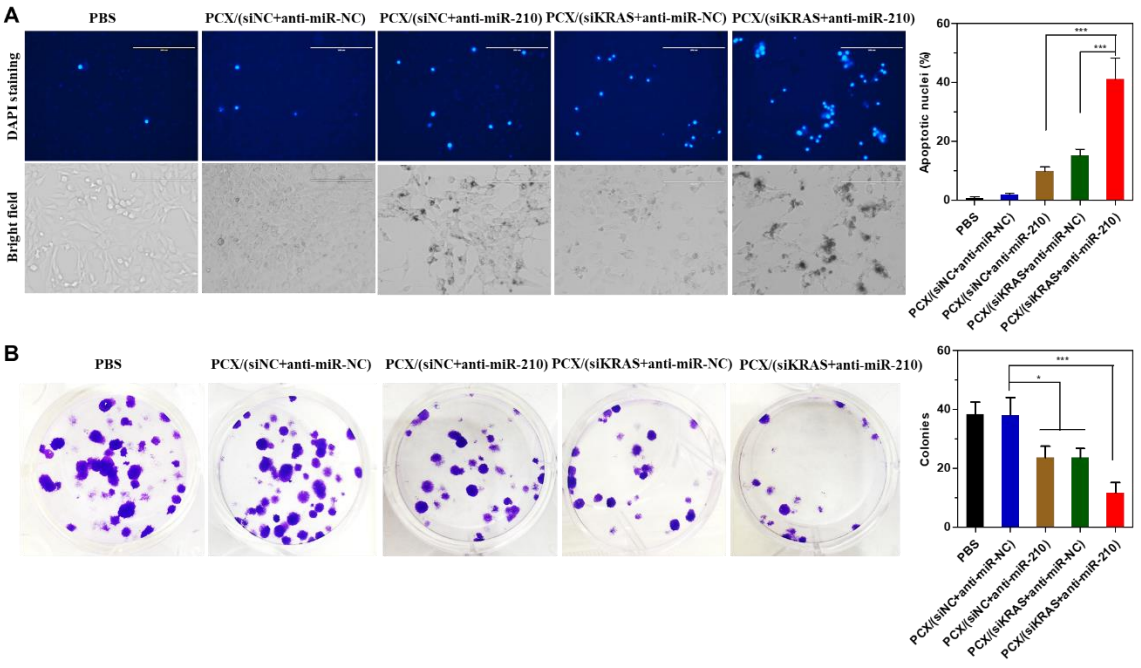

Figure 4.3. Anticancer activity *in vitro*. (A) Apoptotic nuclei were counted after DAPI staining and expressed as a percent of total nuclei. (B) Quantification and representative images of colonies from the colony formation assay for 7 days. Data are shown as mean ± SD (n = 3). **P* < 0.05, ****P* < 0.001.

4.3.4 Blood circulation time and biodistribution

To investigate the circulation time of nanoparticles in blood, AF647-PCX/FAM-siRNA nanoparticles were IV or IP injected into KPC mice. The AF647-PCX fluorescent intensity in each group was normalized by setting 0 h intensity after IV injection as 100%. In the IV injection group, the fluorescence signal of AF647-PCX decreased quickly, remained only 16% at 1 h and then decrease to almost 0% at 24 h due to the fast clearance of nanoparticles from the blood (**Figure 4.4A**). In the IP injection group, the fluorescence intensity firstly increased, reached 18% at 1 h, and then decreased to 0%. The fluorescence intensity after IP injection is a likely a function of absorption from the peritoneal cavity into blood and clearance from blood.

To explore the biodistribution of nanoparticles, AF647-PCX/FAM-siRNA nanoparticles were IV or IP injected into KPC mice. Following animal sacrifice 4h and 24 h post injection, we measured fluorescence (AF647) in the tissues after removal to analyze the biodistribution. In the IV injection mice, the nanoparticles mainly accumulated in the liver and presented poor tumor distribution (**Figure 4.4B**). The nanoparticles were also found in the spleen and lung. In the IP injection mice, specific accumulation of nanoparticles was observed in tumor. The tumor fluorescence intensity increased from 4 h to 24 h due to more penetrated nanoparticles over time. At 24 h, tumoral fluorescence intensity of IP injected mice is 16 folds higher than that of IV injected mice. To further evaluate the ability of the nanoparticles to deliver both PCX and siRNA into the tumors, frozen tumor sections were observed under a confocal microscope. Both AF647-PCX (red) and FAM-siRNA (green) fluorescence were clearly present in the tumor of IP injected mice. Importantly, the nanoparticles were delivered to both peripheral regions and central regions of tumors indicated by widespread fluorescence in the all tumor tissues. However, very weak AF647-PCX and FAM-siRNA

fluorescence were found in the IV injected mice tumor (**Figure 4.4C**). These results confirmed the superior capability of nanoparticles to deliver both PCX and siRNA to orthotopic PC tumor via IP injection than via IV injection.

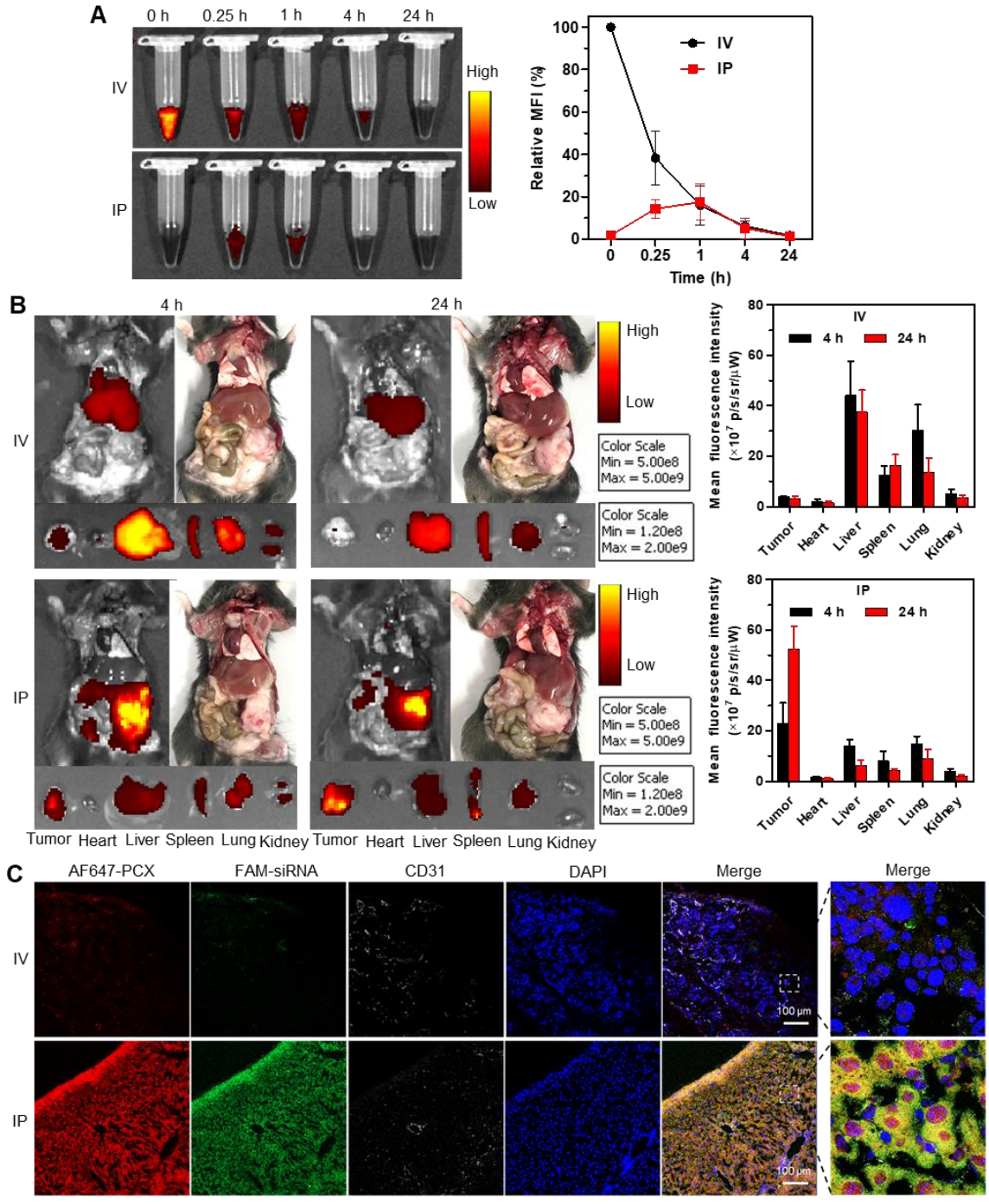

Figure 4.4. The circulation time and biodistribution of nanoparticles *in vivo*. (A) The circulation time of AF647-PCX/FAM-siRNA in blood after IV or IP injection. AF647-PCX was used for visualization. Blood was drawn from mice after IV or IP injection with AF647-PCX/FAM-siRNA nanoparticles at different time and imaged under a

fluorescence imaging system (Ex = 640 nm, Em = 680 nm). The fluorescence intensity of 0 h in each group was normalized as 100%. (B) The biodistribution of AF647-PCX/FAM-siRNA nanoparticles *in vivo*. Mice were administrated with AF647-PCX/FAM-siRNA via IV or IP injection. At 6h and 24h after injection, mice were sacrificed and imaged under a fluorescence imaging system (Ex = 640 nm, Em = 680 nm). The harvested organs and tumors were also imaged. Semiquantitative analysis of the nanoparticle biodistribution was performed. Results are expressed as mean fluorescence intensity ± SD (n = 3). (C) Confocal images of frozen tumor sections. PCX is shown in red (AF647), siRNA in green (FAM), blood vessel in white (Cy3) and the nucleus in blue (DAPI).

4.3.5 Anticancer activity *in vivo*

Therapeutic efficacy of the nanoparticles was tested in a genetic model of spontaneous pancreatic cancer. Mice with mutant KRAS and p53 loss (KPC) were used. At day 14 post-tumor inoculation, mice were received multiple IP injections of nanoparticles (**Figure 4.5A**). As presented by the unchanged body weight during the treatment, PCX/(siRNA+anti-miRNA) nanoparticles had no apparent signs of gross toxicity (**Figure 4.5B**). After treatment, a part of mice (5 per group) were sacrificed for checking primary tumor size and metastasis. Treatment with control PCX/(siNC+anti-miR-NC) nanoparticles showed negligible effect on primary tumor growth (**Figure 4.5 C** and **D**). In comparison with PBS group, both PCX/(siNC+anti-miR-210) and PCX/(siKRAS+anti-miR-NC) significantly inhibited tumor growth by 43% and 47%. PCX/(siKRAS+anti-miR-210) treatment presented enhanced tumor growth inhibition (~60%). These results suggested that CXCR4 inhibition alone has no effect on the growth of primary tumor. Delivery of siKRAS or anti-miR-210 effectively inhibited tumor growth. Co-delivery of siKRAS and anti-miR-210 in PCX nanoparticles achieved combined siRNA/miRNA therapy against primary tumor.

Besides the inhibition activity on primary tumor, the effect of nanoparticles on metastasis was also studied. Widespread tumor metastasis was found in range of organs and tissues, including liver, spleen, kidney, intestine, stomach, abdominal wall and diaphragm (**Figure 4.6A and B**). PCX/(siNC+anti-miR-NC) nanoparticles presented apparent activity to inhibit metastasis, which was indicated by the reduced metastatic frequencies in broad tissues in comparison with PBS group. This metastasis inhibition activity was most likely due to CXCR4 inhibition endowed by PCX. The delivery of siKRAS and anti-miR-210 inhibitor further improved the activity of nanoparticles to inhibit metastasis. PCX/(siKRAS+anti-miR-210) completely inhibited the metastasis to all

observed tissues except spleen (**Figure 4.6B**). PCX/(siKRAS+anti-miR-210) also reduced the macro-metastasis on the surface of liver (**Figure 4.6C**). Moreover, HE staining further showed the decreased tumor metastasis area in tissues (**Figure 4.6D**). These results confirmed the combinational antimetastatic activity of PCX/(siKRAS+miR-210) nanoparticles through simultaneous inhibition of CXCR4 and delivery of siKRAS/miR-210 inhibitor.

PCX/(siKRAS+miR-210) was able to inhibit primary tumor growth and widespread metastasis. Next, we aimed to study the effect of nanoparticles treatment on survival of KPC-derived mice. In comparison with PBS group, PCX/(siNC+miR-NC) treatment significantly increase median survival by 19%. PCX/(siNC+miR-210) and PCX/(siKRAS+miR-NC) further prolonged the survival of mice by 31% and 34%, respectively. PCX/(siKRAS+miR-210) nanoparticles achieved the cooperative activity to significantly improve the survival by 50% (**Figure 4.7**).

3.6 Toxicity evaluation *in vivo*

Blood was collected from nanoparticles treated mice for whole blood analysis and biochemistry test. As shown in **Figure 4.8**, PCX/(siKRAS+miR-210) nanoparticle treatment did not alter white blood cell (WBC), lymphocyte, monocyte, neutrophil and red blood cell (RBC) count in comparison with the PBS group, which suggested no syndrome, such as hemolytic anemia, and acute infection was caused by the nanoparticles. Liver enzymes and renal indicators were also measured. The concentrations of AST, ALT, BUN and creatinine were within the normal range, which indicated no obvious toxicity in the liver or kidney.

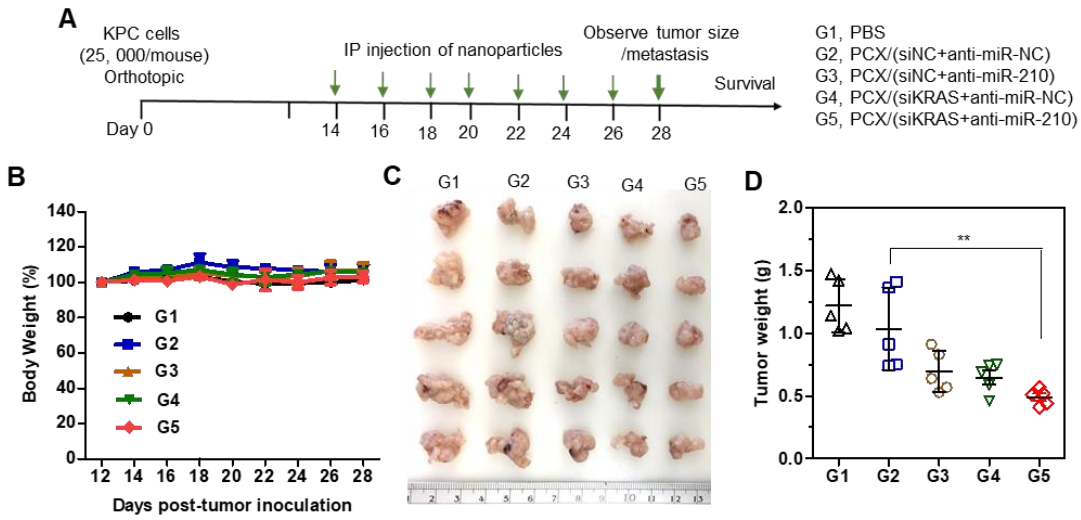

Figure 4.5. Inhibition of tumor growth *in vivo*. (A) Scheme of nanoparticles treatment. G1, PBS; G2, PCX/(siNC+anti-miR-NC); G3, PCX/(siNC+anti-miR-210); G4, PCX/(siKRAS+anti-miR-NC); G5, PCX/(siKRAS+anti-miR-210). (B) Body weight during the treatment. Data are shown as mean ± SD (n = 5). (C) Tumor tissues resected from mice on day 28. (D) Weights of tumors collected from the sacrificed mice. Data are shown as mean ± SD (n = 5). $^{**}P < 0.01$.

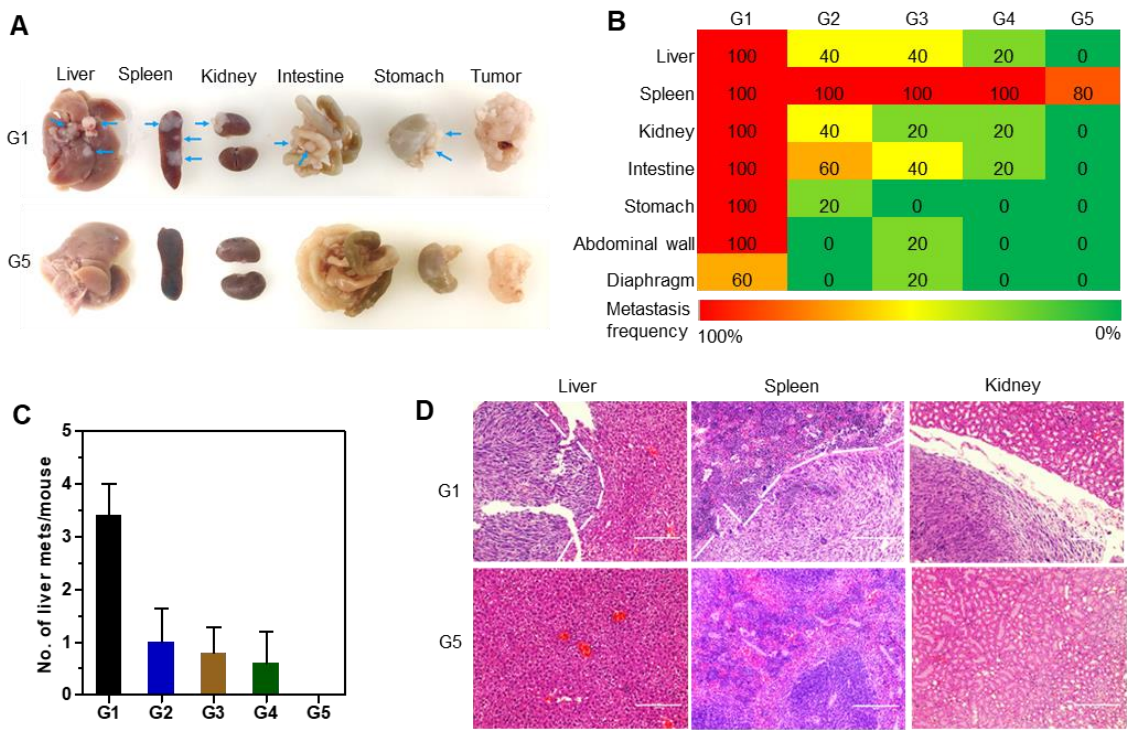

Figure 4.6. Inhibition of metastasis *in vivo*. (A) Tissues resected from mice on day 28. Arrow indicated tumor metastasis. (B) Heat map of tumor metastasis frequency in tissues. (C) Number of maco-metastasis on the surface of liver. (D) H&E staining of tissues. G1, PBS; G2, PCX/(siNC+anti-miR-NC); G3, PCX/(siNC+anti-miR-210); G4, PCX/(siKRAS+anti-miR-NC); G5, PCX/(siKRAS+anti-miR-210).

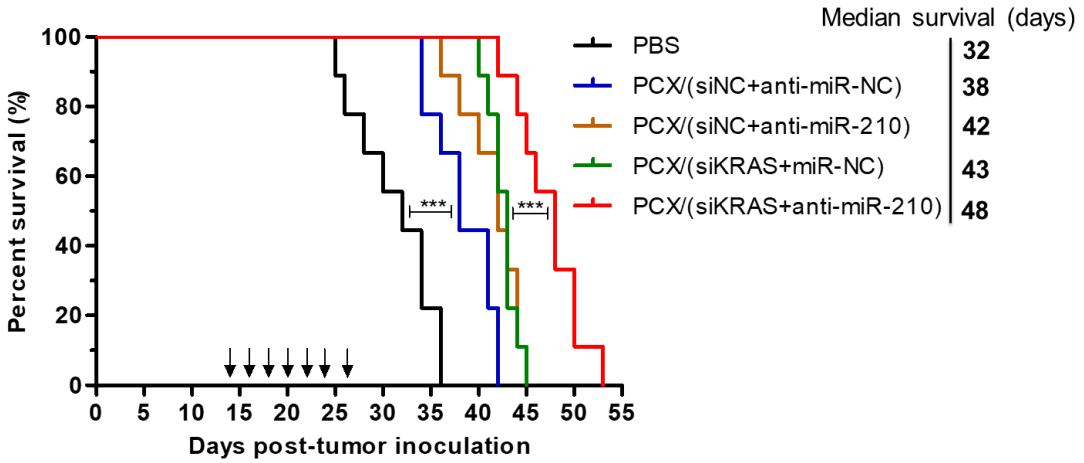

Figure 4.7. Kaplan–Meier survival graph of KPC mice. Log-rank Mantel–Cox test, ***$P <$ 0.0001.

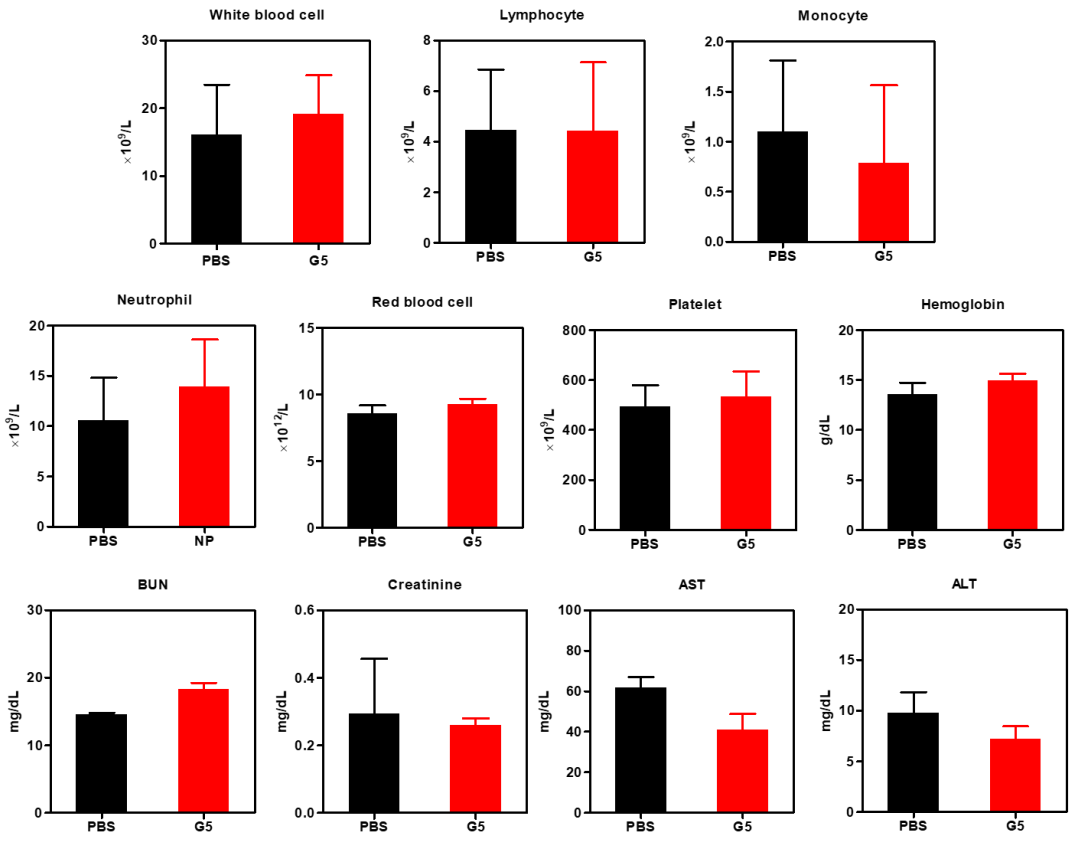

Figure 4.8. Whole blood and biochemistry analysis. G5, PCX/(siKRAS+anti-miR-210). Data are shown as mean ± SD (n = 3).

4.4 Conclusion

In this study, we developed a combination nanoparticle treatment approach through simultaneous inhibition of CXCR4 and knockdown of KRAS and miR-210 for metastatic pancreatic cancer therapy. CXCR4-inhibiting polycation PCX could condense siRNA and miRNA to form nanoparticles. Nanoparticles effectively delivered siRNA and miRNA inhibitor into PC cells and downregulated KRAS and miR-210, which resulted in significant cell killing. The nanoparticles specifically and highly accumulated in orthotopic tumor after IP injection. The IP injected combination nanoparticles achieved improved survival in orthotopic pancreatic cancer mice through inhibiting both primary tumor growth and metastasis. The nanoparticles represent a promising dual-function delivery platform for siRNA/miRNA codelivery and provide safe and effective nanomedicines for metastatic PC therapy.

Chapter 5 – SUMMERY AND FUTURE DIRECTIONS

5.1 Summary

The CXCR4/CXCL12 signaling axis plays a key role in tumor growth, metastasis, angiogenesis and cancer cell-microenvironment interaction. Inhibition of CXCR4 represents an effective strategy for metastatic cancer therapy. On the other hand, miRNAs function as tumor suppressors or oncogenes and participate in the regulation of tumorigenesis and progression. Inhibition of overexpressed oncogenic miRNAs or restitution of downregulated tumor-suppressor miRNAs provides a highly promising approach to treat cancer. Polymeric CXCR4 antagonist PCX is a dual-function polycation to inhibit CXCR4 and deliver nucleic acids. Here, we used PCX to form nanoparticles with therapeutic miRNA and then simultaneously delivered miRNA and inhibited CXCR4 for combined therapy in metastatic cancer.

PCX can inhibit CCA cell migration due to its CXCR4 antagonism. The ability of PCX to form polyplexes with nucleic acids was used for simultaneous delivery of miR-200c mimic into cells. The delivery of miR-200c resulted in reduced expression of the EMT inducer ZEB1. The combination treatment consisting of PCX and miR-200c resulted in cooperative anti-migration activity, most likely by coupling the CXCR4 axis blockade with EMT inhibition in the cholangiocarcinoma cells. PCX/miR-200c nanoparticles is a promising strategy for a combination therapy involving multiple migration pathways in metastatic CCA.

Moreover, we have developed a combination CCA treatment approach through inhibition of CXCR4 and miR-210. PCX could efficiently block the hypoxia-induced migration of CCA cells apparently through CXCR4 and LPA pathways. PCX/anti-miRNA nanoparticles delivered functional anti-miRNA to the CCA cells and downregulated miR-

210 expression, which resulted in significant cell killing through induction of apoptosis. PCX/anti-miR-210 nanoparticles sensitized CCA cells to GEM/CDDP chemotherapy. The combination nanoparticles achieved effective systemic delivery to CCA xenograft tumors and enhanced antitumor therapy *in vivo* through direct tumor growth inhibition and chemotherapy sensitization. The nanoparticles may represent an effective dual-function delivery platform for miRNA delivery and provide safe and effective nanomedicines for systemic CCA therapy.

On the other hand, we developed a combination nanoparticle treatment approach through simultaneous inhibition of CXCR4 and knockdown of mutant KRAS and miR-210 for metastatic pancreatic cancer therapy. PCX could condense siRNA and miRNA to form nanoparticles. Nanoparticles effectively delivered siRNA and miRNA inhibitor into PC cells and downregulated KRAS and miR-210, which resulted in significant cell killing. The nanoparticles specifically accumulated in orthotopic tumor after IP injection. The IP injected combination nanoparticles achieved improved survival in orthotopic PC mice through inhibition of primary tumor growth and metastasis. The CXCR4 targeted nanoparticles may provide a safe and effective platform for therapeutic siRNA/miRNA codelivery in metastatic PC therapy.

5.2 Future directions

Despite the great potential, there are still many challenges for the clinical use of the PCX/miRNA nanomedicines. Future directions will focus on improving their *in vivo* delivery to tumors. For example, recent studies reported that fluorination of polyplexes is able to improve nucleic acid delivery activity while reducing toxicity mainly by increasing stability and membrane transport properties [193-195]. Optimized fluorination of PCX is thus expected to improve their *in vivo* efficiency. Other approaches include zwitterionic

modifications [196, 197], and tumor targeting and penetrating moiety conjugation are also expected to enhance *in vivo* delivery of these nanomedicines [198, 199].

In addition to improving delivery, we also aim to combine the CXCR4 targeted nanomedicines with other therapies like immunotherapy. For example, recent studies confirm that CXCR4 inhibition is able to boost the PD-1/PD-L1 pathway blockade immunotherapy by facilitating T cell infiltration [16, 17, 200]. Intervention of PD-1/PD-L1 pathway via RNA interference (RNAi) also represents an effective approach to boost immunotherapy [201, 202]. Accordingly, use of CXCR4 targeted nanomedicine to deliver PD-L1 siRNA is a potential strategy for improved checkpoint blockade immunotherapy.

Future studies will also focus on the evaluation of the nanoparticles in preclinical animal models which are representative of human disease to facilitate their clinical translation. For example, we aim to test PCX/miR-200c and PCX/miR-210 nanoparticles in orthotopic and metastatic CCA animal models.

Bibliography

1. Xie Y, Wang Y, Li J, Hang Y, Oupický D. Promise of chemokine network-targeted nanoparticles in combination nucleic acid therapies of metastatic cancer. *Wiley Interdisciplinary Reviews: Nanomedicine and Nanobiotechnology* 2018:e1528.
2. Siegel RL, Miller KD, Jemal A. Cancer statistics, 2016. *CA: a cancer journal for clinicians* 2016, 66:7-30.
3. Li J, Wang Y, Zhu Y, Oupický D. Recent advances in delivery of drug–nucleic acid combinations for cancer treatment. *Journal of Controlled Release* 2013, 172:589-600.
4. Gandhi NS, Tekade RK, Chougule MB. Nanocarrier mediated delivery of siRNA/miRNA in combination with chemotherapeutic agents for cancer therapy: current progress and advances. *Journal of Controlled Release* 2014, 194:238-256.
5. Li Y, Maciel D, Rodrigues Jo, Shi X, Tomás H. Biodegradable polymer nanogels for drug/nucleic acid delivery. *Chemical reviews* 2015, 115:8564-8608.
6. Li J, Yu F, Chen Y, Oupický D. Polymeric drugs: Advances in the development of pharmacologically active polymers. *Journal of Controlled Release* 2015, 219:369-382.
7. Xie Y, Murray-Stewart T, Wang Y, Yu F, Li J, Marton LJ, Casero RA, Oupický D. Self-immolative nanoparticles for simultaneous delivery of microRNA and targeting of polyamine metabolism in combination cancer therapy. *Journal of Controlled Release* 2017, 246:110-119.
8. Zhao Y, Wang W, Guo S, Wang Y, Miao L, Xiong Y, Huang L. PolyMetformin combines carrier and anticancer activities for in vivo siRNA delivery. *Nature communications* 2016, 7.

9. Bao X, Wang W, Wang C, Wang Y, Zhou J, Ding Y, Wang X, Jin Y. A chitosan-graft-PEI-candesartan conjugate for targeted co-delivery of drug and gene in anti-angiogenesis cancer therapy. *Biomaterials* 2014, 35:8450-8466.

10. Wang Y, Xie Y, Oupický D. Potential of CXCR4/CXCL12 chemokine axis in cancer drug delivery. *Current pharmacology reports* 2016, 2:1-10.

11. Sleightholm RL, Neilsen BK, Li J, Steele MM, Singh RK, Hollingsworth MA, Oupicky D. Emerging roles of the CXCL12/CXCR4 axis in pancreatic cancer progression and therapy. *Pharmacology & therapeutics* 2017.

12. Guo F, Wang Y, Liu J, Mok S, Xue F, Zhang W. CXCL12/CXCR4: a symbiotic bridge linking cancer cells and their stromal neighbors in oncogenic communication networks. *Oncogene* 2016, 35:816.

13. Taichman RS, Cooper C, Keller ET, Pienta KJ, Taichman NS, McCauley LK. Use of the stromal cell-derived factor-1/CXCR4 pathway in prostate cancer metastasis to bone. *Cancer research* 2002, 62:1832-1837.

14. Zeng Z, Shi YX, Samudio IJ, Wang R-Y, Ling X, Frolova O, Levis M, Rubin JB, Negrin RR, Estey EH. Targeting the leukemia microenvironment by CXCR4 inhibition overcomes resistance to kinase inhibitors and chemotherapy in AML. *Blood* 2009, 113:6215-6224.

15. Singh S, Srivastava S, Bhardwaj A, Owen L, Singh A. CXCL12–CXCR4 signalling axis confers gemcitabine resistance to pancreatic cancer cells: a novel target for therapy. *British journal of cancer* 2010, 103:1671.

16. Feig C, Jones JO, Kraman M, Wells RJ, Deonarine A, Chan DS, Connell CM, Roberts EW, Zhao Q, Caballero OL. Targeting CXCL12 from FAP-expressing carcinoma-associated fibroblasts synergizes with anti–PD-L1 immunotherapy in pancreatic cancer. *Proc Natl Acad Sci U S A* 2013, 110:20212-20217.

17. Chen Y, Ramjiawan RR, Reiberger T, Ng MR, Hato T, Huang Y, Ochiai H, Kitahara S, Unan EC, Reddy TP. CXCR4 inhibition in tumor microenvironment facilitates anti-programmed death receptor-1 immunotherapy in sorafenib-treated hepatocellular carcinoma in mice. *Hepatology* 2015, 61:1591-1602.

18. Li J, Zhu Y, Hazeldine ST, Li C, Oupický D. Dual-Function CXCR4 Antagonist Polyplexes To Deliver Gene Therapy and Inhibit Cancer Cell Invasion. *Angewandte Chemie International Edition* 2012, 51:8740-8743.

19. Wang Y, Hazeldine ST, Li J, Oupický D. Development of functional poly (amido amine) CXCR4 antagonists with the ability to mobilize leukocytes and deliver nucleic acids. *Advanced healthcare materials* 2015, 4:729-738.

20. Li J, Oupický D. Effect of biodegradability on CXCR4 antagonism, transfection efficacy and antimetastatic activity of polymeric Plerixafor. *Biomaterials* 2014, 35:5572-5579.

21. Wang Y, Kumar S, Rachagani S, Sajja BR, Xie Y, Hang Y, Jain M, Li J, Boska MD, Batra SK. Polyplex-mediated inhibition of chemokine receptor CXCR4 and chromatin-remodeling enzyme NCOA3 impedes pancreatic cancer progression and metastasis. *Biomaterials* 2016, 101:108-120.

22. Xie Y, Yu F, Tang W, Alade BO, Peng ZH, Wang Y, Li J, Oupický D. Synthesis and Evaluation of Chloroquine-Containing DMAEMA Copolymers as Efficient Anti-miRNA Delivery Vectors with Improved Endosomal Escape and Antimigratory Activity in Cancer Cells. *Macromolecular Bioscience* 2017.

23. Domanska UM, Kruizinga RC, Nagengast WB, Timmer-Bosscha H, Huls G, de Vries EG, Walenkamp AM. A review on CXCR4/CXCL12 axis in oncology: no place to hide. *European journal of cancer* 2013, 49:219-230.

24. Burger JA, Kipps TJ. CXCR4: a key receptor in the crosstalk between tumor cells and their microenvironment. *Blood* 2006, 107:1761-1767.

25. Kubic JD, Lui JW, Little EC, Ludvik AE, Konda S, Salgia R, Aplin AE, Lang D. PAX3 and FOXD3 promote CXCR4 expression in melanoma. *Journal of Biological Chemistry* 2015, 290:21901-21914.

26. Phillips RJ, Mestas J, Gharaee-Kermani M, Burdick MD, Sica A, Belperio JA, Keane MP, Strieter RM. Epidermal growth factor and hypoxia-induced expression of CXC chemokine receptor 4 on non-small cell lung cancer cells is regulated by the phosphatidylinositol 3-kinase/PTEN/AKT/mammalian target of rapamycin signaling pathway and activation of hypoxia inducible factor-1α. *Journal of Biological Chemistry* 2005, 280:22473-22481.

27. Andre F, Xia W, Conforti R, Wei Y, Boulet T, Tomasic G, Spielmann M, Zoubir M, Berrada N, Arriagada R, et al. CXCR4 Expression in Early Breast Cancer and Risk of Distant Recurrence. *The Oncologist* 2009, 14:1182-1188.

28. Kato M, Kitayama J, Kazama S, Nagawa H. Expression pattern of CXC chemokine receptor-4 is correlated with lymph node metastasis in human invasive ductal carcinoma. *Breast Cancer Research* 2003, 5:R144.

29. Scala S, Ottaiano A, Ascierto PA, Cavalli M, Simeone E, Giuliano P, Napolitano M, Franco R, Botti G, Castello G. Expression of CXCR4 predicts poor prognosis in patients with malignant melanoma. *Clinical Cancer Research* 2005, 11:1835-1841.

30. Sun X, Cheng G, Hao M, Zheng J, Zhou X, Zhang J, Taichman RS, Pienta KJ, Wang J. CXCL12/CXCR4/CXCR7 chemokine axis and cancer progression. *Cancer and Metastasis Reviews* 2010, 29:709-722.

31. Broxmeyer HE, Orschell CM, Clapp DW, Hangoc G, Cooper S, Plett PA, Liles WC, Li X, Graham-Evans B, Campbell TB. Rapid mobilization of murine and human hematopoietic stem and progenitor cells with AMD3100, a CXCR4 antagonist. *Journal of Experimental Medicine* 2005, 201:1307-1318.

32. Burger J, Peled A. CXCR4 antagonists: targeting the microenvironment in leukemia and other cancers. *Leukemia (08876924)* 2009, 23.

33. Hassan S, Buchanan M, Jahan K, Aguilar-Mahecha A, Gaboury L, Muller WJ, Alsawafi Y, Mourskaia AA, Siegel PM, Salvucci O. CXCR4 peptide antagonist inhibits primary breast tumor growth, metastasis and enhances the efficacy of anti-VEGF treatment or docetaxel in a transgenic mouse model. *International journal of cancer* 2011, 129:225-232.

34. Galsky MD, Vogelzang NJ, Conkling P, Raddad E, Polzer J, Roberson S, Stille JR, Saleh M, Thornton D. A phase I trial of LY2510924, a CXCR4 peptide antagonist, in patients with advanced cancer. *Clinical Cancer Research* 2014, 20:3581-3588.

35. Liang Z, Yoon Y, Votaw J, Goodman MM, Williams L, Shim H. Silencing of CXCR4 blocks breast cancer metastasis. *Cancer research* 2005, 65:967-971.

36. Jiang K, Li J, Yin J, Ma Q, Yan B, Zhang X, Wang L, Wang L, Liu T, Zhang Y. Targeted delivery of CXCR4-siRNA by scFv for HER2+ breast cancer therapy. *Biomaterials* 2015, 59:77-87.

37. Nervi B, Ramirez P, Rettig MP, Uy GL, Holt MS, Ritchey JK, Prior JL, Piwnica-Worms D, Bridger G, Ley TJ. Chemosensitization of acute myeloid leukemia (AML) following mobilization by the CXCR4 antagonist AMD3100. *Blood* 2009, 113:6206-6214.

38. Mori T, Doi R, Koizumi M, Toyoda E, Ito D, Kami K, Masui T, Fujimoto K, Tamamura H, Hiramatsu K. CXCR4 antagonist inhibits stromal cell-derived factor 1-induced migration and invasion of human pancreatic cancer. *Molecular Cancer Therapeutics* 2004, 3:29-37.

39. Mei L, Liu Y, Zhang Q, Gao H, Zhang Z, He Q. Enhanced antitumor and anti-metastasis efficiency via combined treatment with CXCR4 antagonist and liposomal doxorubicin. *Journal of Controlled Release* 2014, 196:324-331.

40. Gallo J, Kamaly N, Lavdas I, Stevens E, Nguyen QD, Wylezinska-Arridge M, Aboagye EO, Long NJ. CXCR4-Targeted and MMP-Responsive Iron Oxide Nanoparticles for Enhanced Magnetic Resonance Imaging. *Angewandte Chemie International Edition* 2014, 53:9550-9554.

41. de la Torre C, Casanova I, Acosta G, Coll C, Moreno MJ, Albericio F, Aznar E, Mangues R, Royo M, Sancenón F. Gated Mesoporous Silica Nanoparticles Using a Double-Role Circular Peptide for the Controlled and Target-Preferential Release of Doxorubicin in CXCR4-Expresing Lymphoma Cells. *Advanced Functional Materials* 2015, 25:687-695.

42. Zhao Y, Detering L, Sultan D, Cooper ML, You M, Cho S, Meier SL, Luehmann H, Sun G, Rettig M. Gold Nanoclusters-Doped With 64Cu for CXCR4 Positron Emission Tomography Imaging of Breast Cancer and Metastasis. *ACS nano* 2016, 10:5959.

43. Zhang F, Gong S, Wu J, Li H, Oupicky D, Sun M. CXCR4-Targeted and Redox Responsive Dextrin Nanogel for Metastatic Breast Cancer Therapy. *Biomacromolecules* 2017, 18:1793-1802.

44. Gao D-Y, Lin T-T, Sung Y-C, Liu YC, Chiang W-H, Chang C-C, Liu J-Y, Chen Y. CXCR4-targeted lipid-coated PLGA nanoparticles deliver sorafenib and overcome acquired drug resistance in liver cancer. *Biomaterials* 2015, 67:194-203.

45. Li H, Wang K, Yang X, Zhou Y, Ping Q, Oupicky D, Sun M. Dual-function nanostructured lipid carriers to deliver IR780 for breast cancer treatment: Anti-

metastatic and photothermal anti-tumor therapy. *Acta Biomaterialia* 2017, 53:399-413.

46. Li H, Yang X, Zhou Z, Wang K, Li C, Qiao H, Oupicky D, Sun M. Near-infrared light-triggered drug release from a multiple lipid carrier complex using an all-in-one strategy. *Journal of Controlled Release* 2017, 261:126-137.
47. Daka A, Peer D. RNAi-based nanomedicines for targeted personalized therapy. *Advanced drug delivery reviews* 2012, 64:1508-1521.
48. Lam JK, Chow MY, Zhang Y, Leung SW. siRNA versus miRNA as therapeutics for gene silencing. *Molecular Therapy-Nucleic Acids* 2015, 4:e252.
49. Davidson BL, McCray PB. Current prospects for RNA interference-based therapies. *Nature Reviews Genetics* 2011, 12.
50. Devi G. siRNA-based approaches in cancer therapy. *Cancer gene therapy* 2006, 13.
51. Bartel DP. MicroRNAs: genomics, biogenesis, mechanism, and function. *cell* 2004, 116:281-297.
52. Croce CM. Causes and consequences of microRNA dysregulation in cancer. *Nature reviews. Genetics* 2009, 10:704.
53. Hayes J, Peruzzi PP, Lawler S. MicroRNAs in cancer: biomarkers, functions and therapy. *Trends in molecular medicine* 2014, 20:460-469.
54. Conde J, Artzi N. Are RNAi and miRNA therapeutics truly dead? *Trends in biotechnology* 2015, 33:141-144.
55. Chakraborty C, Sharma A, Sharma G, Doss CGP, Lee S-S. Therapeutic miRNA and siRNA: moving from bench to clinic as next generation medicine. *Molecular Therapy-Nucleic Acids* 2017.
56. Dowdy SF. Overcoming cellular barriers for RNA therapeutics. *Nature Biotechnology* 2017, 35:222-229.

57. Whitehead KA, Langer R, Anderson DG. Knocking down barriers: advances in siRNA delivery. *Nature reviews Drug discovery* 2009, 8.

58. Wang Y, Li J, Chen Y, Oupický D. Balancing polymer hydrophobicity for ligand presentation and siRNA delivery in dual function CXCR4 inhibiting polyplexes. *Biomaterials science* 2015, 3:1114-1123.

59. Xie Y, Wehrkamp CJ, Li J, Wang Y, Wang Y, Mott JL, Oupický D. Delivery of miR-200c mimic with poly (amido amine) CXCR4 antagonists for combined inhibition of cholangiocarcinoma cell invasiveness. *Molecular pharmaceutics* 2016, 13:1073-1080.

60. Peng Z-H, Xie Y, Wang Y, Li J, Oupický D. Dual-Function Polymeric HPMA Prodrugs for the Delivery of miRNA. *Molecular Pharmaceutics* 2017, 14:1395-1404.

61. Liu J-Y, Chiang T, Liu C-H, Chern G-G, Lin T-T, Gao D-Y, Chen Y. Delivery of siRNA using CXCR4-targeted nanoparticles modulates tumor microenvironment and achieves a potent antitumor response in liver cancer. *Molecular Therapy* 2015, 23:1772-1782.

62. Egorova A, Shubina A, Sokolov D, Selkov S, Baranov V, Kiselev A. CXCR4-targeted modular peptide carriers for efficient anti-VEGF siRNA delivery. *International journal of pharmaceutics* 2016, 515:431-440.

63. Landry B, Gül-Uludağ H, Plianwong S, Kucharski C, Zak Z, Parmar MB, Kutsch O, Jiang H, Brandwein J, Uludağ H. Targeting CXCR4/SDF-1 axis by lipopolymer complexes of siRNA in acute myeloid leukemia. *Journal of Controlled Release* 2016, 224:8-21.

64. Rhodes LV, Short SP, Neel NF, Salvo VA, Zhu Y, Elliott S, Wei Y, Yu D, Sun M, Muir SE. Cytokine receptor CXCR4 mediates estrogen-independent

tumorigenesis, metastasis, and resistance to endocrine therapy in human breast cancer. *Cancer research* 2011, 71:603-613.

65. De Clercq E. The bicyclam AMD3100 story. *Nature reviews Drug discovery* 2003, 2:581-587.

66. Debnath B, Xu S, Grande F, Garofalo A, Neamati N. Small molecule inhibitors of CXCR4. *Theranostics* 2013, 3:47.

67. Wong D, Korz W. Translating an antagonist of chemokine receptor CXCR4: from bench to bedside. *Clinical Cancer Research* 2008, 14:7975-7980.

68. Bridger GJ, Skerlj RT, Hernandez-Abad PE, Bogucki DE, Wang Z, Zhou Y, Nan S, Boehringer EM, Wilson T, Crawford J. Synthesis and structure− activity relationships of azamacrocyclic CXC chemokine receptor 4 antagonists: Analogues containing a single azamacrocyclic ring are potent inhibitors of T-cell tropic (X4) HIV-1 replication. *Journal of medicinal chemistry* 2009, 53:1250-1260.

69. Oupicky D, Ogris M, Howard KA, Dash PR, Ulbrich K, Seymour LW. Importance of lateral and steric stabilization of polyelectrolyte gene delivery vectors for extended systemic circulation. *Molecular Therapy* 2002, 5:463-472.

70. Ogris M, Brunner S, Schüller S, Kircheis R, Wagner E. PEGylated DNA/transferrin–PEI complexes: reduced interaction with blood components, extended circulation in blood and potential for systemic gene delivery. *Gene therapy* 1999, 6.

71. Wang Y, Li J, Oupický D. Polymeric plerixafor: effect of PEGylation on CXCR4 antagonism, cancer cell invasion, and DNA transfection. *Pharmaceutical research* 2014, 31:3538-3548.

72. Kumar S, Das S, Rachagani S, Kaur S, Joshi S, Johansson S, Ponnusamy M, Jain M, Batra S. NCOA3-mediated upregulation of mucin expression via

transcriptional and post-translational changes during the development of pancreatic cancer. *Oncogene* 2015, 34:4879-4889.

73. Oishi N, Kumar MR, Roessler S, Ji J, Forgues M, Budhu A, Zhao X, Andersen JB, Ye QH, Jia HL. Transcriptomic profiling reveals hepatic stem-like gene signatures and interplay of miR-200c and epithelial-mesenchymal transition in intrahepatic cholangiocarcinoma. *Hepatology* 2012, 56:1792-1803.

74. Eng CH, Wang Z, Tkach D, Toral-Barza L, Ugwonali S, Liu S, Fitzgerald SL, George E, Frias E, Cochran N. Macroautophagy is dispensable for growth of KRAS mutant tumors and chloroquine efficacy. *Proceedings of the National Academy of Sciences* 2016, 113:182-187.

75. King M, Ganley I, Flemington V. Inhibition of cholesterol metabolism underlies synergy between mTOR pathway inhibition and chloroquine in bladder cancer cells. *Oncogene* 2016, 35:4518-4528.

76. Solomon VR, Lee H. Chloroquine and its analogs: a new promise of an old drug for effective and safe cancer therapies. *European journal of pharmacology* 2009, 625:220-233.

77. Janku F, McConkey DJ, Hong DS, Kurzrock R. Autophagy as a target for anticancer therapy. *Nature reviews Clinical oncology* 2011, 8:528-539.

78. Kim J, Yip MR, Shen X, Li H, Hsin L-YC, Labarge S, Heinrich EL, Lee W, Lu J, Vaidehi N. Identification of anti-malarial compounds as novel antagonists to chemokine receptor CXCR4 in pancreatic cancer cells. *PLoS One* 2012, 7:e31004.

79. Balic A, Sørensen MD, Trabulo SM, Sainz B, Cioffi M, Vieira CR, Miranda-Lorenzo I, Hidalgo M, Kleeff J, Erkan M. Chloroquine targets pancreatic cancer stem cells via inhibition of CXCR4 and hedgehog signaling. *Molecular cancer therapeutics* 2014, 13:1758-1771.

80. Yu F, Xie Y, Wang Y, Peng Z-H, Li J, Oupický D. Chloroquine-containing HPMA copolymers as polymeric inhibitors of cancer cell migration mediated by the CXCR4/SDF-1 chemokine axis. *ACS macro letters* 2016, 5:342.

81. Yu F, Li J, Xie Y, Sleightholm RL, Oupický D. Polymeric chloroquine as an inhibitor of cancer cell migration and experimental lung metastasis. *Journal of Controlled Release* 2016, 244:347-356.

82. Sleightholm R, Yang B, Yu F, Xie Y, Oupický D. Chloroquine-Modified Hydroxyethyl Starch as a Polymeric Drug for Cancer Therapy. *Biomacromolecules* 2017, 18:2247-2257.

83. Pack DW, Hoffman AS, Pun S, Stayton PS. Design and development of polymers for gene delivery. *Nature reviews Drug discovery* 2005, 4:581-593.

84. Perche F, Yi Y, Hespel L, Mi P, Dirisala A, Cabral H, Miyata K, Kataoka K. Hydroxychloroquine-conjugated gold nanoparticles for improved siRNA activity. *Biomaterials* 2016, 90:62-71.

85. Vaupel P, Mayer A. Hypoxia in cancer: significance and impact on clinical outcome. *Cancer and Metastasis Reviews* 2007, 26:225-239.

86. Vaupel P, Kelleher DK, Höckel M. Oxygenation status of malignant tumors: pathogenesis of hypoxia and significance for tumor therapy. In: *Seminars in oncology*: Elsevier; 2001.

87. Samanta D, Gilkes DM, Chaturvedi P, Xiang L, Semenza GL. Hypoxia-inducible factors are required for chemotherapy resistance of breast cancer stem cells. *Proceedings of the National Academy of Sciences* 2014, 111:E5429-E5438.

88. Muz B, de la Puente P, Azab F, Azab AK. The role of hypoxia in cancer progression, angiogenesis, metastasis, and resistance to therapy. *Hypoxia* 2015, 3:83.

89. Schioppa T, Uranchimeg B, Saccani A, Biswas SK, Doni A, Rapisarda A, Bernasconi S, Saccani S, Nebuloni M, Vago L. Regulation of the chemokine receptor CXCR4 by hypoxia. *Journal of Experimental Medicine* 2003, 198:1391-1402.

90. Fiegl M, Samudio I, Clise-Dwyer K, Burks JK, Mnjoyan Z, Andreeff M. CXCR4 expression and biologic activity in acute myeloid leukemia are dependent on oxygen partial pressure. *Blood* 2009, 113:1504-1512.

91. Huang X, Ding L, Bennewith KL, Tong RT, Welford SM, Ang KK, Story M, Le Q-T, Giaccia AJ. Hypoxia-inducible mir-210 regulates normoxic gene expression involved in tumor initiation. *Molecular cell* 2009, 35:856-867.

92. Pulkkinen K, Malm T, Turunen M, Koistinaho J, Ylä-Herttuala S. Hypoxia induces microRNA miR-210 in vitro and in vivo. *FEBS letters* 2008, 582:2397-2401.

93. Chan SY, Loscalzo J. MicroRNA-210: a unique and pleiotropic hypoxamir. *Cell cycle* 2010, 9:1072-1083.

94. Chan YC, Banerjee J, Choi SY, Sen CK. miR-210: The master hypoxamir. *Microcirculation* 2012, 19:215-223.

95. Huang Y-P, Hung C-M, Hsu Y-C, Zhong C-Y, Wang W-R, Chang C-C, Lee M-J. Suppression of breast cancer cell migration by small interfering RNA delivered by polyethylenimine-functionalized graphene oxide. *Nanoscale research letters* 2016, 11:247.

96. Abedini F, Ismail M, Hosseinkhani H, Ibrahim TAT, Omar AR, Chong PP, Bejo MH, Domb AJ. Effects of CXCR4 siRNA/dextran-spermine nanoparticles on CXCR4 expression and serum LDH levels in a mouse model of colorectal cancer metastasis to the liver. *Cancer management and research* 2011, 3:301.

97. Abedini F, Hosseinkhani H, Ismail M, Domb AJ, Omar AR, Chong PP, Hong P-D, Yu D-S, Farber I-Y. Cationized dextran nanoparticle-encapsulated CXCR4-

siRNA enhanced correlation between CXCR4 expression and serum alkaline phosphatase in a mouse model of colorectal cancer. *International journal of nanomedicine* 2012, 7:4159.

98. Patel T. Cholangiocarcinoma—controversies and challenges. *Nature Reviews Gastroenterology and Hepatology* 2011, 8:189-200.

99. Khan SA, Thomas HC, Davidson BR, Taylor-Robinson SD. Cholangiocarcinoma. *The Lancet* 2005, 366:1303-1314.

100. Rizvi S, Gores GJ. Pathogenesis, diagnosis, and management of cholangiocarcinoma. *Gastroenterology* 2013, 145:1215-1229.

101. Okuda K, Nakanuma Y, Miyazaki M. Cholangiocarcinoma: recent progress. Part 2: molecular pathology and treatment. *Journal of gastroenterology and hepatology* 2002, 17:1056-1063.

102. Sia D, Tovar V, Moeini A, Llovet J. Intrahepatic cholangiocarcinoma: pathogenesis and rationale for molecular therapies. *Oncogene* 2013, 32:4861-4870.

103. Wu Y, Crawford M, Yu B, Mao Y, Nana-Sinkam SP, Lee LJ. MicroRNA delivery by cationic lipoplexes for lung cancer therapy. *Molecular pharmaceutics* 2011, 8:1381-1389.

104. Croce CM. Causes and consequences of microRNA dysregulation in cancer. *Nature Reviews Genetics* 2009, 10:704-714.

105. Kasinski AL, Slack FJ. MicroRNAs en route to the clinic: progress in validating and targeting microRNAs for cancer therapy. *Nature reviews Cancer* 2011, 11:849-864.

106. Mott JL. MicroRNAs involved in tumor suppressor and oncogene pathways: implications for hepatobiliary neoplasia. *Hepatology* 2009, 50:630-637.

107. Razumilava N, Bronk SF, Smoot RL, Fingas CD, Werneburg NW, Roberts LR, Mott JL. miR-25 targets TNF-related apoptosis inducing ligand (TRAIL) death receptor-4 and promotes apoptosis resistance in cholangiocarcinoma. *Hepatology* 2012, 55:465-475.

108. Meng F, Henson R, Lang M, Wehbe H, Maheshwari S, Mendell JT, Jiang J, Schmittgen TD, Patel T. Involvement of human micro-RNA in growth and response to chemotherapy in human cholangiocarcinoma cell lines. *Gastroenterology* 2006, 130:2113-2129.

109. Selaru FM, Olaru AV, Kan T, David S, Cheng Y, Mori Y, Yang J, Paun B, Jin Z, Agarwal R. MicroRNA-21 is overexpressed in human cholangiocarcinoma and regulates programmed cell death 4 and tissue inhibitor of metalloproteinase 3. *Hepatology* 2009, 49:1595-1601.

110. Chusorn P, Namwat N, Loilome W, Techasen A, Pairojkul C, Khuntikeo N, Dechakhamphu A, Talabnin C, Chan-On W, Ong C. Overexpression of microRNA-21 regulating PDCD4 during tumorigenesis of liver fluke-associated cholangiocarcinoma contributes to tumor growth and metastasis. *Tumor Biology* 2013, 34:1579-1588.

111. Li B, Han Q, Zhu Y, Yu Y, Wang J, Jiang X. Down-regulation of miR-214 contributes to intrahepatic cholangiocarcinoma metastasis by targeting Twist. *FEBS Journal* 2012, 279:2393-2398.

112. Chen Y, Gao D-Y, Huang L. In vivo delivery of miRNAs for cancer therapy: challenges and strategies. *Advanced drug delivery reviews* 2015, 81:128-141.

113. Cheng CJ, Saltzman WM. Polymer nanoparticle-mediated delivery of microRNA inhibition and alternative splicing. *Molecular pharmaceutics* 2012, 9:1481-1488.

114. Zhang Y, Wang Z, Gemeinhart RA. Progress in microRNA delivery. *Journal of Controlled Release* 2013, 172:962-974.

115. Kumar V, Mondal G, Slavik P, Rachagani S, Batra SK, Mahato RI. Codelivery of small molecule hedgehog inhibitor and miRNA for treating pancreatic cancer. *Mol. Pharm.* 2015, 12:1289-1298.

116. Devulapally R, Sekar NM, Sekar TV, Foygel K, Massoud TF, Willmann JrK, Paulmurugan R. Polymer nanoparticles mediated codelivery of antimiR-10b and antimiR-21 for achieving triple negative breast cancer therapy. *ACS nano* 2015, 9:2290-2302.

117. Hanahan D, Weinberg RA. Hallmarks of cancer: the next generation. *cell* 2011, 144:646-674.

118. Fidler IJ. The pathogenesis of cancer metastasis: the'seed and soil'hypothesis revisited. *Nature Reviews Cancer* 2003, 3:453-458.

119. Ohira S, Sasaki M, Harada K, Sato Y, Zen Y, Isse K, Kozaka K, Ishikawa A, Oda K, Nimura Y. Possible regulation of migration of intrahepatic cholangiocarcinoma cells by interaction of CXCR4 expressed in carcinoma cells with tumor necrosis factor-α and stromal-derived factor-1 released in stroma. *The American journal of pathology* 2006, 168:1155-1168.

120. Guo P, You J-O, Yang J, Moses MA, Auguste DT. Using breast cancer cell CXCR4 surface expression to predict liposome binding and cytotoxicity. *Biomaterials* 2012, 33:8104-8110.

121. Wang B, Guo P, Auguste DT. Mapping the CXCR4 receptor on breast cancer cells. *Biomaterials* 2015, 57:161-168.

122. Kucia M, Reca R, Miekus K, Wanzeck J, Wojakowski W, Janowska-Wieczorek A, Ratajczak J, Ratajczak MZ. Trafficking of Normal Stem Cells and Metastasis of Cancer Stem Cells Involve Similar Mechanisms: Pivotal Role of the SDF-1–CXCR4 Axis. *Stem Cells* 2005, 23:879-894.

123. Smith MC, Luker KE, Garbow JR, Prior JL, Jackson E, Piwnica-Worms D, Luker GD. CXCR4 regulates growth of both primary and metastatic breast cancer. *Cancer research* 2004, 64:8604-8612.

124. Balkwill F. Cancer and the chemokine network. *Nature Reviews Cancer* 2004, 4:540-550.

125. Guo P, You J-O, Yang J, Jia D, Moses MA, Auguste DT. Inhibiting metastatic breast cancer cell migration via the synergy of targeted, pH-triggered siRNA delivery and chemokine axis blockade. *Molecular pharmaceutics* 2014, 11:755-765.

126. Li J, Zhu Y, Hazeldine ST, Li C, Oupicky D. Dual-function CXCR4 antagonist polyplexes to deliver gene therapy and inhibit cancer cell invasion. *Angew Chem Int Ed Engl* 2012, 51:8740-8743.

127. Wang Y, Hazeldine ST, Li J, Oupicky D. Development of Functional Poly(amido amine) CXCR4 Antagonists with the Ability to Mobilize Leukocytes and Deliver Nucleic Acids. *Adv Healthc Mater* 2015, 4:729-738.

128. Wang Y, Li J, Chen Y, Oupicky D. Balancing polymer hydrophobicity for ligand presentation and siRNA delivery in dual function CXCR4 inhibiting polyplexes. *Biomater Sci* 2015, 3:1114-1123.

129. Li J, Oupicky D. Effect of biodegradability on CXCR4 antagonism, transfection efficacy and antimetastatic activity of polymeric Plerixafor. *Biomaterials* 2014, 35:5572-5579.

130. Miyagiwa M, Ichida T, Tokiwa T, Sato J, Sasaki H. A new human cholangiocellular carcinoma cell line (HuCC-T1) producing carbohydrate antigen 19/9 in serum-free medium. *In vitro cellular & developmental biology* 1989, 25:503-510.

131. Wehrkamp CJ, Gutwein AR, Natarajan SK, Phillippi MA, Mott JL. XIAP Antagonist Embelin Inhibited Proliferation of Cholangiocarcinoma Cells. *PloS one* 2014, 9:90238.

132. Gregory PA, Bert AG, Paterson EL, Barry SC, Tsykin A, Farshid G, Vadas MA, Khew-Goodall Y, Goodall GJ. The miR-200 family and miR-205 regulate epithelial to mesenchymal transition by targeting ZEB1 and SIP1. *Nature cell biology* 2008, 10:593-601.

133. Korpal M, Lee ES, Hu G, Kang Y. The miR-200 family inhibits epithelial-mesenchymal transition and cancer cell migration by direct targeting of E-cadherin transcriptional repressors ZEB1 and ZEB2. *Journal of Biological Chemistry* 2008, 283:14910-14914.

134. Xie Y, Wang Y, Li J, Hang Y, Jaramillo L, Wehrkamp CJ, Phillippi MA, Mohr AM, Chen Y, Talmon GA. Cholangiocarcinoma therapy with nanoparticles that combine downregulation of MicroRNA-210 with inhibition of cancer cell invasiveness. *Theranostics* 2018, 8:4305.

135. Razumilava N, Gores GJ. Cholangiocarcinoma. *The Lancet* 2014, 383:2168-2179.

136. Bridgewater J, Galle PR, Khan SA, Llovet JM, Park J-W, Patel T, Pawlik TM, Gores GJ. Guidelines for the diagnosis and management of intrahepatic cholangiocarcinoma. *Journal of hepatology* 2014, 60:1268-1289.

137. Sia D, Tovar V, Moeini A, Llovet J. Intrahepatic cholangiocarcinoma: pathogenesis and rationale for molecular therapies. *Oncogene* 2013, 32:4861.

138. Valle J, Wasan H, Palmer DH, Cunningham D, Anthoney A, Maraveyas A, Madhusudan S, Iveson T, Hughes S, Pereira SP. Cisplatin plus gemcitabine versus gemcitabine for biliary tract cancer. *New England Journal of Medicine* 2010, 362:1273-1281.

139. Valle JW, Wasan H, Johnson P, Jones E, Dixon L, Swindell R, Baka S, Maraveyas A, Corrie P, Falk S. Gemcitabine alone or in combination with cisplatin in patients with advanced or metastatic cholangiocarcinomas or other biliary tract tumours: a multicentre randomised phase II study–The UK ABC-01 Study. *British journal of cancer* 2009, 101:621.

140. Tan X-Y, Chang S, Liu W, Tang H-H. Silencing of CXCR4 inhibits tumor cell proliferation and neural invasion in human hilar cholangiocarcinoma. *Gut and liver* 2014, 8:196.

141. Balkwill F. Cancer and the chemokine network. *Nature Reviews Cancer* 2004, 4:540.

142. Leelawat K, Keeratichamroen S, Leelawat S, Tohtong R. CD24 induces the invasion of cholangiocarcinoma cells by upregulating CXCR4 and increasing the phosphorylation of ERK1/2. *Oncology letters* 2013, 6:1439-1446.

143. Mayr C, Neureiter D, Pichler M, Berr F, Wagner A, Kiesslich T, Namberger K. Cytotoxic effects of chemokine receptor 4 inhibition by AMD3100 in biliary tract cancer cells: Potential drug synergism with gemcitabine. *Molecular medicine reports* 2015, 12:2247-2252.

144. Jung M, Rho J, Kim Y, Jung J, Jin Y, Ko Y, Lee J, Lee S, Lee J, Park M. Upregulation of CXCR4 is functionally crucial for maintenance of stemness in drug-resistant non-small cell lung cancer cells. *Oncogene* 2013, 32:209.

145. Singh AP, Arora S, Bhardwaj A, Srivastava SK, Kadakia MP, Wang B, Grizzle WE, Owen LB, Singh S. CXCL12/CXCR4 Protein Signaling Axis Induces Sonic Hedgehog Expression in Pancreatic Cancer Cells via Extracellular Regulated Kinase-and Akt Kinase-mediated Activation of Nuclear Factor κB IMPLICATIONS FOR BIDIRECTIONAL TUMOR-STROMAL INTERACTIONS. *Journal of Biological Chemistry* 2012, 287:39115-39124.

146. Croce CM. Causes and consequences of microRNA dysregulation in cancer. *Nature reviews genetics* 2009, 10:704.

147. Natarajan SK, Stringham BA, Mohr AM, Wehrkamp CJ, Lu S, Phillippi MA, Harrison-Findik D, Mott JL. FoxO3 increases miR-34a to cause palmitate-induced cholangiocyte lipoapoptosis. *Journal of lipid research* 2017:jlr. M071357.

148. Xie Y, Zhang H, Guo X-J, Feng Y-C, He R-Z, Li X, Yu S, Zhao Y, Shen M, Zhu F. Let-7c inhibits cholangiocarcinoma growth but promotes tumor cell invasion and growth at extrahepatic sites. *Cell death & disease* 2018, 9:249.

149. Li L, Piontek K, Ishida M, Fausther M, Dranoff JA, Fu R, Mezey E, Gould SJ, Fordjour FK, Meltzer SJ. Extracellular vesicles carry microRNA-195 to intrahepatic cholangiocarcinoma and improve survival in a rat model. *Hepatology* 2017, 65:501-514.

150. Kwon H, Song K, Han C, Zhang J, Lu L, Chen W, Wu T. Epigenetic silencing of miRNA-34a in human cholangiocarcinoma via EZH2 and DNA methylation: impact on regulation of notch pathway. *The American journal of pathology* 2017, 187:2288-2299.

151. Li H, Zhou ZQ, Yang ZR, Tong DN, Guan J, Shi BJ, Nie J, Ding XT, Li B, Zhou GW. MicroRNA-191 acts as a tumor promoter by modulating the TET1–p53 pathway in intrahepatic cholangiocarcinoma. *Hepatology* 2017, 66:136-151.

152. Pulkkinen K, Malm T, Turunen M, Koistinaho J, Ylä-Herttuala S. Hypoxia induces microRNA miR-210 in vitro and in vivo: Ephrin-A3 and neuronal pentraxin 1 are potentially regulated by miR-210. *FEBS letters* 2008, 582:2397-2401.

153. Morine Y, Shimada M, Utsunomiya T, Imura S, Ikemoto T, Mori H, Hanaoka J, Kanamoto M, Iwahashi S, Miyake H. Hypoxia inducible factor expression in intrahepatic cholangiocarcinoma. *Hepato-gastroenterology* 2011, 58:1439-1444.

154. Ying Q, Liang L, Guo W, Zha R, Tian Q, Huang S, Yao J, Ding J, Bao M, Ge C. Hypoxia-inducible MicroRNA-210 augments the metastatic potential of tumor cells by targeting vacuole membrane protein 1 in hepatocellular carcinoma. *Hepatology* 2011, 54:2064-2075.

155. Lee D, Sun S, Zhang XQ, De Zhang P, Ho AS, Kiang KM, Fung CF, Lui WM, Leung GK. MicroRNA-210 and endoplasmic reticulum chaperones in the regulation of chemoresistance in glioblastoma. *Journal of Cancer* 2015, 6:227.

156. Lächelt U, Wagner E. Nucleic acid therapeutics using polyplexes: a journey of 50 years (and beyond). *Chemical reviews* 2015, 115:11043-11078.

157. Li J, Zhu Y, Hazeldine ST, Li C, Oupický D. Dual-function CXCR4 antagonist polyplexes to deliver gene therapy and inhibit cancer cell invasion. *Angewandte Chemie* 2012, 124:8870-8873.

158. Su L, Zhang J, Xu H, Wang Y, Chu Y, Liu R, Xiong S. Differential expression of CXCR4 is associated with the metastatic potential of human non–small cell lung cancer cells. *Clinical cancer research* 2005, 11:8273-8280.

159. Mills GB, Moolenaar WH. The emerging role of lysophosphatidic acid in cancer. *Nature Reviews Cancer* 2003, 3:582.

160. Liu S, Umezu-Goto M, Murph M, Lu Y, Liu W, Zhang F, Yu S, Stephens LC, Cui X, Murrow G. Expression of autotaxin and lysophosphatidic acid receptors increases mammary tumorigenesis, invasion, and metastases. *Cancer cell* 2009, 15:539-550.

161. Cadamuro M, Nardo G, Indraccolo S, Dall'Olmo L, Sambado L, Moserle L, Franceschet I, Colledan M, Massani M, Stecca T. Platelet-derived growth factor-D and Rho GTPases regulate recruitment of cancer-associated fibroblasts in cholangiocarcinoma. *Hepatology* 2013, 58:1042-1053.

162. Wang Q, Tang H, Yin S, Dong C. Downregulation of microRNA-138 enhances the proliferation, migration and invasion of cholangiocarcinoma cells through the upregulation of RhoC/p-ERK/MMP-2/MMP-9. *Oncology reports* 2013, 29:2046-2052.

163. Balic A, Sørensen MD, Trabulo SM, Sainz B, Cioffi M, Vieira CR, Miranda-Lorenzo I, Hidalgo M, Kleeff J, Erkan M. Chloroquine targets pancreatic cancer stem cells via inhibition of CXCR4 and hedgehog signaling. *Molecular cancer therapeutics* 2014.

164. Trautmann F, Cojoc M, Kurth I, Melin N, Bouchez LC, Dubrovska A, Peitzsch C. CXCR4 as biomarker for radioresistant cancer stem cells. *International journal of radiation biology* 2014, 90:687-699.

165. Yang W, Wei J, Guo T, Shen Y, Liu F. Knockdown of miR-210 decreases hypoxic glioma stem cells stemness and radioresistance. *Experimental cell research* 2014, 326:22-35.

166. Batlle E, Clevers H. Cancer stem cells revisited. *Nature medicine* 2017, 23:1124.

167. Siegel R, Ma J, Zou Z, Jemal A. Cancer statistics, 2014. *CA: a cancer journal for clinicians* 2014, 64:9-29.

168. Hidalgo M. Pancreatic cancer. *New England Journal of Medicine* 2010, 362:1605-1617.

169. Stathis A, Moore MJ. Advanced pancreatic carcinoma: current treatment and future challenges. *Nature reviews Clinical oncology* 2010, 7:163.

170. Olive KP, Jacobetz MA, Davidson CJ, Gopinathan A, McIntyre D, Honess D, Madhu B, Goldgraben MA, Caldwell ME, Allard D. Inhibition of Hedgehog signaling enhances delivery of chemotherapy in a mouse model of pancreatic cancer. *Science* 2009.

171. Conroy T, Desseigne F, Ychou M, Bouché O, Guimbaud R, Bécouarn Y, Adenis A, Raoul J-L, Gourgou-Bourgade S, de la Fouchardière C. FOLFIRINOX versus gemcitabine for metastatic pancreatic cancer. *New England Journal of Medicine* 2011, 364:1817-1825.

172. Fareh M, Turchi L, Virolle V, Debruyne D, Almairac F, Divonne Sd-l-F, Paquis P, Preynat-Seauve O, Krause K-H, Chneiweiss H. The miR 302-367 cluster drastically affects self-renewal and infiltration properties of glioma-initiating cells through CXCR4 repression and consequent disruption of the SHH-GLI-NANOG network. *Cell death and differentiation* 2012, 19:232.

173. Saur D, Seidler B, Schneider G, Algül H, Beck R, Senekowitsch–Schmidtke R, Schwaiger M, Schmid RM. CXCR4 expression increases liver and lung metastasis in a mouse model of pancreatic cancer. *Gastroenterology* 2005, 129:1237-1250.

174. Li X, Ma Q, Xu Q, Liu H, Lei J, Duan W, Bhat K, Wang F, Wu E, Wang Z. SDF-1/CXCR4 signaling induces pancreatic cancer cell invasion and epithelial–mesenchymal transition in vitro through non-canonical activation of Hedgehog pathway. *Cancer letters* 2012, 322:169-176.

175. Carthew RW, Sontheimer EJ. Origins and mechanisms of miRNAs and siRNAs. *Cell* 2009, 136:642-655.

176. Wittrup A, Lieberman J. Knocking down disease: a progress report on siRNA therapeutics. *Nature Reviews Genetics* 2015, 16:543.

177. Rupaimoole R, Slack FJ. MicroRNA therapeutics: towards a new era for the management of cancer and other diseases. *Nature reviews Drug discovery* 2017, 16:203.

178. Lei Y, Tang L, Xie Y, Xianyu Y, Zhang L, Wang P, Hamada Y, Jiang K, Zheng W, Jiang X. Gold nanoclusters-assisted delivery of NGF siRNA for effective treatment of pancreatic cancer. *Nature communications* 2017, 8:15130.

179. Rachagani S, Macha MA, Heimann N, Seshacharyulu P, Haridas D, Chugh S, Batra SK. Clinical implications of miRNAs in the pathogenesis, diagnosis and therapy of pancreatic cancer. *Advanced drug delivery reviews* 2015, 81:16-33.

180. Gibori H, Eliyahu S, Krivitsky A, Ben-Shushan D, Epshtein Y, Tiram G, Blau R, Ofek P, Lee JS, Ruppin E. Amphiphilic nanocarrier-induced modulation of PLK1 and miR-34a leads to improved therapeutic response in pancreatic cancer. *Nature communications* 2018, 9:16.

181. Xue W, Dahlman JE, Tammela T, Khan OF, Sood S, Dave A, Cai W, Chirino LM, Yang GR, Bronson R. Small RNA combination therapy for lung cancer. *Proceedings of the National Academy of Sciences* 2014, 111:E3553-E3561.

182. Chang DK, Grimmond SM, Biankin AV. Pancreatic cancer genomics. *Current opinion in genetics & development* 2014, 24:74-81.

183. Collins MA, Bednar F, Zhang Y, Brisset J-C, Galbán S, Galbán CJ, Rakshit S, Flannagan KS, Adsay NV, di Magliano MP. Oncogenic Kras is required for both the initiation and maintenance of pancreatic cancer in mice. *The Journal of clinical investigation* 2012, 122:639-653.

184. Collins MA, Brisset J-C, Zhang Y, Bednar F, Pierre J, Heist KA, Galbán CJ, Galbán S, di Magliano MP. Metastatic pancreatic cancer is dependent on oncogenic Kras in mice. *PloS one* 2012, 7:e49707.

185. Ying H, Kimmelman AC, Lyssiotis CA, Hua S, Chu GC, Fletcher-Sananikone E, Locasale JW, Son J, Zhang H, Coloff JL. Oncogenic Kras maintains pancreatic tumors through regulation of anabolic glucose metabolism. *Cell* 2012, 149:656-670.

186. Kamerkar S, LeBleu VS, Sugimoto H, Yang S, Ruivo CF, Melo SA, Lee JJ, Kalluri R. Exosomes facilitate therapeutic targeting of oncogenic KRAS in pancreatic cancer. *Nature* 2017, 546:498.

187. Koong AC, Mehta VK, Le QT, Fisher GA, Terris DJ, Brown JM, Bastidas AJ, Vierra M. Pancreatic tumors show high levels of hypoxia. *International Journal of Radiation Oncology* Biology* Physics* 2000, 48:919-922.

188. Ho AS, Huang X, Cao H, Christman-Skieller C, Bennewith K, Le Q-T, Koong AC. Circulating miR-210 as a novel hypoxia marker in pancreatic cancer. *Translational oncology* 2010, 3:109-113.

189. Huang X, Le Q-T, Giaccia AJ. MiR-210–micromanager of the hypoxia pathway. *Trends in molecular medicine* 2010, 16:230-237.

190. Rothe F, Ignatiadis M, Chaboteaux C, Haibe-Kains B, Kheddoumi N, Majjaj S, Badran B, Fayyad-Kazan H, Desmedt C, Harris AL. Global microRNA expression profiling identifies MiR-210 associated with tumor proliferation, invasion and poor clinical outcome in breast cancer. *PloS one* 2011, 6:e20980.

191. Jung EJ, Santarpia L, Kim J, Esteva FJ, Moretti E, Buzdar AU, Di Leo A, Le XF, Bast Jr RC, Park ST. Plasma microRNA 210 levels correlate with sensitivity to trastuzumab and tumor presence in breast cancer patients. *Cancer* 2012, 118:2603-2614.

192. Chakraborty C, Sharma AR, Sharma G, Doss CGP, Lee S-S. Therapeutic miRNA and siRNA: moving from bench to clinic as next generation medicine. *Molecular Therapy-Nucleic Acids* 2017, 8:132-143.

193. Wang M, Liu H, Li L, Cheng Y. A fluorinated dendrimer achieves excellent gene transfection efficacy at extremely low nitrogen to phosphorus ratios. *Nature communications* 2014, 5:3053.

194. Wang LH, Wu DC, Xu HX, You YZ. High DNA-binding affinity and gene-transfection efficacy of bioreducible cationic nanomicelles with a fluorinated core. *Angewandte Chemie International Edition* 2016, 55:755-759.

195. Chen G, Wang K, Hu Q, Ding L, Yu F, Zhou Z, Zhou Y, Li J, Sun M, Oupický D. Combining fluorination and bioreducibility for improved siRNA polyplex delivery. *ACS applied materials & interfaces* 2017, 9:4457-4466.

196. Jackson MA, Werfel TA, Curvino EJ, Yu F, Kavanaugh TE, Sarett SM, Dockery MD, Kilchrist KV, Jackson AN, Giorgio TD. Zwitterionic Nanocarrier Surface Chemistry Improves siRNA Tumor Delivery and Silencing Activity Relative to Polyethylene Glycol. *ACS nano* 2017.

197. Zhang P, Sun F, Tsao C, Liu S, Jain P, Sinclair A, Hung H-C, Bai T, Wu K, Jiang S. Zwitterionic gel encapsulation promotes protein stability, enhances pharmacokinetics, and reduces immunogenicity. *Proceedings of the National Academy of Sciences* 2015, 112:12046-12051.

198. Wang Y, Xie Y, Li J, Peng Z-H, Sheinin Y, Zhou J, Oupický D. Tumor-Penetrating Nanoparticles for Enhanced Anticancer Activity of Combined Photodynamic and Hypoxia-Activated Therapy. *ACS nano* 2017, 11:2227-2238.

199. Xu X, Wu J, Liu Y, Yu M, Zhao L, Zhu X, Bhasin S, Li Q, Ha E, Shi J. Ultra-pH-Responsive and Tumor-Penetrating Nanoplatform for Targeted siRNA Delivery with Robust Anti-Cancer Efficacy. *Angewandte Chemie International Edition* 2016, 55:7091-7094.

200. Miao L, Li J, Liu Q, Feng R, Das M, Lin CM, Goodwin TJ, Dorosheva O, Liu R, Huang L. Transient and local expression of chemokine and immune checkpoint traps to treat pancreatic cancer. *ACS nano* 2017, 11:8690-8706.

201. Hobo W, Maas F, Adisty N, de Witte T, Schaap N, van der Voort R, Dolstra H. siRNA silencing of PD-L1 and PD-L2 on dendritic cells augments expansion and

function of minor histocompatibility antigen–specific CD8+ T cells. *Blood* 2010, 116:4501-4511.

202. Wang D, Wang T, Liu J, Yu H, Jiao S, Feng B, Zhou F, Fu Y, Yin Q, Zhang P. Acid-activatable versatile micelleplexes for PD-L1 blockade-enhanced cancer photodynamic immunotherapy. *Nano letters* 2016, 16:5503-5513.